2012

UNCONVENTIONAL SUPERHALOGENS: DESIGN AND APPLICATIONS

Devleena Samanta
Virginia Commonwealth University

UNCONVENTIONAL SUPERHALOGENS: DESIGN AND APPLICATIONS

A thesis submitted in partial fulfillment of the requirements for the degree of Master of Science

at Virginia Commonwealth University

By

Devleena Samanta
B.Sc., St. Xavier's College (autonomous), Kolkata, India, 2010

Director: Purusottam Jena, Ph. D
Distinguished Professor, Department of Physics

Virginia Commonwealth University
Richmond, Virginia
May, 2012

Acknowledgement

This is perhaps the most difficult section to write in this thesis. Ordinarily, one would begin by expressing his/her gratitude towards his/her advisor, the one person without whom it would be impossible to finish this journey. But mine is no ordinary case. How do I thank someone when all the good words can never be enough? Professor Puru Jena has not merely been an advisor to me, but he has been a teacher, a mentor, a guide, and someone whose wisdom I could trust. He has taught me how to think, how to write and how to present. Coming from a traditional chemistry background, many a time, just as we were about to start a project, I had not believed in his hypotheses which were based on a physicist's apparently simple logic. And I must say that I had been surprised every time! Once I carried out his suggested calculations, I was amazed to see that his expectations were correct, and impressed at the deep level of understanding he must possess to be able to accurately predict these results. I think he is a brilliant scientist, and I am deeply and sincerely indebted to him for helping to shape me as a researcher.

My acknowledgement would be incomplete without expressing my warm and hearty thanks to my former and current group members Rosy (Swayamprabha Behera), Miao Miao (Dr. Miao Miao Wu), Li Sa (Dr. Sa Li), Wang-san (Dr. Qian Wang), Sun-san (Dr. Qiang Sun), Bikash-da (Dr. Bikash Gupta), Mary (Mary Willis), Kalpa (Dr. Kalpataru Pradhan) and Anil (Dr. Anil K. Kandalam) for helping me to start and continue my research. Additionally, I would also like to thank my committee members as well as Dr. Sarah Rutan and Dr. Everett Carpenter.

A special vote of thanks to my fellow student Ahmed (Dr. Ahmed Hamid), who has helped me time and again on numerous occasions in the course of my graduate study at VCU.

Thank you my friends Pooja (Pooja Ponnusamy) and Kavita (Kavita Iyer) for keeping me company (and sane) in a foreign land amidst my quest for knowledge.

Last but not the least, I would like to thank my family for being a constant source of support. Ma (Dr. Chhanda Samanta), you inspire me every day. I hope to be a successful scientist like you one day. Dada (Dr. Indraneel Samanta), without your perspective, advice and good wishes, my journey would not have been so smooth. Finally, Baba (Late Prabhat Kumar Samanta), thank you for watching over me and for always having believed in me.

Table of Contents

List of Figures

List of Tables

Abstract

UNCONVENTIONAL SUPERHALOGENS: DESIGN AND APPLICATIONS

By Devleena Samanta, M.S.

A thesis submitted in partial fulfillment of the requirements for the degree of Master of Science at Virginia Commonwealth University

Virginia Commonwealth University, 2012

Director: PURUSOTTAM JENA

Distinguished Professor, Department of Physics

Electron affinity is one of the most important parameters that guide chemical reactivity. Halogens have the highest electron affinities among all elements. A class of molecules called superhalogens has electron affinities even greater than that of Cl, the element with the largest electron affinity (3.62 eV). Traditionally, these are metal-halogen complexes which need one electron to close their electronic shell. Superhalogens have been known to chemistry for the past 30 years and all superhalogens investigated in this period are either based on the 8-electron rule

or the 18-electron rule. In this work, we have studied two classes of unconventional superhalogens: borane-based superhalogens designed using the Wade-Mingo's rule that describes the stability of *closo*-boranes, and pseudohalogen based superhalogens. In addition, we have shown that superhalogens can be utilized to build hyperhalogens, which have electron affinities exceeding that of the constituent superhalogens, and also to stabilize unusually high oxidation states of metals.

Chapter 1 Introduction

Electron affinity (EA) is the energy released when an electron is added to a species. It is one of the major factors that govern reactivity. Molecules with high electron affinity form very stable negative ions which are important in the chemical and health industry as they purify air,[1,2] lift mood[3] and most importantly, act as strong oxidizing agents.[4] They can oxidize species with high ionization potential, thereby forming novel and unusual salts. It is well known that noble gases have closed electronic shell structure and hence have high ionization potentials and low electron affinities, due to which they are chemically inert and resistant to salt formation under most conditions. This changed in 1962 when Bartlett synthesized the first salt of xenon, $XePtF_6$.[5] This was possible since PtF_6 has a very high electron affinity value of 7.00±0.35 eV[6] rendering it ability to ionize xenon.

In the periodic table, halogens have the highest electron affinity since they have ns^2np^5 configuration and need only one electron to attain the noble gas configuration. In fact, the electron affinity of Cl, 3.62 eV is the largest of all the elements.[7] The discovery of Bartlett and coworkers has led to a search for other molecules that also can have large electron affinities. The motivation has been to design strong oxidants that can generate new chemistry. In 1981, Gutsev and Boldyrev showed that when a central metal atom is decorated with halogen ligands, the electron affinity of the resulting species is much above that of Cl. They called these species "superhalogens".[8]

Subsequent studies have shown that the central metal atom can be a main group[9-21] as well as a transition metal atom[22-34] and the halogen ligand can be substituted by other electronegative ligands such as oxygen, hydroxyl radical etc.[35-46] However, all superhalogens studied in the past 30 years are based on either the 8-electron rule[8-46] or the 18-electron rule.[47]

In this work, we have shown that a new class of superhalogens can be designed by tuning the size and composition of borane derivatives.[48] These superhalogens are based on the Wade-Mingo's rule, well-known for describing the stability of *closo*-boranes.[49-52] We have also studied a second class of unconventional superhalogens where pseudohalogens have been used in place of halogens.[53-54] In addition, we have examined the potential of superhalogens for applications, namely, in the design of "hyperhalogens"[48] and in stabilizing unusually high oxidation states of metals.[55]

This work is primarily theoretical in nature. Predicted values have been compared against experimental data, when available. Due to the choice of the theoretical methods, there is good agreement between experiment and theory.

This brief introduction is followed by Chapter 2 in which existing literature (both theoretical and experimental) on superhalogens is discussed. Chapter 3 states the objectives of the project undertaken and Chapter 4 elaborates on the theoretical methods employed in determining the results. The results are divided into two sections, beginning with Chapter 5 which focuses on the design of unconventional superhalogens and continuing to Chapter 6 which demonstrates the

applications of superhalogens. Finally, in Chapter 7, the main conclusions of this study are summarized.

Chapter 2 Background and Overview

2.1 Superhalogens

Superhalogens are molecules which have electron affinities (EA) greater than that of Cl, the element with the highest EA (3.62 eV).[7] In 1981, Gutsev and Boldyrev generalized the formula of one class of superhalogens to be MX_{n+1} where M is a central metal atom with a valency n and X is a monovalent halogen atom.[8] This can be rationalized by realizing that MX_n is a closed-shell neutral salt. Addition of another halogen ligand results in a molecule that needs one electron to close the outer shell. When an electron is added to this system, the negative charge can delocalize over (n+1) X atoms as opposed to just one, and hence the energy of the anion is lowered considerably. As a result, the EA of such a cluster is greater than that of the constituent halogen atom. For example, the electron affinity of NaCl, a salt, is 0.727 eV[56] and that of $NaCl_2$, a superhalogen, is 5.77 eV[15], which is about 1.5 times that of Cl (see Figure 1).

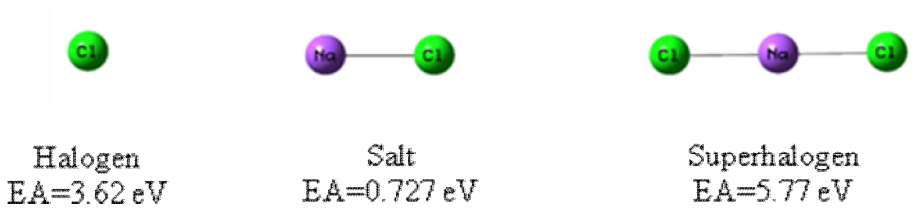

Figure 1. Electron affinity: From halogen to superhalogen

Simple electron counting rules can be employed to design new superhalogens and to understand their stability. These are discussed in the following section.

2.2 Electron Counting Rules

Electron counting rules have been known to play an important role in describing the stability and chemistry of atoms and compounds. For example, the octet rule[57-58] is responsible not only for the inertness of noble gas atoms but also for the reactivity of elements such as alkali metals and halogens. The 18-electron rule,[59-61] on the other hand, is mainly associated with compounds composed of transition metal atoms such as $Cr(C_6H_6)_2$ and $V(CO)_6^-$. These two electron counting rules can be used to form stable negative ions.

2.2.1 Octet Rule

According to the octet rule, eight electrons are required to complete the valence of a simple element and attain a noble gas configuration. Therefore, elements combine in such a manner so that each element has a full octet. The simplest example is that of a halogen atom which has ns^2np^5 as its outermost orbital. Since only one electron is needed to satisfy the octet rule, the EAs of halogens atoms are high (3.0-3.6 eV).[62] The octet rule is followed (with few exceptions) by most main group elements. Considerable research over the past three decades has demonstrated that the octet rule can be used to design and synthesize superhalogens.[8-46] For example, $NaCl_2$ could be hypothetically thought of as (NaCl)Cl where the Na and Cl atoms in NaCl have complete octets but the second Cl atom does not. Therefore, addition of one extra electron completes the electronic shell and stabilizes $NaCl_2^-$. This makes the corresponding neutral a superhalogen.[15]

2.2.2 18-electron Rule

The 18-electron rule governs the stability of many transition metal complexes. As per this rule, 18 valence electrons (10 *d*-electrons, 2 *s*-electrons and 6 *p*-electrons) are required to complete the electronic shell of the central atom. Ferrocene [$Fe(C_5H_5)_2$] and nickel carbonyl [$Ni(CO)_4$]are prime examples of molecules whose stability is dictated by the 18-electron rule. It has been shown that, using this rule clusters composed of only metal atoms, such as $M@Au_{12}$ (M=V, Nb, Ta) clusters can also form superhalogens.[47]

From these two rules it is evident that to be a superhalogen, a molecule needs to have an optimal size and one electron less than that required to complete the electronic shell.

2.3 Theoretical and Experimental Studies

A substantial number of superhalogens have been studied[9-47] theoretically as well as experimentally since the pioneering work of Gutsev and Boldyrev.[8] The superhalogen properties of a cluster can be characterized theoretically by calculating the difference in the energies between the neutral and the anionic cluster. A value greater than 3.62 eV corresponds to superhalogen behavior. Note that a particular molecular formula may correspond to multiple isomers with different relative energies. Depending on the structure of the neutral and the anion clusters chosen, the electron binding energy (EBE) may correspond to an adiabatic detachment energy, a vertical detachment energy or the electron affinity. Methods for calculating each of these parameters is described in section 5.2.2. Typically, first principle calculations such as *ab initio* methods and density functional theory (DFT) are used to predict these values.

Experimentally, the electron affinities can be determined using photoelectron spectroscopy (UV PES). Here, a mass selected cluster anion is crossed with photons of fixed frequency, ν and the kinetic energy, E_{kin} of the photo-ejected electron is measured. Spectroscopic properties are studied by using the energy conserving equation,

$$E_{anion} + h\nu = E_{neutral} + E_{kin},$$

where hν is the energy of the photon, E_{anion} is the energy of the anion and $E_{neutral}$ is the energy of the neutral that results following photodetachment. The electron binding energy is given by,

$$EBE = E_{neutral} - E_{anion} = h\nu - E_{kin.}$$

The simplest superhalogens are of the form MX_2 where M is a monovalent metal (M=Li, Na, Cu; X=F, Cl, Br, I).[15,17,24,25] The first experiments on superhalogens carried out using photoelectron spectroscopy have shown that vertical detachment energies of the clusters studied (M=Li, Na; X=Cl, Br, I) lie between 4.5-6.0 eV.[17] Superhalogens of divalent and trivalent metal atoms of the form MX_3 (M=Be, Mg, Ca; X=F, Cl, Br) and MX_4 (M=B, Al; X=F, Cl, Br) respectively, have also been studied.[9-11,16,18-20] In general, the electron affinity increases with increasing size of the cluster and electronegativity of the ligand. Though initially majority of the work was done using *sp*-block metals[9-21] as the central metal atom, gradually there has been increasing work on *d*-block transition metals.[22-34] Transition elements have variable valency. For example, the oxidation state of Mn can range from -3 to +7. Therefore, it is not clear for what value of n, an MX_n cluster (M=transition metal) will behave as a superhalogen. Recent studies on MCl_n (M=Sc, Y, La and n=1-5) have been aimed at addressing this question.[28] Other transition metals that have been studied as central atoms in superhalogens include Cu[24,25], Ag[25], Au[25], Pt[29,34], Mn[27,30], Cr[32] etc.

Superhalogens with more than one metal centers have also been studied.[30,63-68] Examples include Mg_2F_5, Mg_3Cl_7, Na_nCl_{n+1}, Cu_mCl_n etc. There has been some effort in building superhalogens without halogens. Other electronegative ligands such as O, OH, etc. have been studied as halogen alternatives.[35-46] Moreover, unusual superhalogens such as those composed solely of metals such as $Ta@Au_{12}$ have been theoretically studied and confirmed experimentally.[47] It has also been demonstrated that clusters without halogen atoms (such as MH_n)[37,38] or without metal atoms (such as H_nF_{n+1}, BO_2 and ClO_4)[69-71] can behave as superhalogens. Currently, the highest predicted vertical detachment energy of a molecule is 13.871 eV for the cluster $H_{12}F_{13}^-$.[69]

2.4 Applications

Superhalogens are important as they form very stable negative ions. Therefore, they are common anions in many known salts, some of which are notable for their strong oxidizing properties (e.g. $KMnO_4$ and $KClO_4$). They are also promising candidates as building units of novel chemical compounds.

In 2010, Willis et al. showed that hierarchical structures called "hyperhalogens" can be made by replacing the halogen atoms in a traditional superhalogen with other superhalogens.[72] The hyperhalogens have electron affinities that even surpass that of the constituent superhalogens. This was shown with the example of $Au(BO_2)_2$. Here, BO_2 is a superhalogen with an EA of 4.32 eV[71], $AuBO_2$ is salt with an EA of 2.80 eV and $Au(BO_2)_2$ is a hyperhalogen whose EA is 5.70 eV[72] (see Figure 2). In general, hyperhalogens would obey the formula MY_{n+1} where Y is a superhalogen.

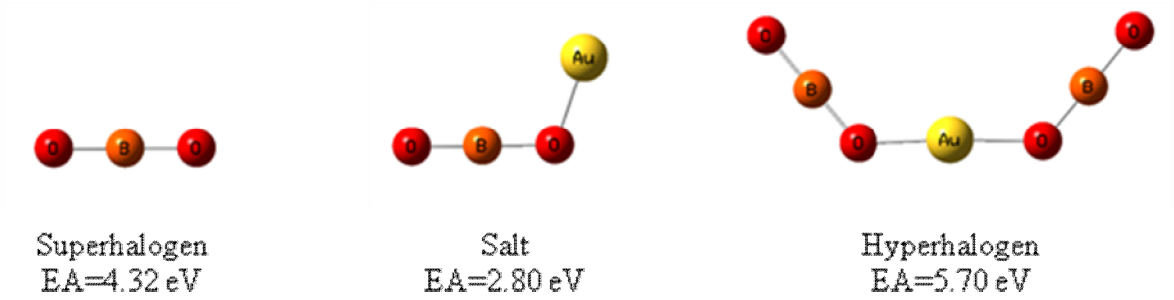

Figure 2. Electron affinity: From superhalogen to hyperhalogen

In 2011, the discovery of a class of polynuclear magnetic superhalogens of the form Mn_nCl_{2n+1} (n=1, 2, 3...) was reported.[30] It was shown that these molecules could be used to build salts. In the particular example of $KMnCl_3$, it was proposed that the bulk phase would exhibit antiferromagnetic properties. Existing literature on this well-known perovskite salt confirms this prediction.

Recently, it has also been demonstrated that superhalogens can oxidize certain neutral species (SiO_2, NH_3, etc.) with moderately high ionization potentials to form stable ionic salts.[73] Superhalogens have also been shown to increase the work function of graphene.[74] This property could be utilized in designing graphene-based electrodes. Other potential applications of superhalogens include but are not limited to synthesis of organic superconductors[75] and materials with non-linear optical properties.[76]

2.5 Unexplored Territories

Though there has been significant work in the arena of superhalogens, there is much that is left to be explored. The simplest of these is to complete a comprehensive study of superhalogens using

elements spanning the entire periodic stable. This would give us valuable insight into how the superhalogen behavior varies down a group, across a row and as a function of composition. Moreover, this may lead to the discovery of useful halogen-free superhalogens with very large electron affinities. Halogens (especially F) are corrosive and therefore require special handling care. This poses as an obstacle during the synthesis of superhalogens. It is possible that halogen-free superhalogens may be prepared under less hazardous conditions. Investigating the stability of these superhalogens compared to that of conventional metal-halogen superhalogens would be important. It would also be an interesting study to see if the stability can be modified if electron counting rules, other than the 8 and 18 electron rules were used to generate these superhalogens.

Moreover, most studied superhalogens are binary i.e. they consist of two elements. Not much is known about the behavior of superhalogens whose composition extends beyond binary species. One could think of building such superhalogens by replacing the halogen atoms by pseudohalogens such as CN, SCN, NCO etc. This possibility has been somewhat explored in the work of Smuczynska and Skurski using Li, Na, Be, Mg, Ca, B and Al as the central metal atoms.[77] However, a more systematic and elaborate study is required to understand how these superhalogens compare with traditional ones.

A majority of the work done on superhalogens is theoretical, awaiting experimental validation. Therefore, while experiments are encouraged, it is also important to theoretically study those systems which could be replicated in experiments without posing difficulties. This would also increase the chances of practical applications of these superhalogens.

Suggesting and testing applications of superhalogens are complex problems. For example, due to their large electron affinities, it can be expected that superhalogens may also be able to stabilize unusually high oxidation states of metals. Question remains if this is possible in practice, and how stable the resulting compounds would be. A link between superhalogens and weakly coordinating ions, which are known to be stabilizing ligands, would facilitate this investigation and give rise to new chemistry.

Chapter 3 Objectives

This work addresses some of the problems on superhalogens that remain unexplored. Specifically, the main motivation of this work is to answer the following questions:

(1) Is it possible to use any other electron counting rule (apart from 8-electron and 18-electron rules) to design superhalogens?
(2) Must superhalogens consist of a metal and/or a halogen atom?
(3) Can pseudohalogens be used in place of halogens to design superhalogens containing transition metal atoms?
(4) How do pseudohalogen-based superhalogens compare with conventional superhalogens?
(5) Can unconventional superhalogens also be used to design hyperhalogens?
(6) Are superhalogens strong enough to oxidize metals beyond their normal valence?

Questions (1) and (2) are addressed in section 5.1 Answers to questions (3) and (4) are explored in section 5.2 Sections 6.1 and 6.2 deal with questions (5) and (6), respectively.

Chapter 4 Theoretical Methods

This chapter provides a brief overview of the theoretical methods that have been used to study the systems of interest. Namely, Density Functional Theory (DFT) has been employed to carry out all calculations using B3LYP hybrid functional for exchange-correlation. Different basis sets have been chosen depending on the system studied. The Gaussian 03 and Gaussian 09 softwares have been employed to perform the calculations. The following sections begin with quantum mechanics and thereafter DFT is introduced.

4.1 The Schrodinger Equation

The chemistry of elements and compounds is guided by their electronic configuration. To have a theoretical understanding of the structure, stability and reactivity of chemical species, it is therefore important to calculate electronic properties.

Using wave mechanics as a tool, in 1926, Schrodinger proposed an equation solving which the exact energy of a system can be determined.[78] The time-independent non-relativistic Schrodinger equation is defined as an eigenvalue problem of the form

$$\hat{H}\Psi = E\Psi \qquad 4.1$$

where $\hat{H}$ is the Hamiltonian operator which operates on Ψ, the wave function of the system and returns E, the energy eigenvalue. This is a second order differential equation as will be seen from the description of $\hat{H}$.

In a system consisting of N electrons and M nuclei,

$$\Psi_i = \Psi_i(\vec{x}_1, \vec{x}_2, \dots, \vec{x}_N, \vec{R}_1, \vec{R}_2, \dots, \vec{R}_M) \quad 4.2$$

and it represents the wave function of the i[th] state of a system. It is dependent on $3N$ spatial co-ordinates $\{\vec{r}_i\}$ and N spin co-ordinates $\{s_i\}$, which are collectively represented by $\{\vec{x}_i\}$ as well as the $3M$ spatial co-ordinates of the nuclei. In absence of any external magnetic or electric field the Hamiltonian operator $\hat{H}$ comprises of

i) the kinetic energy operator of the electrons given by

$$\hat{T} = -\frac{h^2}{8\pi^2 m_e}\sum_{i=1}^{N}\nabla_i^2 \quad 4.3$$

ii) the kinetic energy operator of the nuclei described as

$$\hat{T}_{nuc} = -\frac{h^2}{8\pi^2 M_A}\sum_{A=1}^{M}\nabla_A^2 \quad 4.4$$

iii) the potential acting on the electrons due to the nuclei (often called external potential in density functional theory)

$$\hat{V}_{ext} = -e^2\sum_{i=1}^{N}\sum_{A=1}^{M}\frac{Z_A}{r_{iA}} \quad 4.5$$

iv) the electron-electron interaction term

$$\hat{V}_{ee} = e^2 \sum_{i=1}^{N} \sum_{j>i}^{N} \frac{1}{r_{ij}} \quad 4.6$$

v) the repulsive electrostatic interaction between the nuclei

$$\hat{V}_{NN} = e^2 \sum_{A=1}^{M} \sum_{B>A}^{M} \frac{Z_A Z_B}{R_{AB}} \quad 4.7$$

Therefore, the net Hamiltonian is given by

$$\hat{H} = \hat{T} + \hat{T}_{nuc} + \hat{V}_{ext} + \hat{V}_{ee} + \hat{V}_{NN} \quad 4.8$$

Here, h is the Planck's constant, m_e is the mass of an electron, M_A is the mass of the A^{th} nucleus, e is the charge of an electron, Z_A is the nuclear charge of the A^{th} nucleus. Subscripts i and j run over N electrons, while A and B run over M nuclei. The Laplacian operator ∇_q^2 is defined as a sum of differential operators in Cartesian co-ordinates as

$$\nabla_q^2 = \frac{\partial^2}{\partial x_q^2} + \frac{\partial^2}{\partial y_q^2} + \frac{\partial^2}{\partial z_q^2} \quad 4.9$$

It is a common practice to write these quantum mechanical equations without the use of fundamental physical constants. Therefore, m_e, e, $h/2\pi$, $4\pi\epsilon_0$ (permittivity of free space) are all set to one. Other physical quantities are expressed as multiples of these constants. Therefore, the Hamiltonian can now be written as

$$\hat{H} = -\frac{1}{2}\sum_{i=1}^{N}\nabla_i^2 - \frac{1}{2M_A}\sum_{A=1}^{M}\nabla_A^2 - \sum_{i=1}^{N}\sum_{A=1}^{M}\frac{Z_A}{r_{iA}} + \sum_{i=1}^{N}\sum_{j>i}^{N}\frac{1}{r_{ij}} + \sum_{A=1}^{M}\sum_{B>A}^{M}\frac{Z_A Z_B}{R_{AB}}$$

4.10

4.2 The Born-Oppenheimer Approximation

Equation 4.10 is a partial differential equation in $4N+3M$ co-ordinates ($3N$ electronic spatial co-ordinates, N electronic spin co-ordinates, and $3M$ nuclear spatial co-ordinates) and therefore, impossible to solve analytically for systems with more than one electron. However, systems of interest to chemists are mostly multi-atomic systems, let alone multi-electronic systems. Such studies are computationally expensive and require simplified schemes.

The Schrodinger equation can be simplified with the aid of several approximations. The first approximation given by Born and Oppenheimer takes into account the significant mass difference between an electron and nuclei. The mass of the lightest nucleus (i.e. mass of a proton, ^1H), is about 1800 times greater than that of an electron. Consequently, electrons move much faster than nuclei. In other words, the kinetic energy of the nuclei is negligible compared to that of the electrons. The Born-Oppenheimer approximation[79] assumes the nuclear kinetic energy to be zero. This fixes $\vec{R}_A$ and therefore, the inter-nuclear repulsion becomes a constant.

The Hamiltonian is reduced to

$$\hat{H} = -\frac{1}{2}\sum_{i=1}^{N}\nabla_i^2 - \sum_{i=1}^{N}\sum_{A=1}^{M}\frac{Z_A}{r_{iA}} + \sum_{i=1}^{N}\sum_{j>i}^{N}\frac{1}{r_{ij}} + \sum_{A=1}^{M}\sum_{B>A}^{M}\frac{Z_A Z_B}{R_{AB}}$$

4.11

the last term being a constant.

Moreover, the Hamiltonian can now be separated into two components: nuclear and electronic, where the electronic Hamiltonian is given by

$$\hat{H}_{elec} = \hat{T} + \hat{V}_{Ne} + \hat{V}_{ee} = -\frac{1}{2}\sum_{i=1}^{N}\nabla_i^2 - \sum_{i=1}^{N}\sum_{A=1}^{M}\frac{Z_A}{r_{iA}} + \sum_{i=1}^{N}\sum_{j>i}^{N}\frac{1}{r_{ij}} \qquad 4.12$$

The problem of electronic structure calculation has now been simplified to solving the electronic Schrodinger equation given by

$$\hat{H}_{elec}\Psi_{elec} = E_{elec}\Psi_{elec} \qquad 4.13$$

where

$$\Psi_{elec} = \Psi_{elec}(\vec{x}_1, \vec{x}_2, \dots, \vec{x}_N). \qquad 4.14$$

As subsequent discussions will focus only on the electronic Schrodinger equation, the subscript '*elec*' is dropped hereafter.

Ψ itself is not an observable. However, $|\Psi(\vec{x}_1, \vec{x}_2, \dots, \vec{x}_N)|^2 d\vec{x}_1 d\vec{x}_2 \dots d\vec{x}_N$ represents the probability that all N electrons can be simultaneously found within the volume element $d\vec{x}_1 d\vec{x}_2 \dots d\vec{x}_N$. If the co-ordinates of two electrons are interchanged, this probability should remain unchanged i.e.

$$\left|\Psi(\vec{x}_1, \vec{x}_2, \dots, \vec{x}_i, \vec{x}_j, \dots, \vec{x}_N)\right|^2 = \left|\Psi(\vec{x}_1, \vec{x}_2, \dots, \vec{x}_j, \vec{x}_i, \dots, \vec{x}_N)\right|^2. \qquad 4.15$$

Electrons are fermions with half-integral spin. Consequently they have anti-symmetric wave functions. This implies that interchanging the state of two electrons would result in a sign change in the wave function i.e.

$$\Psi(\vec{x}_1, \vec{x}_2, \dots, \vec{x}_i, \vec{x}_j, \dots, \vec{x}_N) = -\Psi(\vec{x}_1, \vec{x}_2, \dots, \vec{x}_j, \vec{x}_i, \dots, \vec{x}_N). \quad 4.16$$

This anti-symmetry principle validates the Pauli exclusion principle, which states that no two electrons can occupy the same state.

4.3 The Variational Principle

To solve the Schrodinger equation, first the Hamiltonian has to be set up. Using equation 4.1 we get,

$$\hat{H}\Psi_i = E\Psi_i \quad 4.17$$

Multiplying both sides by Ψ_i^*, the complex conjugate of Ψ_i, and integrating over all space, we get,

$$\int \Psi_i^* \hat{H} \Psi_i d\vec{x}_1 d\vec{x}_2 \dots d\vec{x}_N = \int \Psi_i^* E_i \Psi_i d\vec{x}_1 d\vec{x}_2 \dots d\vec{x}_N \quad 4.18$$

When Ψ_i is normalized,

$$\int \Psi_i^* \Psi_i d\vec{x}_1 d\vec{x}_2 \dots d\vec{x}_N = 1 \quad 4.19$$

and hence

$$E_i = \int \Psi_i^* \hat{H} \Psi_i d\vec{x}_1 d\vec{x}_2 \dots d\vec{x}_N \quad 4.20$$

In Dirac notation,

$$E_i = \langle \Psi_i | \hat{H} | \Psi_i \rangle. \quad 4.21$$

Therefore, by determining Ψ_i, the total energy E_i can be calculated. However, this task is more challenging than it appears as the equation above can be solved only for selected trivial cases.

Approximations can be applied to determine Ψ_i and E_i. One of the most important approximations that is widely used to approach the problem is the variational principle. According to this, if a trial wave function Ψ_{trial} is used to estimate the total energy E_{trial} of the system, then,

$$\langle \Psi_{trial} | \hat{H} | \Psi_{trial} \rangle = E_{trial} \geq E_0 = \langle \Psi_0 | \hat{H} | \Psi_0 \rangle \qquad 4.22$$

where E_0 is the true energy of the ground state of the system. The equality holds when Ψ_{trial} and Ψ_0 are identical. Therefore, by minimizing the total energy, the energy of the ground state can be obtained. The total energy $E[\Psi]$ is called a functional as it is a function of another function $\Psi(\vec{x})$. Mathematically, the variational principle can be expressed as

$$E_0 = \min E[\Psi] = \min \langle \Psi | \hat{H} | \Psi \rangle = \min \langle \Psi | \hat{T} + \hat{V}_{Ne} + \hat{V}_{ee} | \Psi \rangle \qquad 4.23$$

4.4 The Hartree Approximation

The Hartree approximation[80] separates the one-*N* electron problem into *N*-one electron Schrodinger equations. The Hamiltonian is defined as

$$\hat{H} = \sum_{i=1}^{N} \hat{h}(i) \qquad 4.24$$

where

$$\hat{h}(i) = -\frac{1}{2}\sum_{i=1}^{N} \nabla_i^2 - \sum_{A=1}^{M} \frac{Z_A}{r_{iA}} + \sum_{j=1}^{N} \frac{1}{r_{ij}} \qquad 4.25$$

Electrons are assumed to be non-interacting and therefore, the total wave function is expressed as a product of the one-electron wave functions, called the Hartree product wave function, given below:

$$\Psi^{HP}(\vec{x}_1, \vec{x}_2, \dots, \vec{x}_N) = \chi_1(\vec{x}_1)\chi_2(\vec{x}_2) \dots \chi_N(\vec{x}_N) \quad 4.26$$

The one electron wave functions $\chi_i(\vec{x}_i)$, called spin orbitals, are composed of a spatial orbital $\phi_i(\vec{r}_i)$ and one of the two spin functions $\alpha(s)$ or $\beta(s)$ i.e.

$$\chi_i(\vec{x}_i) = \phi_i(\vec{r}_i)\sigma(s) \text{ where } \sigma = \alpha \text{ or } \beta. \quad 4.27$$

Each one-electron wave function can be solved using the equation

$$\hat{h}(i)\chi_i(\vec{x}_i) = \epsilon_i\chi_i(\vec{x}_i) \quad 4.28$$

The total energy of the system is given by

$$E = \sum_{i=1}^{N} \epsilon_i \quad 4.29$$

Though the Hartree approximation greatly simplifies electronic calculations, it has some severe limitations. It neither follows the antisymmetry principle nor the Pauli exclusion principle. Moreover, particular electrons are assigned to particular orbitals. This is inconsistent with electrons being indistinguishable. In addition, the electrons are assumed to behave independent of each other (i.e. they are uncorrelated) which implies that the probability of finding an electron is totally independent of that of finding another electron. This is untrue for a real system.

4.5 The Hartree-Fock Approximation

To account for the antisymmetry of the electronic wavefunction, the Hartree-Fock method[81] approximates the N electron wave function by a Slater determinant ϕ_{SD} of the form

$$\phi_{SD} = \frac{1}{\sqrt{N!}} \begin{vmatrix} \chi_1(\vec{x}_1) & \chi_2(\vec{x}_1) & \cdots & \chi_N(\vec{x}_1) \\ \chi_1(\vec{x}_2) & \chi_2(\vec{x}_2) & \cdots & \chi_N(\vec{x}_2) \\ \cdots & \cdots & \cdots & \cdots \\ \chi_1(\vec{x}_N) & \chi_2(\vec{x}_N) & \cdots & \chi_N(\vec{x}_N) \end{vmatrix} \qquad 4.30$$

which is an antisymmetrized product of N single electron wave functions $\chi_i(\vec{x}_i)$. The wave function ϕ_{SD} is antisymmetric as interchanging two rows or two columns in the Slater determinant results in a change in sign. If two electrons are assigned to the same orbital, that is, $\chi_i = \chi_j$, $\phi_{SD} = 0$. Therefore, ϕ_{SD} follows the Pauli exclusion principle. Using the variational principle under the condition that $\chi_i(\vec{x}_i)$ are orthonormal, the Hartree-Fock energy can be obtained by minimizing $E[\phi_{SD}]$. This results in a set of *N* one electron Hartree-Fock equations of the form

$$\hat{f}(i)\chi_i(\vec{x}_i) = \epsilon_i\chi_i(\vec{x}_i) \qquad i = 1 \text{ to } N \qquad 4.31$$

where ϵ_i is the eigen solution and $\hat{f}(i)$ is an effective one electron operator called the Fock operator. It is given by

$$\hat{f}(i) = -\frac{1}{2}\nabla_i^2 - \sum_{A=1}^{M} \frac{Z_A}{r_{iA}} + V_{HF}(i) \qquad 4.32$$

$V_{HF}(i)$ is the Hartree-Fock potential which is the average repulsive potential experienced by an electron due to the presence of other *N-1* electrons. This simplifies the complex two electron operator $1/r_{ij}$ to a one electron operator $V_{HF}(i)$.

$V_{HF}(i)$ is composed of the Coulomb operator $\hat{J}$ and the exchange operator $\hat{K}$. Mathematically,

$$V_{HF}(\vec{x}_1) = \sum_{j=1}^{N} \left(\hat{J}_j(\vec{x}_1) - \hat{K}_j(\vec{x}_1) \right)$$

4.33

where

$$\hat{J}_j(\vec{x}_1) = \int \left|\chi_j(\vec{x}_2)\right|^2 \frac{1}{r_{12}} d\vec{x}_2$$

4.34

and

$$\hat{K}_j(\vec{x}_1)\chi_i(\vec{x}_1) = \int \chi_j^*(\vec{x}_2) \frac{1}{r_{12}} \chi_i(\vec{x}_2) d\vec{x}_2 \, \chi_j(\vec{x}_1)$$

4.35

The Coulomb operator represents the potential experienced by an electron at a position due to an electron in another spin orbital and is integrated over all space. The exchange operator arises because two electrons can exchange their positions. It is to be noted that only electrons of same spin can interchange position. If the electrons are of different spins the value of the exchange potential is zero. Another point to note from equation 4.34 is that when $i=j$ an electron can interact with itself. However, this self-interaction term is cancelled out as the Coulomb and exchange integrals are equal and opposite in magnitude for $i=j$.

The Hartree-Fock method utilizes the self-consistent field (SCF) method to solve for the energy. In this method, an initial set of orbitals is 'guessed' and used to construct the $V_{HF}(i)$. Then $V_{HF}(i)$ is used to solve the Hartree-Fock equations and a new set of orbitals is obtained. This

process is iteratively continued till the input and output set of orbitals match within a certain degree of precision.

The Hartree-Fock method is computationally more expensive than the Hartree method as a number of two electron integrals have to be computed. Though it gives better results, it does not account for the dynamic correlation between electrons arising out of inter-electronic repulsions within a short range. To include dynamic correlation, the wave function is better represented as a linear combination of several Slater determinants. In several theoretical methods (e.g. Moller-Plesset Perturbation theory[82], Coupled-Cluster theory[83]) the Hartree-Fock energy is calculated first and then the correction due to electronic correlation is incorporated.

4.6 Density Functional Theory

There is significant computational expense associated with the Hartree-Fock method as the wave function is dependent on $3N$ electronic spatial co-ordinates and N electronic spin co-ordinates. The earliest formulation of density functional theory led to a simplification of this problem by expressing the wave function as a function of the electron density which depends only on three spatial co-ordinates.

4.6.1 Thomas-Fermi-Dirac Approximation

In 1927, Thomas and Fermi[84,85] showed that the kinetic energy of an electronic system E_{TF} can be expressed as a function of the electron density $\rho(\vec{r})$. Electrons were assumed to be non-interacting with a homogeneous gas density. The electron density is similar to the probability density and is given by

$$\rho(\vec{r}) = |\Psi(\vec{r})|^2 = \left|\Psi\left(\vec{x}_1, \vec{x}_2, \dots, \vec{x}_i, \vec{x}_j, \dots \vec{x}_N\right)\right|^2 \quad 4.36$$

where $\rho(\vec{r})$ holds the property

$$\int \rho(\vec{r}) d\vec{r} = N \quad 4.37$$

$\rho(\vec{r})$ denotes the probability of finding the ith electron out of N electrons at any point within a given volume $d\vec{r}$ where $d\vec{r} = d\vec{x}_1 d\vec{x}_2 \dots d\vec{x}_N$.

The Thomas-Femi kinetic energy is then given by

$$T_{TF}[\rho(\vec{r})] = \frac{3}{10}(3\pi^2)^{\frac{2}{3}} \int [\rho(\vec{r})]^{\frac{5}{3}} d\vec{r} \quad 4.38$$

The total energy of the system is then give by

$$E_{TF}[\rho(\vec{r})] = \frac{3}{10}(3\pi^2)^{\frac{2}{3}} \int [\rho(\vec{r})]^{\frac{5}{3}} d\vec{r} - Z \int \frac{\rho(\vec{r})}{r} d\vec{r} + \frac{1}{2} \int \int \frac{\rho(\vec{r}_1)\rho(\vec{r}_2)}{r_{12}} d\vec{r}_1 d\vec{r}_2 \quad 4.39$$

where the second term represents the attractive nucleus-electron Coulombic interaction and the third term represents the inter-electronic repulsion. It is to be noted that this expression does not account for the electron-electron exchange energy.

In 1930, Dirac introduced an exchange term[86] in the Thomas-Fermi energy

$$K_{D[\rho]} = -\frac{3}{4}\left(\frac{3}{\pi}\right)^{\frac{1}{3}} \int [\rho(\vec{r})]^{\frac{4}{3}} d\vec{r} \quad 4.40$$

and the resulting energy functional is therefore given by the Thomas-Fermi-Dirac approximation shown below.

$$E_{TFD}[\rho(\vec{r})] = E_{TF}[\rho(\vec{r})] + K_{D[\rho]} \qquad 4.41$$

The importance of the Thomas-Fermi-Dirac approximation is that it could express the kinetic energy as a functional of the electron density. Also it reduced the many-body problem involving 3*N* spatial co-ordinates to 3 spatial co-ordinates. However, this method does not estimate the energies accurately. This drawback arises from assuming electrons to be uniformly distributed in space as a gas.

4.6.2 Hohenberg-Kohn Formulation

Modern day density functional theory is founded upon two theorems published by Hohenberg and Kohn[87] in 1964. These theorems apply to a system consisting of electrons moving under the influence of an external potential $V_{ext}(\vec{r})$.

The first theorem states

> *The external potential $V_{ext}(\vec{r})$ is (to within a constant) a unique functional of $\rho(\vec{r})$; since, in turn $V_{ext}(\vec{r})$ fixes $\hat{H}$ we see that the total energy is a unique functional of $\rho(\vec{r})$.*

From equation 4.12, we see that under the Born-Oppenheimer approximation

$$\hat{H}_{elec} = \hat{T} + \hat{V}_{Ne} + \hat{V}_{ee} = -\frac{1}{2}\sum_{i=1}^{N}\nabla_i^2 - \sum_{i=1}^{N}\sum_{A=1}^{M}\frac{Z_A}{r_{iA}} + \sum_{i=1}^{N}\sum_{j>i}^{N}\frac{1}{r_{ij}}$$

The second term represents the external potential $V_{ext}(\vec{r})$. The equation implies by fixing $V_{ext}(\vec{r})$, the Hamiltonian $\widehat{H}$ is completely fixed. The first theorem of Hohenberg and Kohn justifies that $V_{ext}(\vec{r})$ can be expressed as a function of the electron density $\rho(\vec{r})$. They proved that two different external potentials $V_{ext}(\vec{r})$ and $V'_{ext}(\vec{r})$ cannot result in the same $\rho(\vec{r})$. They further proposed that the kinetic energy of the electrons and the inter-electronic repulsion could also be expressed as functionals of $\rho(\vec{r})$. That is, by knowing the ground state density, the Hamiltonian of a many-electron system can be fully determined.

The total energy, given as a functional of the electron density is

$$E[\rho] = T[\rho] + V_{ext}[\rho] + V_{ee}[\rho] \qquad 4.42$$

where the first term is the kinetic energy of the electrons, the second term is the external potential (i.e. the attraction between nuclei and electrons) and the third term is the inter-electronic repulsion. This inter-electronic repulsion can be written as a sum of the Coulomb electrostatic interaction and the non-classical exchange-correlation energy E_{XC}:

$$V_{ee} = \frac{1}{2}\int\int \frac{\rho(\vec{r}_1)\rho(\vec{r}_2)}{r_{12}} d\vec{r}_1 d\vec{r}_2 + E_{XC} \qquad 4.43$$

Equation 4.42 can be re-written as

$$E[\rho] = F_{HK}[\rho] + \int \rho(\vec{r})\, V_{ext}(\vec{r}) d\vec{r} \qquad 4.44$$

where

$$F_{HK}[\rho] = T[\rho] + V_{ee}[\rho] \qquad 4.45$$

It is to be noted that $F_{HK}[\rho]$ is independent of the external potential and is therefore a universal functional, identical for all systems.

The second Hohenberg-Kohn theorem applies the variational theorem to the ground state energy which is a functional of the electron density. It states

The density that minimizes the energy functional is the exact ground state density.

Mathematically, the ground state energy can be obtained by

$$E_0[\rho] = \min \left(F_{HK}[\rho] + \int \rho(\vec{r})\, V_{ext}(\vec{r}) d\vec{r} \right) \quad 4.46$$

It is to be noted that though the Hohenberg-Kohn theorems state that the kinetic energy and the Hamiltonian can be constructed from the electron density, it does not tell us how. Therefore, it is unclear from these theorems what the functional form of $F_{HK}[\rho]$ is. The Kohn-Sham equations published in 1965 address these issues.

4.6.3 Kohn-Sham Equations

The central assertion of the Kohn-Sham scheme[88] is that for a particular ground state density $\rho(\vec{r})$ of a system of interacting particles, there exists a system of non-interacting particles. Calculations are performed on this fictitious system of non-interacting particles to yield the ground state total energy of the system of interest. The total wave function of the system is given by a Slater determinant of independent single electron orbitals ϕ_i, called the Kohn-Sham orbitals. The electron density is given by

$$\rho = \sum_{i=1}^{N} |\phi_i|^2$$

4.47

where $\phi_i = \phi_i(\vec{r})$.

The Hamiltonian for the system can be constructed as follows:

$$\hat{H} = \left[-\frac{1}{2}\nabla^2 + \hat{V}_{eff}(\vec{r})\right] \quad 4.48$$

The first term on the right hand side of this equation is the kinetic energy operator and the second term represents the "effective potential". The effective potential includes the effects from the external potential (i.e. the electron-nucleus interaction), the inter-electronic Coulomb repulsion and the exchange-correlation. The Kohn-Sham wave functions therefore satisfy the equation

$$\left[-\frac{1}{2}\nabla^2 + \hat{V}_{eff}(\vec{r})\right] = \epsilon_i \phi_i \quad 4.49$$

The total energy of the interacting system is given by

$$E_{KS} = T[\rho] + J[\rho] + E_{Ne}[\rho] + E_{XC}[\rho] \quad 4.50$$

where

$$T[\rho] = \sum_{i=1}^{N} \left\langle \phi_i \left| -\frac{1}{2}\nabla^2 \right| \phi_i \right\rangle$$

4.51

which is the exact kinetic energy of the non-interacting system. The Coulomb repulsion can be expressed as

$$J[\rho] = \frac{1}{2}\sum_{i=1}^{N}\sum_{j>i}^{N}\int\int \frac{|\phi_i(\vec{r}_1)|^2|\phi_i(\vec{r}_2)|^2}{r_{12}} d\vec{r}_1 d\vec{r}_2$$

4.52

The nucleus-electron interaction is given by

$$E_{Ne}[\rho] = -\sum_{i=1}^{N}\int\sum_{A=1}^{M}\frac{Z_A}{r_{1A}}|\phi_i(\vec{r}_1)|^2\, d\vec{r}_1$$

4.53

The Kohn-Sham equations are solved self-consistently. An initial density is first chosen and the effective potential is constructed. The solution yields a new initial density. This process is continued till the input and output densities are the same within the precision level desired.

The importance of the Kohn-Sham method is that it converted the many-body problem into an independent particle problem. The exact kinetic energy of the system of non-interacting particles is first calculated and then the contributions from the inter-electronic interactions are estimated as E_{XC}.

It is important to note that the total energy only depends on the electron density $\rho(\vec{r})$ and that except E_{XC}, all energy component of the total energy have explicit functional forms. The approximations that have been made to construct the functional form of E_{XC} will be discussed in the next section. As will be shown, E_{XC} can be expressed as a functional of $\rho(\vec{r})$.

4.6.4 Functionals for Exchange-Correlation

In density functional theory (DFT), the exchange correlation energy E_{XC} is expressed as a function of the electron density. However, it is a difficult task to find the exact functional form of E_{XC}. Therefore, the value of E_{XC} is found out by using approximations. The exchange-correlation energy E_{XC} is better treated by separating it into two terms, one term dealing with the exchange energy E_X and the other term dealing with the correlation energy E_C. Therefore, E_{XC} can be expressed as

$$E_{XC}[\rho] = E_X[\rho] + E_C[\rho] \qquad 4.54$$

E_X and E_C correspond to the Kohn-Sham orbitals given in equation 4.49.

It should be emphasized that the exchange energy is numerically larger than the corresponding correlation energy.

4.6.4.1 The Local Density Approximation (LDA)

The Local Density Approximation is applied to estimate the value of E_X and E_C. Here, it is assumed that the electron density $\rho(\vec{r})$ is a slowly varying function of $\vec{r}$. That is, the electron density is treated locally as a uniform electron gas. Under this approximation, the exchange energy is given as

$$E_X^{LDA} = \int \rho(\vec{r})\epsilon_x d\vec{r} = -\frac{3}{4}\left(\frac{3}{\pi}\right)^{\frac{1}{3}} \int [\rho(\vec{r})]^{\frac{4}{3}} d\vec{r} \qquad 4.55$$

where ϵ_x is the exchange energy per particle given by

$$\epsilon_x = -\frac{3}{4}\left(\frac{3}{\pi}\right)^{\frac{1}{3}}[\rho(\vec{r})]^{\frac{1}{3}} \qquad 4.56$$

For a homogeneous electron gas, the correlation energy E_C cannot be expressed analytically. However, it can be determined to great accuracy by using Quantum Monte Carlo methods. One of the most widely prevalent LDA functionals used for E_C is given by Vosko, Wilk and Nusair, and referred to as the VWN potential.[89]

The advantage of the LDA method is that it is relatively simple and computationally inexpensive. The main disadvantages on the other hand is that this method overestimates bonding (that is, underestimates bond lengths) and underestimates equilibrium volume as well as band gap. Also, the functional cannot describe reaction barriers or calculate total energies correctly. This arises from the issue that the LDA method underestimates exchange energy by about 10% and overestimates correlation energy to be double of the actual value.

4.6.4.2 The Generalized Gradient Approximation (GGA)

The LDA method approximates the energy of the true density by the energy of a local constant density. Therefore, in situations where the density $\rho(\vec{r})$ varies rapidly with $\vec{r}$ such as in molecules), the true energy of the system is poorly represented. To overcome the limitations of LDA, the Generalized Gradient Approximation (GGA) is used. Here, the exchange correlation function E_{XC} is dependent on both the density and the density gradient. Mathematically, the gradient-corrected exchange correlation function can be expressed as

$$E_{XC}^{GGA} = E_{XC}[\rho(\vec{r}), \nabla\rho(\vec{r})] \qquad 4.57$$

There are several functionals that are used for GGA exchange and correlation. Examples include the B88 functional for exchange[90], the LYP functional for correlation and the PW91 functional for exchange and correlation[91]. The gradient-corrected exchange functional proposed by Becke in 1988 termed as B88 is given as

$$E_X^{B88} = E_X^{LDA} + \Delta E_X^{B88} \tag{4.58}$$

where

$$\Delta E_X^{B88} = -\beta \rho^{\frac{1}{3}} \frac{x^2}{1 + 6\beta x \sinh^{-1} x} \tag{4.59}$$

The parameter β is determined from atomic data while

$$x = \frac{|\nabla \rho|}{\rho^{\frac{1}{3}}} \tag{4.60}$$

4.7 The B3LYP Hybrid Functional

In 1993, Becke proposed a gradient corrected exchange functional that combines the exact Hartree-Fock (HF) exchange and the DFT exchange energies[92]. Therefore, this functional is called a hybrid functional. This 3-parameter exchange functional together with the correlation functional proposed by Lee, Yang and Parr[93] is called the B3LYP. The B3LYP hybrid functional can be mathematically expressed as

$$E_{XC}^{B3LYP} = E_X^{LDA} + a_0(E_X^{HF} - E_X^{LDA}) + a_x \Delta E_X^{B88} + E_C^{VWN} + a_c(E_c^{LYP} - E_C^{VWN}) \tag{4.61}$$

where $a_0 = 0.20$; $a_x = 0.72$; $a_c = 0.81$ which are semi-empirical constants obtained by fitting experimental data.

As can be seen, the B3LYP functional is combination of the LDA exchange, HF exchange, Becke's gradient corrected exchange with the Lee-Yang-Parr gradient corrected correlation functionals.

An important thing to point out would be that though hybrid functionals partially account for the electron-electron self-interaction term, effects of this non-physical term is not totally canceled in density functional theory.

4.8 Basis sets

Molecular orbitals are often represented as a Linear Combination of Atomic Orbitals (LCAO) as follows

$$\Psi_i = \sum_{\mu=1}^{N} C_{\mu i}\chi_\mu \qquad 4.62$$

where χ_μ represents a predefined set of basis functions for the μ^{th} orbital and $C_{\mu i}$ are expansion coefficients.

There are two types of basis functions that used in the Kohn-Sham DFT regime of electronic structure calculations. They are the Slater Type Orbitals (STOs)[94] and the Gaussian Type Orbitals (GTOs)[95].

The Slater Type Orbitals decay exponentially with increasing distance from the nucleus and are given by

$$\chi(r,\theta,\phi) = Nr^{n-1}e^{-\zeta r}Y_{l,m}(\theta,\phi) \qquad 4.63$$

where N is a normalization constant, ζ is called the "Slater orbital exponent", (r,θ,ϕ) are spherical co-ordinates and $Y_{l,m}$ represent the conventional spherical harmonics.

One problem with STOs is that there are no radial nodes predicted from the analytical expression. Therefore, to account for radial nodes, atomic orbitals are given as a combination of STOs. When the electron is near the nucleus, they are well-represented by STOs. However, it is substantially computationally expensive to calculate 3 or 4 centered electron integrals in SCF calculations. Therefore, STOs are used mainly for atomic and linear systems.

It was realized by Frank Boys that STOs can be represented as a linear combination of Gaussian orbitals. Since it is relatively easier to calculate integrals (such as overlap integral and so on) using Gaussian orbitals, the Gaussian Type Orbitals (GTOs) are widely used today. GTOs can be expressed as

$$\chi(x,y,z) = Nx^{l_x}y^{l_y}z^{l_z}e^{-\zeta r^2} \qquad 4.64$$

where l_x, l_y, l_z are the angular part of the orbitals and ζ represents the radial part of the function. The main drawback of GTOs is that a zero slope is obtained near the nucleus, instead of a cusp.

In general it takes about three times as many GTOs as STOs to achieve a particular degree of accuracy. Therefore, a number of GTOs are combined to form one contracted Gaussian function (CGF). The simplest basis sets have only one basis function (or one contracted function in case of CGF) to represent each atomic orbital and are therefore called minimal basis sets. One of the most widely used minimal basis sets is the STO-nG basis set which is constructed by a linear

combination of n primitive GTO functions.[96] For example, the STO-3G basis set is made of 3 GTO functions. In higher basis sets, called double-zeta basis sets, two functions are used for each atomic orbital. Now, given that only the valence electrons are involved in bonding, the core electrons can be treated by minimal basis sets while the valence electrons can be represented by double/triple/quadruple zeta basis sets. Such kind of basis sets developed by Pople and coworkers are called split valence basis sets.[97,98] They are represented as X-YZG (for double-zeta basis sets). This means that X primitive GTOs are used to represent each of the core electrons and the outer electrons are each represented by two basis functions each consisting of Z and Y primitive GTOs, respectively. For example, in the 6-311G basis, 6 primitive GTOs make up each of the core orbitals and the valence orbitals are represented by 3 basis functions each of which is composed of 3, 1 and 1 gaussian functions, respectively. Polarization functions (represented as *) and diffuse functions (represented as +) are added to improve basis sets. The former allows flexibility for atoms to form chemical bonds while the latter helps to improve the predicted properties of systems with diffuse electron density such as anions.

The inert core electrons of atoms heavier than krypton (such as gold) are often modeled by an effective core potential (ECP) called a pseudopotential. The pseudopotential is called relativistic if relativistic effects have been incorporated into it. For example, the Stuttgart pseudopotential (SDD) is a common relativistic pseudopotential used for gold.[99,100]

4.9 Computational Methodology

In this work, structural, electronic and spectroscopic properties of clusters, specifically superhalogens, have been studied using density functional theory and the B3LYP hybrid

functional[92,93] for exchange-correlation. Different basis sets have been chosen depending on the system under investigation. The choice was based on earlier literature available for similar systems that gave reliable results in good agreement with experiments.

We used the 6-311++G** basis set[97,98] for Li, Na, K, B, and H, and the Stuttgart pseudopotential[99,100] SDD for Rb and Cs in sections 5.1 and 6.1 . In section 5.2 we used the 6-311+G* basis set for C and N while using the Stuttgart pseudopotential SDD basis set for Au. In section 6.2 we used the 6-311+G* basis set for Zn, F, B and O and the Stuttgart pseudopotential SDD for Au.

In all cases, the structures were optimized to find out geometry and the corresponding total energies were calculated. These energies were utilized to compute the vertical detachment energies (VDE) and the adiabatic detachment energies (ADE) of the clusters. Detailed description and definitions of VDE and ADE are given in section 5.2.2 To find out the lowest energy geometry, several initial geometries were chosen and then their structures were optimized. The convergence in the total energy and force were set at $1x10^{-6}$ eV and $1x10^{-2}$ eV/Å, respectively. The dynamical stability of the clusters was confirmed by carrying out frequency calculations which were all found to be positive. In addition, Natural Bond Orbital (NBO) analysis was performed to give an indication of the nature of bonding involved in the clusters.

All calculations were performed using the Gaussian 03 and Gaussian 09 softwares.[101,102]

Chapter 5 Design of Unconventional Superhalogens

5.1 Borane-based Superhalogens

5.1.1 Introduction

Boranes belong to a class of compounds with rich chemistry. Boranes and their derivatives, created by replacing B with C (carboranes), B with metal atoms (metalloboranes), and H with halogens (F and Cl) have far reaching applications. They are used in boron neutron capture therapy,[103-107] pharmaceuticals,[108] and as ligands in the synthesis of unusual coordination compounds.[109] They are also useful as superacids,[110] weakly coordinating anions[111] and potential candidates for hydrogen storage.[112-114] Larger boranes form polyhedral complexes and exist as highly stable anions. To realize the full potential of this class of compounds a fundamental understanding of the stability of boranes and how they can be tuned by tailoring size and substitution is important. In this section we focus on the stability of the *closo*-boranes and show that by using simple electron counting rules one can choose the appropriate size and substituent to render boranes not only enhanced stability but also high electron affinity far exceeding the value of any halogen atom.

The stability of *closo*-boranes ($B_nH_n^{2-}$),[115] is governed by the Wade-Mingos rule[49-52] which states that in polyhedral borane clusters with n vertices (n+1) pairs of electrons are needed for cage

bonding. Here, the H atoms are radially bonded to the B atoms and two of the four electrons of the BH pair are tied up in n covalent bonds. This leaves 2n electrons of a B_nH_n polyhedral cluster for cage bonding. Since (2n+2) or (n+1) pairs of electrons are needed for stability, the dianions of B_nH_n are stable. This rule has recently been used for the focused discovery of numerous Al-H clusters with potential applications in hydrogen storage.[116]

Here, we show that an entirely new class of superhalogens can be created by using the Wade-Mingos rule without the benefit of either a metal or a halogen atom. To demonstrate the power of this rule we concentrate on replacing B with C or adding an extra H or alkali metal atom to the well known $B_{12}H_{12}$ cluster, thus opening the door to a vast list of rationally designed stable borane derivatives. This finding also extends the pool of highly electronegative ions which play an important role in chemical industry.

5.1.2 Results and Discussion

A conventional superhalogen has the formula MX_{n+1} where n is the maximal valence of the metal atom M and X represents a halogen atom.[8] The electron affinities of MX_{n+1} clusters are larger than those of X atoms since the extra electron is distributed over (n+1) X atoms. However, our prime target is to demonstrate that Wade-Mingos rule can also be used to predict new superhalogens. We show this by performing a systematic study based on density functional theory, focusing on borane derivatives. We note that while $B_nH_n^{2-}$ clusters for $n \leq 11$ are unstable against auto ejection of the second electron,[117,118] $B_{12}H_{12}^{2-}$ is stable. In other words, the total energy of $B_{12}H_{12}^{2-}$ is lower than that of $B_{12}H_{12}^{-}$. When one hydrogen atom is added to $B_{12}H_{12}$, this can only bind on the bridge site forming a 2-electron 3-center bond or cap a polar face of the

cluster forming a 2-electron 4-center bond. In either case, the electron associated with this extra hydrogen atom would be contributed to the cage bonding. Since $B_{12}H_{13}$ cluster is isoelectronic with $B_{12}H_{12}^-$ it would require only one electron to satisfy the Wade-Mingos rule for stability. Consequently, the electron affinity of $B_{12}H_{13}$ cluster should be higher than that of a halogen atom, making it a candidate for a superhalogen. Similarly, consider the case of carboranes. These are created by replacing one or more of the B atoms with C. For example, it is legitimate to expect that $CB_{11}H_{12}$ which is isoelectronic with $B_{12}H_{13}$, may also be a superhalogen. One can also imagine that $M(B_{12}H_{12})$ (M=Li, Na, K, Rb, Cs) clusters could be superhalogens since they are isoelectronic with $CB_{11}H_{12}$. However, there is a difference between $CB_{11}H_{12}$ and $MB_{12}H_{12}$. In the former, C replaces a B atom in the $B_{12}H_{12}$ polyhedron while in the latter, the alkali metal atom would donate an electron to the $B_{12}H_{12}$ moiety. Note that unlike conventional superhalogens where an alkali atom needs at least two halogen atoms, here only one $B_{12}H_{12}$ moiety will be sufficient.

To prove the above hypotheses we have carried out calculations using density functional theory and hybrid B3LYP functional for exchange-correlation.[92,93] The predictive power of this theoretical method has already been demonstrated in previous publications.[25,72] The electron affinities predicted are in good agreement with experiment. This method also compares well with coupled cluster calculations. For example, the EA of MnF calculated at the B3LYP/6-311+G (3df basis) level of theory is 1.34 eV which agrees well with the 1.13 eV value calculated at the RCCSD(T)/5-zeta basis.[119] Moreover, in case of 4d and 5d transition metal atoms, it is found that density functional theory (using B3LYP) gives better performance than CCSD(T) in predicting electron affinities.[120]

In Figure 3, we show the geometries of neutral and anionic $B_{12}H_{12}$, $B_{12}H_{13}$, $CB_{11}H_{12}$, and $Na(B_{12}H_{12})$ clusters. The geometry of $B_{12}H_{12}^-$ in Figure 3 (b) has D_{3d} symmetry with B-B bond lengths ranging from 1.73 to 1.82 Å and all B-H bond lengths are around 1.19 Å. However, when the extra electron is removed, the neutral $B_{12}H_{12}$ cluster (Figure 3 (a)) undergoes significant structural distortion with two of the B-B bonds stretched to 2.00 Å and one of the H atoms bound to two B atoms instead of radially bonding to only one B atom. This, as will be discussed later, is reflected in the large difference between the electron affinity and vertical detachment energy of the $B_{12}H_{12}$ cluster. The geometries of neutral and anionic $B_{12}H_{13}$ clusters given in Figure 3 (c) and (d) are rather similar with only small differences in B-B bond lengths. They range from 1.75 to 1.97 Å in the neutral cluster and 1.76 to 1.96Å in the anionic cluster. In both the structures the 13^{th} H atom is bonded on the face. When this H atom was placed on the bridge site, it moved readily to the surface site during optimization, indicating that the energy barrier is very small. These results are in agreement with previous calculations.[118] The effect of the H atom capping a surface site will be apparent later when we discuss the electronic structure of these clusters.

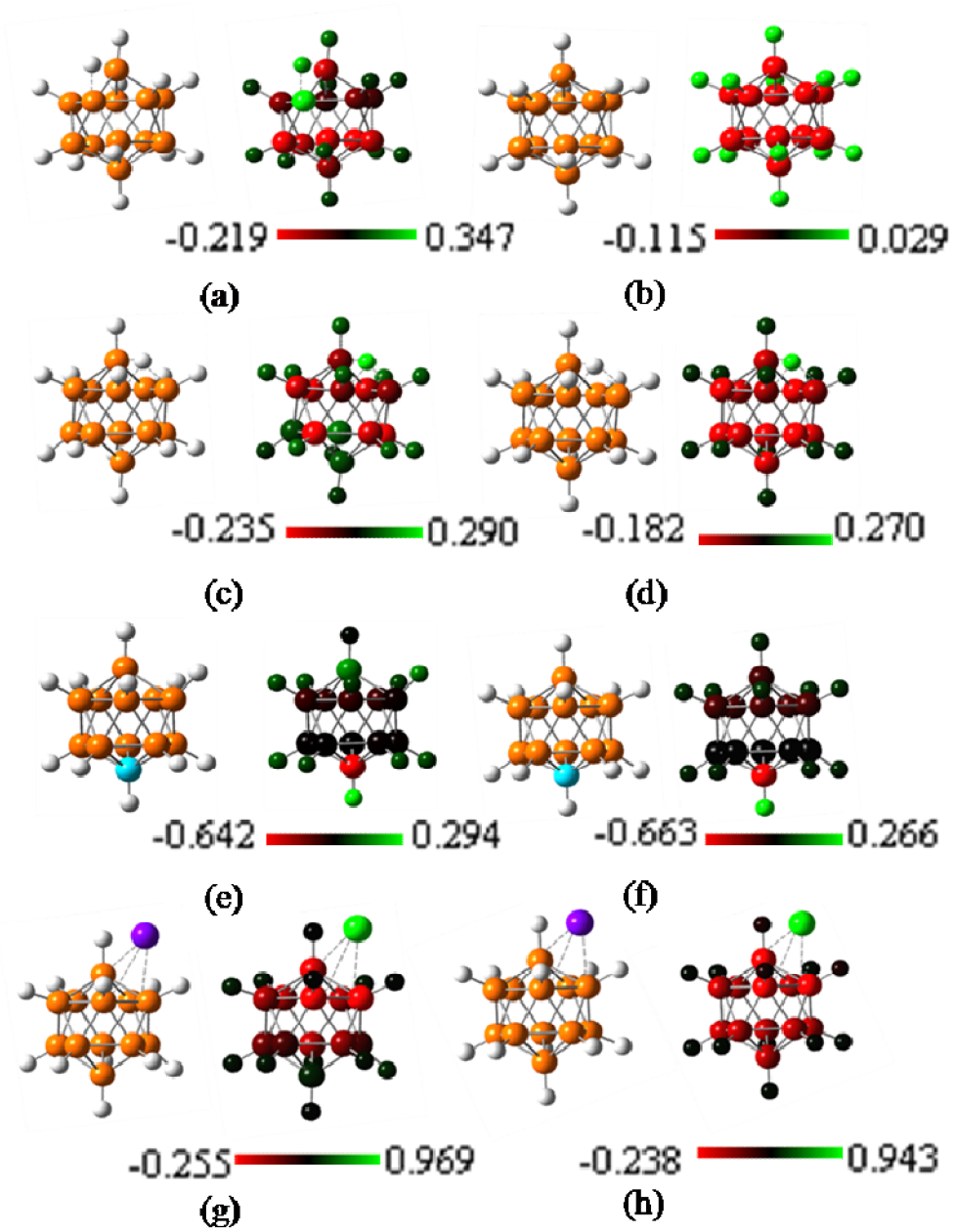

Figure 3. Geometries (left) and NBO charge distributions (right) of (a) $B_{12}H_{12}$, (b) $B_{12}H_{12}^-$, (c) $B_{12}H_{13}$, (d) $B_{12}H_{13}^-$, (e) $CB_{11}H_{12}$, (f) $CB_{11}H_{12}^-$, (g) $Na(B_{12}H_{13})$ and (h) $Na(B_{12}H_{13})^-$

The geometries of neutral and anionic $CB_{11}H_{12}$ clusters are given in Figure 3 (e) and (f) respectively. The anion is slightly more symmetric (C_5 symmetry) than the neutral (C_1 symmetry). The nearest C-B distances in neutral and anionic $CB_{11}H_{12}$ clusters are respectively

1.70 Å and 1.71 Å. Both the structures have icosahedric form. The geometries of all M($B_{12}H_{12}$) (M=Li, ,Na, K, Rb, and Cs) clusters are similar except the distance between the alkali metal atom and the nearest B atom. Therefore, we present in Figure 3 (g) and (h) only the geometries of neutral and anionic Na($B_{12}H_{12}$). The distances between alkali metal atoms Li, Na, K, Rb, and Cs and the nearest B atom are, respectively, 2.20, 2.60, 2.99, 3.24 and 3.42 Å for neutrals and 2.14, 2.52, 2.89, 3.12 and 3.28 Å for the anions. We note that the distances in anions are consistently smaller than those in the neutral clusters indicating that the bonding becomes stronger as an electron is attached. From the NBO charge distributions displayed in Figure 3 we see that, compared to the neutrals, the negative charge is more evenly distributed in the anions. In $B_{12}H_{12}^-$ the negative charge rests evenly on all the B atoms and H atoms remain mostly charge neutral. This is to be expected as the bonding between radial H atom and B atom is covalent. In $B_{12}H_{13}^-$ cluster which is isoelectronic with $B_{12}H_{12}^{2-}$, the 13th H atom carries a positive charge of +0.270. This small charge donation makes the charge on the B and H atoms in $B_{12}H_{13}^-$ more uniform than that in neutral $B_{12}H_{13}$. When a C atom is substituted for the B atom, the charge on the C atom in $CB_{11}H_{12}$ is -0.642. This is consistent with the fact that the electronegativity of C is larger than that of B. There are three kinds of B atoms in terms of their charge; those forming the pentagon closest to the C atom carry an average charge of -0.014/atom while those in the upper pentagon carry a charge of -0.117/atom. The B atom at the apex, however, carries a charge of +0.150. In the corresponding anion cluster the B atoms in the lower pentagon carry a charge of -0.002/atom while those in the upper pentagon carry a charge of -0.166/atom. The apical B has a charge of -0.141. We also note that the geometries of the $B_{12}H_{12}$ cage in neutral and anionic Na($B_{12}H_{12}$) clusters are very similar to those in corresponding $B_{12}H_{13}$ cluster. This implies that the added hydrogen and alkali metal atoms behave in a similar manner, namely the electron donated by

these atoms is uniformly distributed over the remaining atoms. However, the charges on Li, Na, Rb, K, and Cs in both neutral and anionic $M(B_{12}H_{12})$ clusters are close to +1 while the charge on the 13^{th} H atom in neutral and anionic $B_{12}H_{13}$ is +0.290 and +0.270, respectively.

To further probe the effect of electron delocalization in the anions, we have calculated the electron affinities (EA) and vertical detachment energies (VDE) of these clusters (see Table 1). The former is calculated from the energy difference between the ground states of the anion and neutral while the later is calculated from the energy difference between the anion ground state and the neutral at the anion geometry. The difference between the EA and VDE, therefore, provides a measure of the relaxation the cluster undergoes when the electron is photo-detached from the anion. We note that $B_{12}H_{12}$ is already a superhalogen with electron affinity of 4.56 eV. The VDE of $B_{12}H_{12}$ is 1.2 eV larger than that of its EA. This is a consequence of the large geometry change the anion undergoes when the extra electron is removed. The difference between the EA and VDE of the remaining clusters ($B_{12}H_{13}$, $CB_{11}H_{12}$ and $MB_{12}H_{12}$) is between 0.4 to 0.5 eV. Although these are significantly smaller than the difference noted in $B_{12}H_{12}$, they represent structural distortion suffered by these clusters following electron detachment. The important point we wish to make is that all these clusters are superhalogens. Further, electron affinities decrease with increasing size of the alkali atom, a characteristic that can be related to the strength of bonding.

Table 1. Electron affinities (EA) and Vertical Detachment Energies (VDE) of superhalogen clusters of $B_{12}H_{12}$, $B_{12}H_{13}$, $CB_{11}H_{12}$, and $M(B_{12}H_{12})$ for (M=Li, Na, K, Rb, Cs).

Cluster	EA (eV)	VDE (eV)
$B_{12}H_{12}$	4.56	5.75
$B_{12}H_{13}$	5.42	5.92
$CB_{11}H_{12}$	5.39	5.82
$Li(B_{12}H_{12})$	4.75	5.19
$Na(B_{12}H_{12})$	4.43	4.92
$K(B_{12}H_{12})$	4.21	4.66
$Rb(B_{12}H_{12})$	4.01	4.44
$Cs(B_{12}H_{12})$	3.92	4.36

Note that $B_{12}H_{13}$ and $CB_{11}H_{12}$ do not possess a single metal atom or a halogen, yet these have electron affinities larger than those of halogen atoms. We recall that BO_2 which does not possess either a metal atom or a halogen atom is also a superhalogen with an electron affinity of 4.46 eV.[71] However, this superhalogen property arises due to the octet rule as BO_2^- is isoelectronic with CO_2. Furthermore, O is far more electronegative than H. The underlying reason for the stability of all the anions we have studied here is that this class of clusters needs an extra electron for cage bonding to satisfy the Wade-Mingos rule.

5.1.3 Conclusions

In summary, we have shown that Wade-Mingos rule provides another window for the design and synthesis of a new class of superhalogens with exceptionally high electron affinities. Equally important, we also show that it is not necessary for a molecule to contain either a metal atom or a halogen atom to be a superhalogen. Moreover, whereas at least two halogen ligands are required in a conventional superhalogen, here one borane moiety by itself is a superhalogen. Many borane and carborane derivatives with high electron affinities can be formed.

5.2 Pseudohalogen-based Superhalogens

5.2.1 Introduction

In this section, we consider a different class of electronegative moieties, called pseudohalogens, as building blocks of superhalogens. Like halogens, these molecules also need one electron to close their electronic shell, and form very stable singly charged negative ions. Thus, they mimic the chemistry of halogens.[121] Pseudohalides are composed of two or more atoms and the nature of bonding between these atoms is not affected in chemical reactions where they resemble halogens. Typical examples of such moieties include CN, NCO, SCN, N_3 etc. Due to the similarity in chemical reactivity with halogens, it can be expected that pseudohalogens can also be used as building blocks of superhalogens. In a recent paper, Smuczynska and Skurski have shown that Li, Na, Be, Mg, Ca, B, and Al can be used as core atoms to form superhalogens with pseudohalogens as building blocks.[77]

In our work, we have performed a systematic study of $Au(CN)_n$ complexes where n=1 to 6 and calculated their equilibrium structure, nature of bonding, and spectroscopic properties. We have chosen gold since it is a noble metal and because of the aurophilic interaction its chemistry is of interest to a vast range of disciplines. Moreover, gold has a high electronegativity and can have a range of oxidation states from -1 to +5, the +1 and +3 states being the most widely prevalent.[122] The oxidation state of +6, however, is highly debated. Though Au has an oxidation state of +6 in AuF_6 neutral, some argue that it will either soon transform to AuF_6^- due to its large electron affinity or dissociate. We chose to study the interaction of CN (EA 3.82 eV)[123] with Au since cyanide is the simplest pseudohalogen and gold cyanides have an extensive chemistry. In fact,

cyanidation is one of the major methods for extraction of gold from its ore in the form of water soluble $Au(CN)_2^-$ complex.[124] Gold cyanides are also used in electroplating.[125] The objectives of this work are twofold. First we demonstrate that noble metals like Au can also form superhalogens when decorated by CN ligands. Second, we study the extent to which the CN ligand mimics the halogen ligands with respect to its interaction with Au in forming superhalogens. For the first phase, we have done extensive calculations using density functional theory, and for the second we have compared our data with those available for AuF_n complexes,[25] which are traditional superhalogens.

5.2.2 Computational Methods

The total energies and geometries of the low lying isomers of both anions and corresponding neutral clusters were calculated using density functional theory (DFT) with hybrid functional B3LYP for exchange-correlation potential.[92,93] To find the global minimum structure we have considered several initial geometries by attaching Au to N or C atom of CN as well as allowing CN molecules to cluster. In all cases, the structures were optimized within the given symmetry.

The calculated energies of the optimized clusters are used to probe their spectroscopic properties. These results can be compared with photoelectron spectroscopy (PES) experiment. The vertical detachment energy (VDE) is the electron binding energy (EBE) corresponding to optimal Franck-Condon (FC) overlap between the ground state of the anion and the corresponding neutral at the structure of that anion, i.e., straight up or vertically from the anion's ground state. For an electronic transition, the VDE is taken as the EBE of the peak of that transition, i.e., the maximum FC overlap of the anion's and neutral's wave functions producing a maximum in

electron intensity. Theoretically, it is calculated as the energy difference between the lowest energy isomer of the anion and its neutral at this anion geometry. The adiabatic electron affinity (EA), on the other hand, is the energy difference between the ground vibronic state of the lowest energy anion isomer and that of the corresponding lowest energy neutral isomer. It is the thermodynamic EA. With vibrational spectral structure and an assignment, one can identify the transition in the vibronic envelope that corresponds to the EA. Without it, one is left to estimate its location near the low EBE side of the ground anion to ground neutral transition. With no vibrational hot bands, it is at the threshold, but the problem is that there are often some hot bands. The problem gets further complicated if the anion possesses energetically nearly degenerate isomers and/or if the geometries of the lowest energy anion and the lowest energy neutral isomers are very different. In the latter case, the neutral resulting from the photodetached anion will be in an electronically excited state. Its geometric structure may not be that of the geometric neutral isomer. What the experiment will then measure is not the EA, but what we term as the adiabatic detachment energy (ADE). We define this ADE as the transition energy from the ground vibronic state of an anion to the ground vibronic state of the structurally similar neutral isomer. This is calculated by optimizing the neutral geometry by starting with the geometry of the ground state of the anion isomer. The resulting neutral structure clearly belongs to one of the local minima on the potential energy surface. The geometry of the lowest energy neutral isomer, as mentioned before, is determined by starting from different initial structures and optimizing the geometry. This indeed is one of the hardest quantities to calculate since there may be numerous local minima on the potential energy surface. Several techniques such as genetic algorithm and basin hopping methods have been developed to make this task easier. However, geometries lying within 0.2 eV of each other are often referred to as nearly degenerate

as this is beyond the accuracies of current computations. We will illustrate the distinction between EA and ADE in the following.

5.2.3 Results and Discussions

5.2.3.1 $Au(CN)_n$ (n=1-6) Superhalogens

First we have considered the dissociative attachment of CN ligands with Au, that is, attachment of CN without association into $(CN)_n$. Since CN is a well known ambident ligand, it can attach with gold in two possible ways. It can either form gold cyanide clusters in which C atom of CN is bonded with Au (AuCN) or it can form gold isocyanide cluster where the N end of CN is bonded with Au (AuNC). For all the cases studied, we have found that gold cyanides (AuCN) are lower in energy than their isomeric gold isocyanide clusters (AuNC). All these structures are similar in geometry to the corresponding AuF_n clusters.[25] Furthermore, analogous to AuF_n clusters, $Au(CN)_n$ clusters have lowest energy for minimum spin multiplicities, i.e. species with odd number of electrons prefer to be doublet while species with even number of electrons prefer to be singlet. This is expected since CN^- is known to be a strong field ligand according to the spectrochemical series.[126]

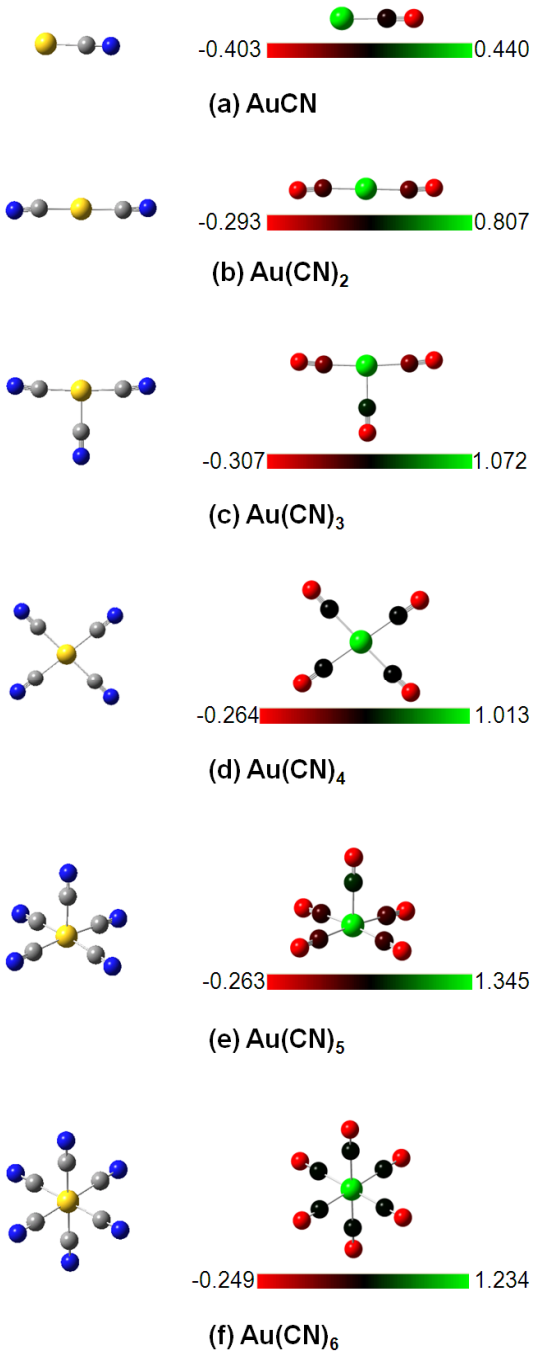

Figure 4. Optimized structures (left) and natural bond orbital (NBO) charge distribution (right) of $Au(CN)_n$ neutral complexes.
Yellow represents Au, blue represents N and grey represents C.

In Figure 4, we present the geometries and charge distributions of neutral $Au(CN)_n$ clusters. The Au-C bond length lies between 1.94 Å and 2.05 Å. The C-N bond length is about 1.16 Å in each

case which is same as that in a free CN moiety. This means that the nature of the C-N bond is not affected when the CN ligand binds with Au as should be the case for a true pseudohalogen. AuCN is linear. $Au(CN)_2$ is pseudolinear and slightly trans in geometry, the Au-C-N angle being about 175˚ and the C-Au-C angle being about 180˚. The Au-C bond lengths are 1.99 Å. An earlier calculation at the PW91/TZ2P level using density functional theory indicates that neutral $Au(CN)_2$ is linear.[127] When we forced the molecule to be linear, the total energy of the molecule was 0.09 eV greater. This is within the errors associated with DFT level theories. However, it is known that different levels of theory may result in different optimized structures. $Au(CN)_3$ is T-shaped with C_{2v} symmetry where all the Au-C bonds are not equivalent. The Au-C bond length between the Au atom and the CN ligands which form the head of the T is about 2.01 Å whereas, the Au-C bond length for the CN ligand attached perpendicular to the head is 1.94 Å signifying that this bond is stronger. $Au(CN)_4$ is planar with a D_{2h} symmetry and all bond lengths are about 2.02 Å. One pair of C-Au-C angle is about 80˚ while the other pair is about 100˚. $Au(CN)_5$ has C_{4v} symmetry. Here, four of the CN ligands lie in the same plane as Au and one CN ligand is perpendicular to this plane. As in case of $Au(CN)_3$, there are two kinds of Au-C bonds. The Au-C bonds between the Au and the CN in the same plane are all equivalent and about 2.03 Å whereas the remaining Au-C bond length is 1.98 Å. $Au(CN)_6$ has D_{3d} symmetry and all the Au-C bonds are equivalent with a bond length of 2.05 Å. As indicated in section 5.2.2, we have used tolerance level of 0.1 in assigning cluster symmetry. Note that this assignment may vary depending upon the tolerance level chosen. For example, if this tolerance level is increased to 0.6, the symmetries of $Au(CN)_4$ and $Au(CN)_6$ are respectively D_{4h} and O_h.

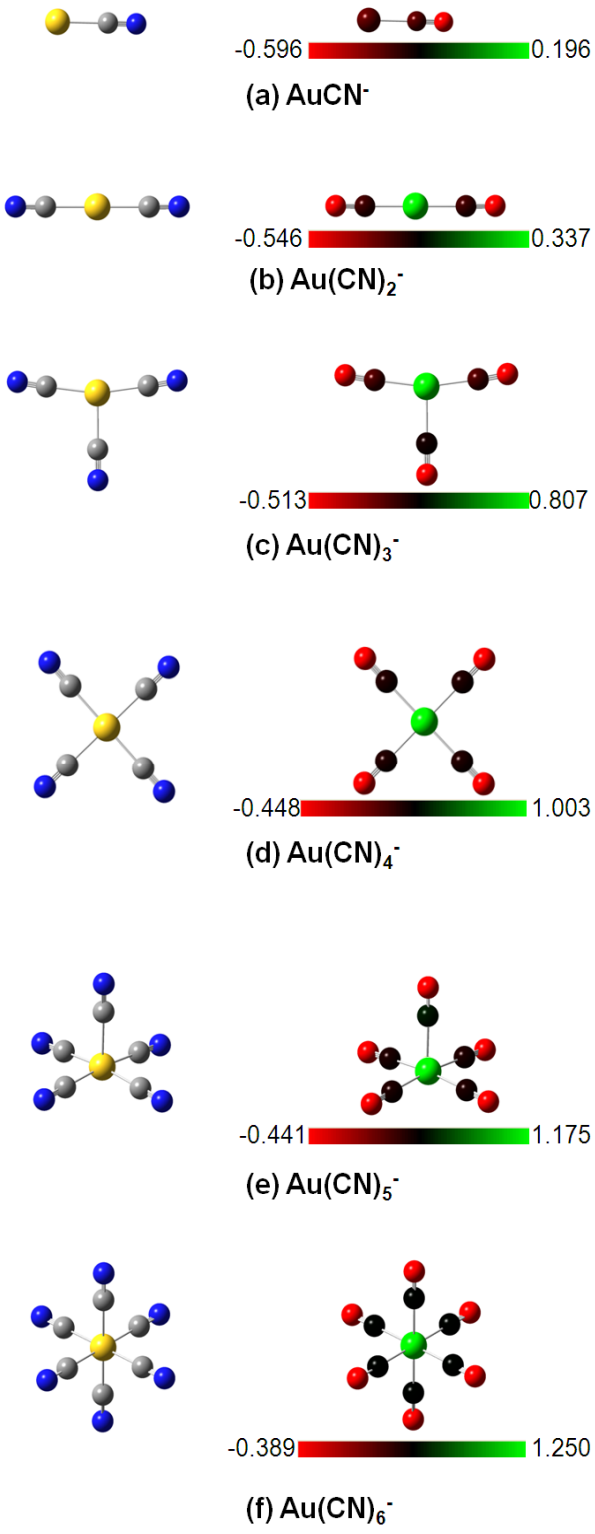

Figure 5. Optimized structures (left) and NBO charge distribution (right) of $Au(CN)_n^-$ complexes

The anionic clusters shown in Figure 5 have similar geometry as that of the neutrals. This is reflected in the small difference between the calculated vertical detachment energies (VDE) and the adiabatic detachment energies (ADE) as discussed below. The average C-N bond distance is 1.16 Å as in the case of the neutrals. However, the Au-C distances are slightly longer compared to those in the neutrals and lie between 2.02 Å and 2.26 Å. The symmetries of $Au(CN)_n$ are C_{infv}, D_{infh}, C_{2v}, D_{4h}, C_{4v} and C_{4h} for n=1 to 6, respectively. These are the lowest energy structures for dissociative attachment of CN.

Table 2. Theoretical and experimental ADE and VDE of $Au(CN)_n$ complexes for dissociative attachment of CN ligands.

Complex	ADE (eV)		VDE (eV)	
	Theo	**Expt**	**Theo**	**Expt**
AuCN	2.12	2.07[128]	2.25	2.19[128]
$Au(CN)_2$	6.08	6.09[127]	6.10	6.09[127]
$Au(CN)_3$	5.07	-	5.44	-
$Au(CN)_4$	7.61	-	7.95	-
$Au(CN)_5$	7.02	-	7.45	-
$Au(CN)_6$	8.40	-	8.48	-

The adiabatic detachment energies (ADE) and vertical detachment energies (VDE) of the complexes were computed. ADE provides a measure of the stability of the anion over the neutral and its electron accepting capacity. The ADE and the VDE values are given above in Table 2 and compared with available experimental data. Note that the ADE of $Au(CN)_2$ is almost a factor of 3 larger than that of AuCN and a factor 2 larger than that of Cl. Hence, it is a superhalogen. These results are in excellent agreement with previous theoretical and experimental data.[127] The ADEs of clusters for $n \geq 3$ are more than twice the electron affinity of Cl and reach values as high as 8.4 eV in $Au(CN)_6$. This indicates that these $Au(CN)_n$ complexes are indeed

superhalogens. We also note that Smuczynska and Skurski recently studied $Na(CN)_2$, $Mg(CN)_3$, and $Al(CN)_4$ and found these to be superhalogens as well.[77]

The difference between the ADE and VDE is a measure of the geometry change of the anion when the electron is removed. The small magnitude of this (between 0.02 eV and 0.43 eV) signifies that the neutrals and anions studied here are analogous in symmetry and structure as is evidenced from Figure 4 and Figure 5.

From the above data we observe that very high ADEs, much higher than that of Cl, are obtained. These values are comparable with those of corresponding AuF_n complexes (2.46 eV to 8.38 eV for n=1 to 6).[25] We further notice that there is an odd-even alternation in the electron affinities. When n is odd, the ADE is low and when n is even the ADE is high. The explanation is simple. For odd n, the neutrals have even number of electrons and closed shell. Thus, the ADE is comparatively small when an extra electron is added. When n is even, the neutrals have odd number of electrons and open shell. Since their anions have even number of electrons and closed shell, energies are lowered when the electron is attached. This increases their ADE values.

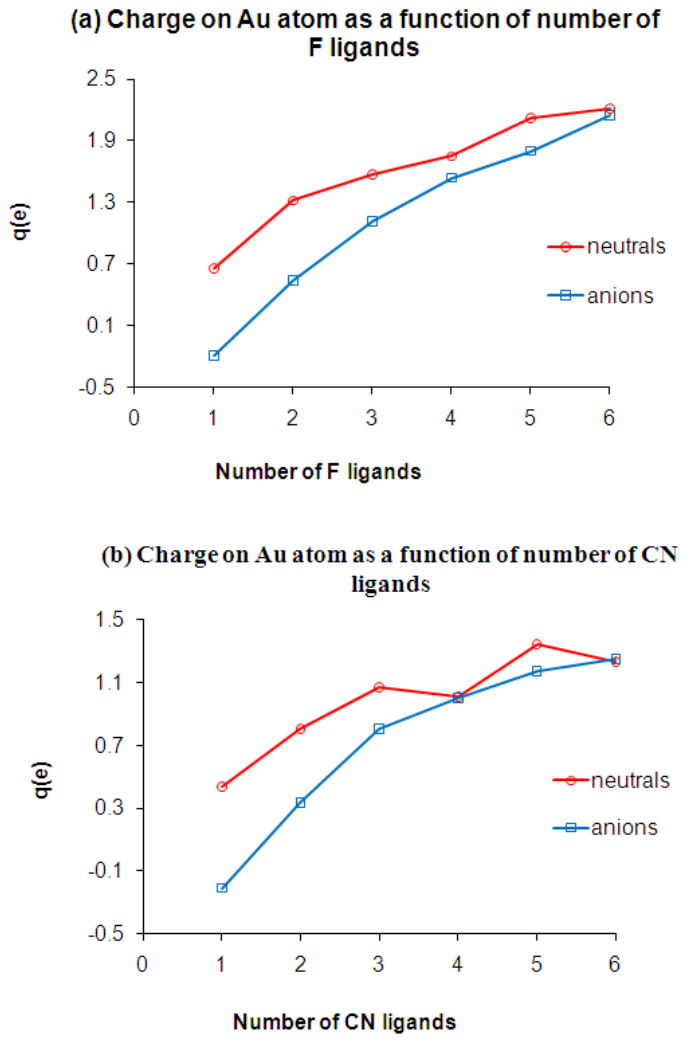

Figure 6. NBO charge on Au in (a) AuF_n and (b) $Au(CN)_n$ complexes

To understand the nature of bonding we also calculated the NBO charges [q(e)] on the Au atom in both the neutral and the anionic structures (see Figure 4 and Figure 5). The results are plotted in Figure 6 and compared with that in AuF_n clusters. As we can see, gold is positively charged in all the neutral clusters and all the anionic clusters except in $AuCN^-$. CN, due to its high electron affinity, withdraws electron density from Au, thus rendering it a positive charge in the clusters. However, AuCN is a small closed shell molecule. Thus, on addition, the extra electron in $AuCN^-$ is delocalized over all the three atoms. This process is further facilitated since Au, though a

metal, has quite a high electronegativity. In fact, the closed shell nature of AuCN explains why its ADE is low. The charge on the Au atom increases with the number of ligands in both the neutral and anionic clusters. However, the difference between the charges gets smaller as the number of ligand atoms increases and becomes vanishingly small at n=4. This is to be expected when one considers the oxidation state of Au to be +3. In $Au(CN)_4^-$, the extra electron is distributed over the CN moieties and hence charge on Au is same as that in neutral $Au(CN)_4$. The charge distribution in $Au(CN)_n$ compares well with that in AuF_n, although the magnitudes are different. This shows that as long as CN moieties are bound to Au dissociatively, the pseudohalogen behaves like a halogen. Moreover, we see that the charges on Au are greater when F is attached than when CN is attached. It should also be mentioned that the small NBO charges on Au in AuCN and $Au(CN)_2^-$ establishes the covalent nature of the Au-C bond corroborating earlier experimental work.[127,128]

5.2.3.2 Stability with respect to fragmentation

Since all the molecules studied above have no imaginary frequencies, they at least belong to minima on the potential energy surface. However, to test their stability against fragmentation, we have considered several dissociation pathways of structures given in Figure 4 and Figure 5. Here, the neutral clusters can fragment by ejecting a CN or $(CN)_2$. In the case of anions, we also have to consider whether the charge is carried by the CN or the $Au(CN)_n$ moiety. In Table 3, we list the dissociation energies corresponding to the most thermodynamically preferred channel. When dissociation energy is positive, fragmentation will be endothermic implying that the parent cluster is stable. Both AuCN and $AuCN^-$ are stable. However, $Au(CN)_n$ complexes are unstable with respect to dissociation for n>1 in case of neutrals and n>3 in case of anions. This is in stark

contrast with AuF_n complexes which are stable with respect to dissociation up to n=5 for neutrals and n=6 for anions.[25] This difference arises because of the difference in the F-F bond energy in F_2 molecule and C-C bond energy in cyanogen gas (NCCN). The binding energy of $(CN)_2$ (NCCN), namely 5.84 eV,[123] is about 3.5 times the binding energy of F_2, namely 1.82 eV.[129] Moreover the Au-F bond energy (2.65 eV)[25] > F-F bond energy (1.82 eV) whereas, the Au-CN bond energy (3.65 eV) < NC-CN bond energy (5.84 eV). Hence, CN would preferentially bind to itself than with Au whereas F would preferentially bind to Au than with itself. Similarly $Au(CN)_n^-$ are less stable against fragmentation than corresponding AuF_n^-.

Table 3. Fragmentation energies for neutral and anionic $Au(CN)_n$ clusters

Complex (A)	Preferred fragmentation product (B)	Fragmentation energy/eV (Energy of B-A)
AuCN	Au+CN	3.65
$AuCN^-$	$Au+CN^-$	1.70
$Au(CN)_2$	$Au+(CN)_2$	-0.49
$Au(CN)_2^-$	$Au^-+(CN)_2$	3.39
$Au(CN)_3$	$AuCN+(CN)_2$	-1.42
$Au(CN)_3^-$	$AuCN^-+(CN)_2$	1.53
$Au(CN)_4$	$Au+2(CN)_2$	-2.44
$Au(CN)_4^-$	$Au(CN)_2^-+(CN)_2$	-0.42
$Au(CN)_5$	$AuCN+2(CN)_2$	-5.02
$Au(CN)_5^-$	$Au(CN)_3^-+(CN)_2$	-1.65
$Au(CN)_6$	$Au+3(CN)_2$	-6.32
$Au(CN)_6^-$	$Au(CN)_2^-+2(CN)_2$	-3.50

This brings us to examine the case of $Au(CN)_2$ more closely. We note from Table 3 that while neutral $Au(CN)_2$ is unstable and fragments to Au and NCCN, its anionic counterpart is stable. The question then arises: What prevents the neutral following electron detachment of the anion to remain in the metastable state? To gain further insight we have calculated the energy barrier

between the metastable and dissociated lower energy state by keeping the C-Au-C fixed at a particular angle and optimizing all other parameters. Partial geometry optimizations were carried out by varying the ∠C-Au-C angle from 30º to 180˚ in 10º increments. This simple procedure gave us the potential energy diagram for fragmentation (Figure 7). We also calculated the structure and energy of the transition state. The difference in the energy of the TS and $Au(CN)_2$ gave the barrier height. This energy barrier is 1.86 eV which is substantial indicating that though $Au(CN)_2$ is metastable, it has a long lifetime. In this connection, it should also be mentioned that fragmentation through other pathways such as $Au(CN)_2 \rightarrow AuCN+CN$ are thermodynamically unlikely, as in this case the energy of the fragmented products is 2.12 eV higher than that of $Au(CN)_2$. This is even higher than the energy barrier for fragmentation into $Au+(CN)_2$.

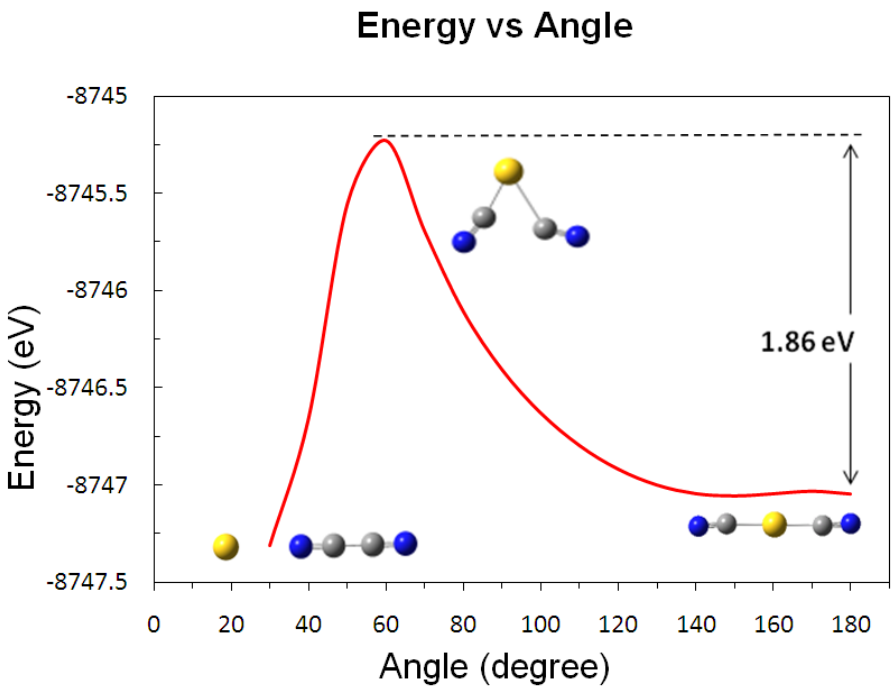

Figure 7. Calculation of energy barrier for the fragmentation of $Au(CN)_2$ to Au and $(CN)_2$

Note that Wang et al.[127] probed the nature of bonding in $Au(CN)_2^-$ using PES and found the spectrum to be quite narrow indicating that the anion and neutral have similar geometries. We want to emphasize that what Wang et al. measured is the adiabatic detachment energy (ADE) which should not be confused with the electron affinity (EA).

5.2.3.3 More stable isomers and the importance of metastability

Since neutral $Au(CN)_2$ structure shown in Figure 4 is not the global minimum and clusters with larger CN concentration are metastable, we searched for lower energy isomers where CN molecules may dimerize to form $(CN)_2$ or trimerize to form $(CN)_3$. We concentrated our search only on $Au(CN)_3$ and $Au(CN)_4$ where strong bonding is observed. We have not considered van der Waals type clusters in which cyanogen gas molecules can also dimerize to form $(CN)_4$ and then interact with Au.

First, we determined the minimum energy structures of $(CN)_n$ for n=2 and 3. This gave an indication of the relative C-C, C-N and N-C bond strengths in the $(CN)_n$ moieties and accordingly we proceeded in our search for lowest energy $Au(CN)_n$ structures. The geometries of some isomers of $(CN)_2$ and $(CN)_3$ are given in Figure 5. It is to be noted that all the structures were found to have no imaginary frequencies indicating they are dynamically stable. In case of neutral $(CN)_2$, we found that cyanogen (NCCN) has lower energy than isocyanogen (NCNC), which in turn, has lower energy than and diisocyanogen (CNNC). This indicates that when cyanide binds with gold after dimerization, it will preferentially attach as NCCN moiety. The N-C bond lengths are 1.16 Å and the C-C bond length is 1.38 Å. In case of $(CN)_2^-$, we found that again, $NCCN^-$ with C_{2h} symmetry has the lowest energy. The N-C bond lengths increase to 1.20

Å and the C-C bond length remains at 1.38 Å. Our results agree with previous reports.[130-132] We found several isomers for $(CN)_3$, some of which are shown in Figure 5. Of these, the NCNCCN structure with C_s symmetry has the lowest energy, in both neutral and anionic forms. Here, a cyanide moiety is attached to the cyanogen molecule. The energies of the different isomers relative to the ground state (ΔE) isomers are listed in Figure 8. ΔE is defined as the energy of the converged structure minus the energy of the lowest energy structure.

With these results in mind, we proceeded to the investigation of lower energy structures of $Au(CN)_n$ clusters. We expected that structures where $(CN)_2$ and $(CN)_3$ attach as NCCN and CNNCCN respectively, will have lower energy. We did not find any energetically lower isomers of AuCN and $Au(CN)_2$ than those given in Figure 4 and Figure 5. However, for $Au(CN)_3$, $Au(CN)_3^-$ and $Au(CN)_4$ we were able to find lower energy structures, in accordance with our expectations. These are shown in Figure 9. The energies of these structures are lower from those given in Figure 4 and Figure 5 by 2.69, 0.08 and 2.97 eV, respectively. No structures of $Au(CN)_4^-$ with energies lower than that shown in Figure 5 was found.

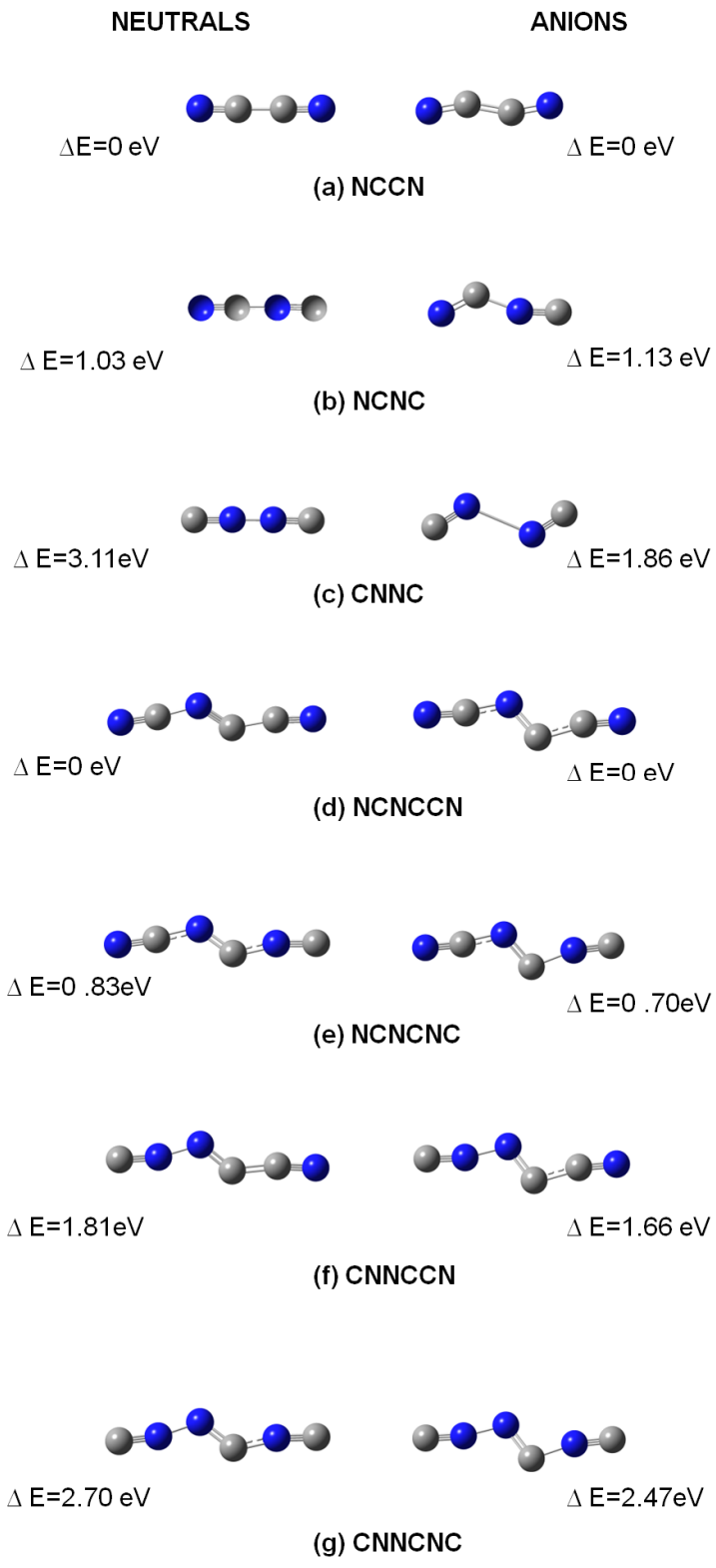

Figure 8. (a)-(c) Some low energy isomers of $(CN)_2$; (d)-(g) Some low energy isomers of $(CN)_3$

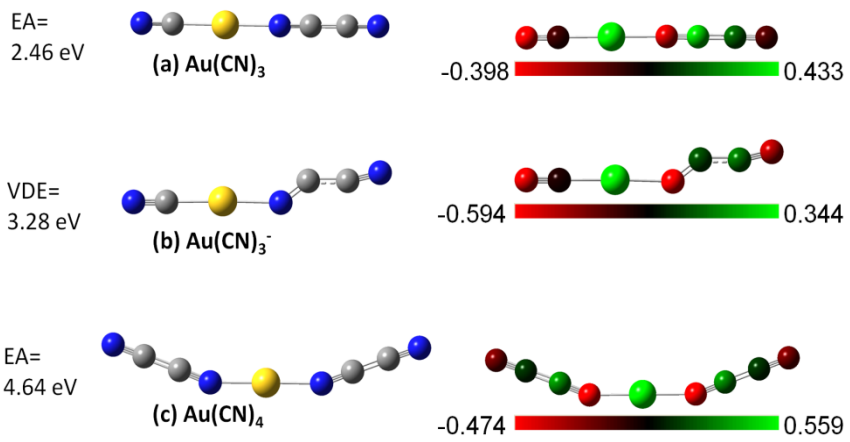

Figure 9. Ground state geometries of $Au(CN)_3$, $Au(CN)_3^-$ and $Au(CN)_4$

Neutral $Au(CN)_3$ is linear with C_{infv} symmetry. The Au-C bond length is 1.96 Å which is slightly longer than that in AuCN (1.94 Å). The N-Au bond length is 2.04 Å signifying that this bond is much weaker. The structure of $Au(CN)_3^-$ is quite different. The Au-C bond length is 1.98 Å and the Au-C-N atoms lie in a plane. However, the $(CN)_2$ moiety on the other side has a slight trans nature with the Au-N bond length of 2.04 Å. Considering Au to be in +1 oxidation state, we see that AuCN has a closed shell. Hence, most of the negative charge (-0.755) in $NCAuNCCN^-$ goes to the $(CN)_2$ moiety and thus its structure is similar to that of free $NCCN^-$. Moreover, the difference between VDE and ADE (which is also the EA in this case) of $NCAuNCCN^-$ is 0.82 eV which is equal to the VDE of $NCCN^-$. We note that the $Au(CN)_3^-$ isomer in Figure 9 is only 0.08 eV lower in energy than that in Figure 5 where CN moieties bind dissociatively. This energy difference is less than the accuracy of DFT methods and hence the two geometries are nearly degenerate.

Neutral $Au(CN)_4$ has C_{2v} symmetry with two linear cyanogen groups in a cis conformation, the C-N-Au angles being 159˚ each and the N-Au-N angle being about 180˚. The Au-N bond length

is 1.98 Å. It is interesting to note that while their isomers in which CN molecules have attached to Au dissociatively are unstable with respect to fragmentation, these lower energy structures are all stable and also have no imaginary frequencies. The fragmentation energies of the lower energy structures along the same path as for the metastable ones are 1.26 eV, 1.60 eV and 0.53 eV for $Au(CN)_3$, $Au(CN)_3^-$ and $Au(CN)_4$ respectively.

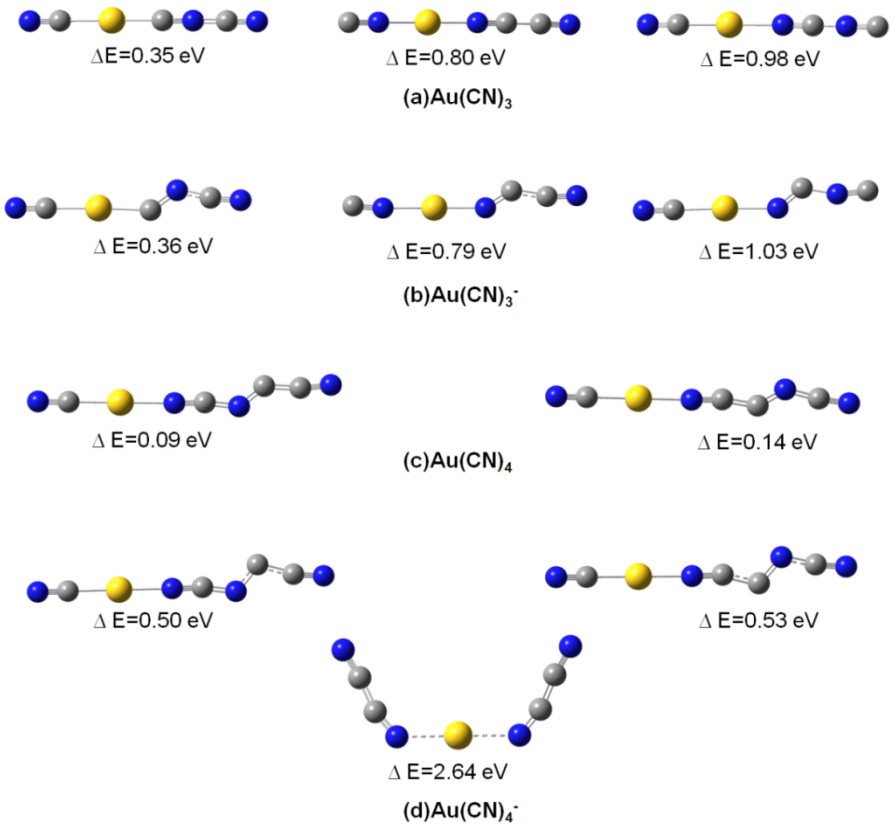

Figure 10. Some higher energy structures of $Au(CN)_3$, $Au(CN)_3^-$, $Au(CN)_4$ and $Au(CN)_4^-$

We also found several energetically higher structures for these three complexes. These were obtained by permutations of the relative positions of the C and N atoms with respect to gold. Some of the structures are shown below in Figure 10. Optimization of $Au(CN)_4^-$, starting with different initial configurations led to structures all of which have higher energies than the

structure in Figure 5 (d). However, these structures are also dynamically stable and belong to local minima on the potential energy surface. The energies of the higher energy structures relative to the ground state (ΔE) are incorporated in Figure 10. Beyond this limit, cyanogen dimerization sets in.

This suggests that what will be observed experimentally may depend on the initial reaction conditions. In gas phase synthesis of gold cyanide clusters, if the vapor pressure of CN molecules is low, the most likely products will have the structures shown in Figure 4 and Figure 5. This is because reaction occurs when two species collide with each other. Lower CN vapor pressure minimizes the chances of CN-CN collisions. On the contrary, if the vapor pressure of CN is high, structures as shown in Figure 9 may form. However, it is likely that in both cases a mixture of isomeric products may exist.

Our results also lead us to the important conclusion that there is a difference between the electron affinity (EA) and the adiabatic detachment energy (ADE). In fact, the EA of $Au(CN)_3$ is the energy difference between structures (a) and (b) in Figure 9 which is 2.46 eV. The energy difference between the structures in Figure 4 (c) and Figure 5 (c) is simply the ADE. From Figure 9, we see that $Au(CN)_3$ can be considered to be composed of a pseudo closed-shell dipolar AuCN moiety which binds to the pseudo closed-shell $(CN)_2$ moiety by inducing a dipole moment in it. This explains the low value of EA. The VDE is 3.28 eV. Similarly, the EA of $Au(CN)_4$ is 4.64 eV, the energy difference between the structures in Figure 5 (d) and Figure 9 (c). The VDE is 7.95 eV as tabulated in Table 2. The large difference of 3.3 eV between the EA and VDE accounts for the fact that the geometries of the neutral and the anion are drastically

different in this case. Since we note that there is a substantial difference between the lowest energy structure of the neutral and the lowest energy structure of the anion in several cases, one has to be careful while assigning a value to EA experimentally. If the structures shown in Figure 4 and Figure 5 are relevant to experimental conditions, one would measure ADE as the transition energy from the anion's ground state to the ground state of the structurally similar neutral isomer. We earlier demonstrated this to be the case for $Au(CN)_2$. Experimental studies of larger $Au(CN)_n$ complexes will be very useful.

A very important realization that we make from our data is that, to exhibit superhalogen behavior it is essential that the CN moieties attach dissociatively with Au so that effective electron delocalization can take place. Most of the structures studied are metastable and their fragmented counterparts are lower in energy. However, to exploit the superhalogen properties of these clusters, it is these metastable clusters that are important. Experiments can tell us if the formation of $Au(CN)_n$ clusters will be driven kinetically or thermodynamically and if the spectroscopic properties carry the signature of metastable states.

5.2.3.4 A closer look at $Au(CN)_3$

We note an unusual property of $Au(CN)_3$: Its anion is found to possess two energetically nearly degenerate isomers that are only 0.08 eV apart, while the resulting neutral isomers lie 2.69 eV apart. In addition, the anion isomers have strikingly different spectroscopic properties. The vertical detachment energy (VDE) of one isomer is 5.44 eV while it is only 3.28 eV for the other. In the former isomer the Au atom is attached to three individual CN ligands in a T-shaped configuration while in the latter isomer Au binds to cyanogen (NCCN) and a separate CN

moiety. The vast difference in the VDE arises because the stabilities of the two anion isomers are governed by very different mechanisms. The former isomer is stabilized by its superhalogen behavior while the latter draws its stability from the unusually large binding energy of cyanogen. Following electron detachment, the degeneracy in the corresponding neutrals is lifted as the anions relax towards their nearest equilibrium configuration. In spite of the large energy difference (2.69 eV) between the two neutral isomers, the photoelectron spectra resulting from these anion isomers are expected to be sharp. This is because chemical bonds need to break for the higher energy neutral isomer to reach its ground state structure and this would involve crossing large energy barriers. Photoelectron spectroscopy experiments should be able to verify these predictions.

It is well known that structure and properties of matter are intertwined and a fundamental understanding of these relationships is important for the synthesis of nanomaterials with tailored properties. Clusters are the ultimate nanoparticles where every atom and every electron count. Unfortunately, there are no current experimental techniques that can unambiguously determine the structures of clusters without the benefit of theoretical input. This becomes an even more difficult task when the energy differences between the nearly degenerate isomers are beyond the accuracy of theoretical methods. We find $Au(CN)_3$ to be a unique example of such a cluster where photoelectron spectra in combination with theory can unmistakably distinguish between the nearly degenerate anion isomers. Due to this interesting property of $Au(CN)_3$ we have further investigated it.

To obtain the ground state geometry of $Au(CN)_3$ anion, we used 22 initial structures where CN moieties are bound to a Au atom either individually or in dimerized/trimerized form. In the former case Au has a choice to bind to either C or N. For the later configurations the choices are more complex since $(CN)_2$ and $(CN)_3$ can have many isomers of their own.[130-132] For the dimerized configuration we used NC-Au-NCCN, NC-Au-NCNC, NC-Au-CNCN, NC-Au-CNNC as well as CN-Au-NCCN, CN-Au-NCNC, CN-Au-CNCN, and CN-Au-CNNC. Similarly, there are also a number of ways $(CN)_3$ can attach to Au and one such example is Au-NCCNCN. All the different isomers for the various different ways of attachment of CN with Au are shown in Figure S1, S2 and S3. For each configuration the geometries were fully optimized without any symmetry constraint. The convergence in total energy and forces was set to $1x10^{-6}$ eV and $1x10^{-2}$ eV/Å, respectively. The geometries of the neutral clusters were obtained by using anion geometries as starting points and optimizing the geometries following electron detachment with the same constraints outlined above.

In Figure 11, we show the geometries of the low lying isomers of $Au(CN)_3$ for different modes of CN attachment. We begin with the geometries of the $Au(CN)_3^-$. The ground state geometry has NC-Au-NCCN configuration. Here two of the CN moieties dimerize and bind to Au while the third CN moiety binds to Au on the opposite side with C pointing towards Au. The structure has a pseudo-linear form with the NCCN moiety having a bent structure. We note that this has the same form as $(CN)_2^-$. Au exists in the oxidation state of +1 and the added electron is distributed over the cyanogen (NCCN) moiety. The next higher energy structure lying only 0.08 eV above the ground state has three CN moieties attached to Au separately. In this configuration Au has an oxidation state of +2. With the extra electron in the anion, there are enough electrons to break the

NC-CN bond. The near degeneracy of these two structures results from separate mechanisms. The stability of the ground state structure arises because the binding energy of $(CN)_2$ is 5.84 eV.[123] The stability of the next higher energy structure arises because the extra electron is distributed over three CN moieties and hence leads to high binding energy, namely 5.07 eV. Thus, this isomer behaves as a superhalogen. Calculations indicate both the isomers are stable with respect to fragmentation into $AuCN^-$ and NCCN (see Table 3). Furthermore, we note that the lowest energy structure where trimerized form of $(CN)_3$ attaches to the Au atom is significantly higher in energy than the isomers discussed above.

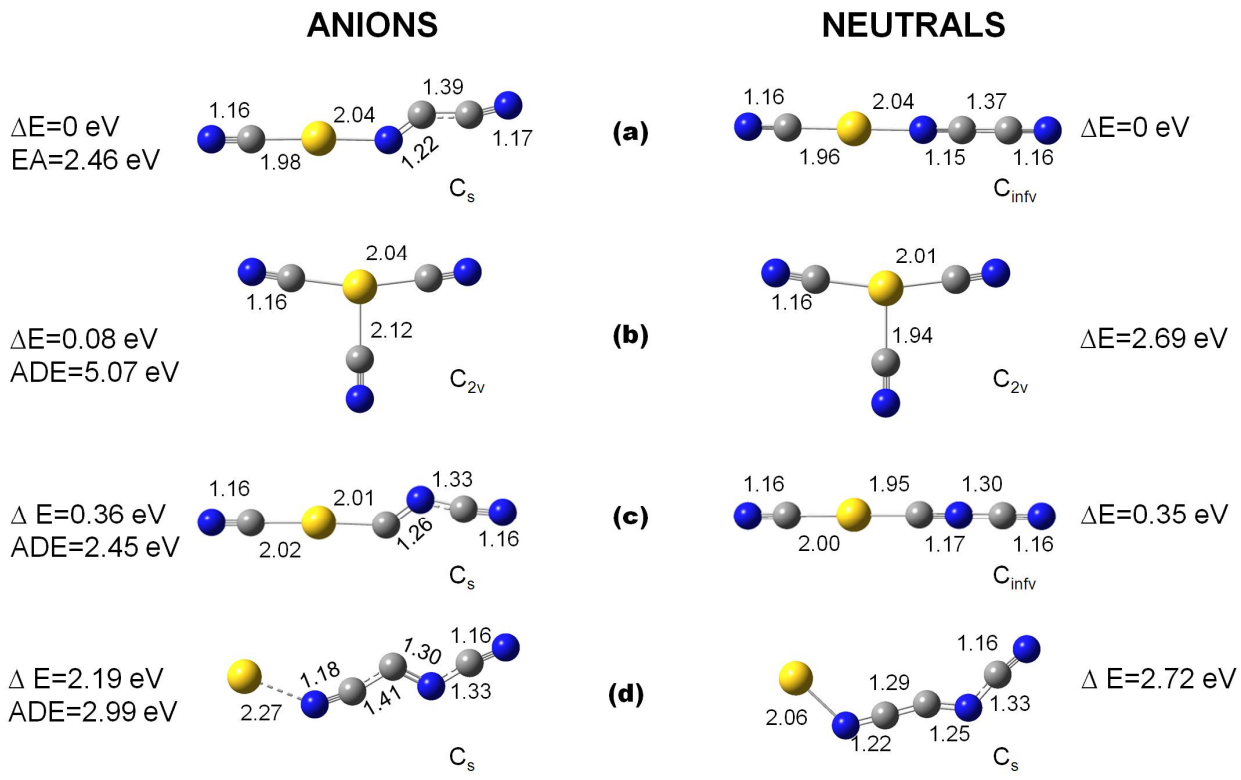

Figure 11. Geometries of low lying isomers of anionic (left) and neutral (right) $Au(CN)_3$ isomers [(a)-(d)].
The bond lengths are in Å. The energies are measured with respect to the ground states of the anion and neutral in (a). Blue represents N, grey represents C and yellow represents Au.

Next we discuss the geometries of the neutral isomers. Here, the ground state is a linear chain with Au bonded to C of CN and N of NCCN moieties. The oxidation state of Au is +2 and the stability of the structure is due to the large binding energy of cyanogen (NCCN). The structure where the CN moieties bind separately is 2.69 eV higher in energy than the ground state. Here Au exists in +3 oxidation state, but the cluster does not gain the same energy it did in the anion due to distribution of the added electron over all the three ligands. Hence, we see that while the linear isomer is bound against fragmentation into AuCN and NCCN (by 1.26 eV), the T-shaped neutral isomer is not (by 1.42 eV). However, there are other linear structures of $Au(CN)_3$ whose energies are closer to the ground state. Here $(CN)_2$ binds either as CNCN and NCCN or CNNC. Once again, Au bound to $(CN)_3$ namely Au-NCCNCN has much higher energy.

To confirm the validity of our results, we have repeated the calculations for ADE and VDE for the two nearly degenerate $Au(CN)_3^-$ anions at different levels of theory to study the effect of changing method as well as basis set. The results are given below in Table 4. At the B3LYP level we used LANL2DZ[133] and SDD pseudopotentials[99,100] for Au and 6-311+G*[97,98] and aug-cc-pVTZ basis sets for C and N. At the B3PW91[91,92] and M06[134] levels we used SDD basis set for Au (as it is superior to LANL2DZ) and aug-cc-pVTZ[135] for C and N. As can be seen, the ADE and VDE values lie within 0.2 eV of each other for the different methods and different basis sets tested here. This is within the error limit associated with these calculations. We did not include corrections for zero-point vibrational energy or basis set superposition error as these do not significantly alter the ADE and VDE. In all cases, geometries were optimized. The energy difference between the isomers varied between 2.56-2.91 eV for the neutral and 0.05-0.22 eV for the anion depending on the theoretical method used, the energy being lower for the isomers

where CN moieties were dimerized. For extensive calculations we have chosen the B3LYP[92,93] hybrid functional with SDD basis[99,100] for Au and 6-311+G* basis for C and N since this method has been found to provide results very close to experimental values particularly for gold cyanide clusters. For example, the ADE and VDE of $AuCN^-$ predicted using this method are 2.12 eV and 2.25 eV respectively which matches very well with the experimentally determined values (2.07 eV and 2.19 eV respectively).[127,128] UCCSD(T) calculations done using aug-cc-pVTZ basis set for C and N and aug-cc-pVTZ-pp basis for Au predict these values to be 1.97 eV and 2.08 eV respectively.[128] Similarly, the calculated VDE value for $Au(CN)_2^-$ using the above B3LYP level of theory is 6.10 eV. This also compares very well with the CASSCF/CCSD(T) value of 6.02 eV, and experimental value of 6.09 eV, respectively.[127] Therefore, to save computation time, we have not performed CCSD(T) calculations for the $Au(CN)_3$ complexes .

Table 4. ADE and VDE of the two lowest energy $Au(CN)_3^-$ clusters calculated at different theoretical levels

Cluster	Method	B3LYP				B3PW91	M06
	Au	SDD		LANL2DZ		SDD	SDD
	Basis C, N	6-311+G*	aug-cc-pvtz	6-311+G*	aug-cc-pvtz	aug-cc-pvtz	aug-cc-pvtz
$Au(CN)_3^-$	ADE	5.07	5.00	5.07	4.99	4.91	4.89
	VDE	5.44	5.41	5.47	5.36	5.26	5.29
NC-Au-NCCN$^-$	ADE	2.46	2.40	2.44	2.40	2.42	2.20
	VDE	3.28	3.20	3.26	3.19	3.16	2.79

One of the ideal experiments to probe the electronic properties of clusters is the photoelectron spectroscopy (PES). Here, a mass isolated anion is interjected with a fixed frequency laser and the energy of the photo-ejected electron is measured. The resulting PES carries information on the vertical and adiabatic detachment energies as well as electron affinity. In fact, several

superhalogens have been studied using PES experiments and VDEs as large as about 7 eV have been measured.[23,127] In anion clusters that do not possess nearly degenerate isomers, interpretation of the PES is simple. Sharp spectra correspond to the geometry of the neutral that is very similar to that of its anion. Broad spectra, on the other hand, reflect the fact that the neutral and anion ground state geometries are significantly different. In the event that nearly degenerate isomers of the anion exist, interpretation of the PES becomes complex, particularly if the isomers have very different geometries. This is the case here. The VDE and ADE of the isomer in Figure 11(a) yields 3.28 eV and 2.46 eV, respectively while those corresponding to Figure 11 (b) the energies are 5.44eV and 5.07 eV. Since the geometries of the anions and the corresponding neutrals in Figure 11 (a) and (b) are similar, the PES spectra of both the isomers are expected to be sharp. Going from the anion geometry in Figure 11 (a) to the neutral geometry in Figure 11 (b) or from the anion geometry in Figure 11 (b) to neutral geometry in Figure 11 (a) will be difficult as it would require breaking chemical bonds and hence encountering large energy barriers.

The PES contains more information than just the VDE, ADE and EA. The many peaks in the spectrum reflect the density of states of the neutral cluster. These are commonly studied in theory by broadening the discrete molecular orbital energy levels. Since most calculations are carried out by using density functional theory one should recall that single particle energy levels in DFT do not have any formal meaning. Consequently, Gutsev et al. had suggested a different procedure where more information can be gleaned from DFT calculations to compare with PES experiment.[136] This deals with energy gaps between the two lowest peaks in the PES.

Note that when an electron is removed from an anion with spin multiplicity M, the corresponding spin multiplicity of the neutral can be either M+1 or M-1, depending upon whether the electron is removed from the spin-down or spin-up state. The difference between these two energies yields the energy separation between the two lowest peaks in the PES. In Figure 12, we provide the vertical detachment energies associated with the two nearly degenerate isomers from the doublet spin state to the singlet and triplet states of the corresponding neutrals. These would correspond to the two low energy peaks in the PES and provide further data against which experiment can be compared.

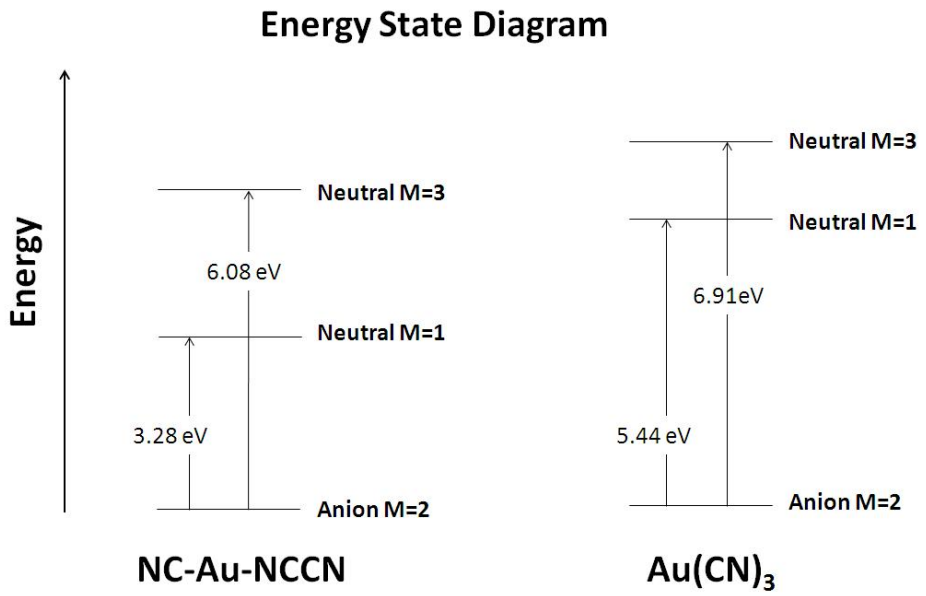

Figure 12. Vertical detachment energies of the two nearly degenerate $Au(CN)_3^-$ anions

5.2.4 Conclusions

Our systematic study of $Au(CN)_n$ clusters shows several important results. (1) The calculated vertical and adiabatic detachment energies of AuCN and $Au(CN)_2$ agree with previous experiments.[127,128] However, we show that neutral $Au(CN)_2$ is metastable and PES study only

yields the adiabatic detachment energy and not the electron affinity as initially believed. (2) Our result confirms the earlier observation[77] that pseudohalogens can be used to build superhalogens. However, in our study we show that large electron affinities can be attained without changing the identities of the reactant molecules, simply by tuning the number of ligands allowed to interact with the central metal atom. Moreover, we observe a fundamental difference between how the halogens and pseudohalogens lead to the formation of superhalogens. For example AuF_n forms superhalogens up to n=6.[25] Pseudohalogens can do the same if experimental conditions are such that they bind individually to the metal atom. (3) The reaction of halogens and pseudohalogens with a metal atom is different which arises due to the fact that pseudohalogens can dimerize more easily due to their large binding energy. (4) It is to be noted that for superhalogen behavior, it is essential to have ligands attaching dissociatively rather than after dimerization. This is demonstrated for $Au(CN)_3$ whose electron affinity corresponding to the lowest energy anion isomer is 2.46 eV while for its isomer in Figure 9, the adiabatic detachment energy is 5.07 eV. Therefore, as per the definition of electron affinity, $Au(CN)_3$ is *not* a superhalogen! This is in sharp contrast with AuF_3 which is a superhalogen with an electron affinity of 5.15 eV. Thus, even if pseudohalogens mimic the chemistry of halogens, they may not form superhalogens the same way halogens do. This is the limitation! Hence, we see that the possible existence of metastable isomers can make the task of experimental determination of electron affinity difficult. In such cases, there may be a discrepancy between the electron affinity and the adiabatic detachment energy of a species and theoretical work is essential. We hope our work will provide direction in the synthesis of new superhalogens and in a fundamental understanding of their behavior.

Chapter 6 Applications of Superhalogens

6.1 Salts and Hyperhalogens

6.1.1 Introduction

For practical applications of superhalogens, it is important that they can be used as building blocks of materials. To be a superhalogen and a strong oxidizing agent, not only does its electron affinity have to be larger than those of halogen atoms, but like halogens, the cluster should also form ionic bond reminiscent of salts. Since these are closed shells, their electron affinities should also be very small. To confirm that superhalogens based on the Wade-Mingo's rule can be utilized to form salts, we have calculated the equilibrium structures and total energies of neutral and anionic $M(B_{12}H_{13})$ and $M(CB_{11}H_{12})$ (M=Li, Na, K, Rb, and Cs) clusters. Moreover, we have investigated if these superhalogens could also be used to build hyperhalogens. Hyperhalogens constitute another class of highly electronegative species which was discovered recently.[72] They are created when a metal atom is decorated with superhalogen moieties just as conventional superhalogens are created when a metal atom is surrounded with halogen atoms. The electron affinities of hyperhalogens are, therefore, larger than their superhalogen building blocks. Our results are discussed in the following sections.

6.1.2 Results and Discussion

6.1.2.1 Salts

The geometries for all these clusters are similar and hence we only show the geometries and NBO charges of neutral and anionic Na($B_{12}H_{13}$) and Na($CB_{11}H_{12}$) in Figure 13. The shortest M-B distance increases gradually from Li to Cs. For M($B_{12}H_{13}$) (M=Li, Na, K, Rb and Cs) clusters, these are 2.19, 2.59, 3.00, 3.24 and 3.43 Å for the neutrals and 2.42, 2.99, 3.32, 3.63 and 3.81 Å for the anions, respectively. For M($CB_{11}H_{12}$) (M=Li, Na, K, Rb and Cs) clusters, the shortest M-B distances are 2.20, 2.59, 2.99, 3.24 and 3.43 Å for the neutrals and 2.42, 2.97, 3.31, 3.63 and 3.79 Å for the anions, respectively. These distances are larger in negative ions than in neutrals.

It is to be noted that the neutral M($B_{12}H_{13}$) and M($CB_{11}H_{12}$) are ionic just like metal halide salts since the NBO charge on the metal atom is almost +1 (ranging from 0.898 for Li to 1.002 for Cs). The vertical detachment energies and electron affinities are given in Table 5. We see that electron affinities of $B_{12}H_{13}$ and $CB_{11}H_{12}$ superhalogens are reduced to nearly 1 eV when attached to an alkali atom.

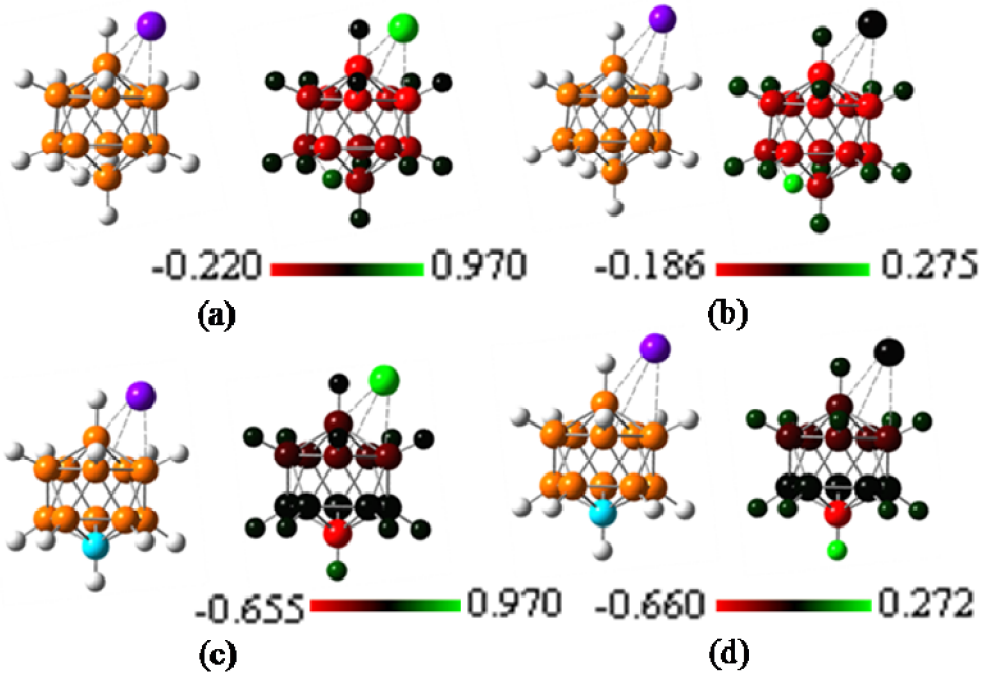

Figure 13. Geometries (left) and NBO charge distributions (right) of (a) $Na(B_{12}H_{13})$, (b) $Na(B_{12}H_{13})^-$, (c) $Na(CB_{11}H_{12})$ and (d) $Na(CB_{11}H_{12})^-$

Table 5. Electron affinities and Vertical Detachment Energies of closed-shell clusters of $M(B_{12}H_{13})$ and $M(CB_{11}H_{12})$ and hyperhalogen clusters of $M(B_{12}H_{13})_2$ and $M(CB_{11}H_{12})_2$ (M=Li, Na, K, Rb, Cs).

Cluster	EA (eV)	VDE (eV)	Cluster	EA (eV)	VDE (eV)
$Li(B_{12}H_{13})$	0.91	1.07	$Li(B_{12}H_{13})_2$	6.55	6.85
$Na(B_{12}H_{13})$	1.27	1.55	$Na(B_{12}H_{13})_2$	6.53	6.74
$K(B_{12}H_{13})$	1.06	1.21	$K(B_{12}H_{13})_2$	6.48	6.68
$Rb(B_{12}H_{13})$	1.14	1.30	$Rb(B_{12}H_{13})_2$	6.42	6.67
$Cs(B_{12}H_{13})$	1.05	1.18	$Cs(B_{12}H_{13})_2$	6.38	6.53
$Li(CB_{11}H_{12})$	0.90	1.05	$Li(CB_{11}H_{12})_2$	6.49	6.68
$Na(CB_{11}H_{12})$	1.25	1.51	$Na(CB_{11}H_{12})_2$	6.47	6.65
$K(CB_{11}H_{12})$	1.05	1.19	$K(CB_{11}H_{12})_2$	6.42	6.58
$Rb(CB_{11}H_{12})$	1.13	1.29	$Rb(CB_{11}H_{12})_2$	6.36	6.50
$Cs(CB_{11}H_{12})$	1.05	1.17	$Cs(CB_{11}H_{12})_2$	6.31	6.46

6.1.2.2 Hyperhalogens

To see if Wade-Mingos rule can be applied to create hyperhalogens as well, we have considered $M(B_{12}H_{13})_2$ and $M(CB_{11}H_{12})_2$ where M=Li, Na, K, Rb, and Cs. In Figure 14 the geometries of only $Na(B_{12}H_{13})_2$ and $Na(CB_{11}H_{12})_2$ are given for illustrative purpose. Note that the NBO charges on the metal atoms are close to +1 indicating ionic bonding with the cage. As seen before, the charge distribution in the case of anionic clusters is more uniform than that in the neutral species.

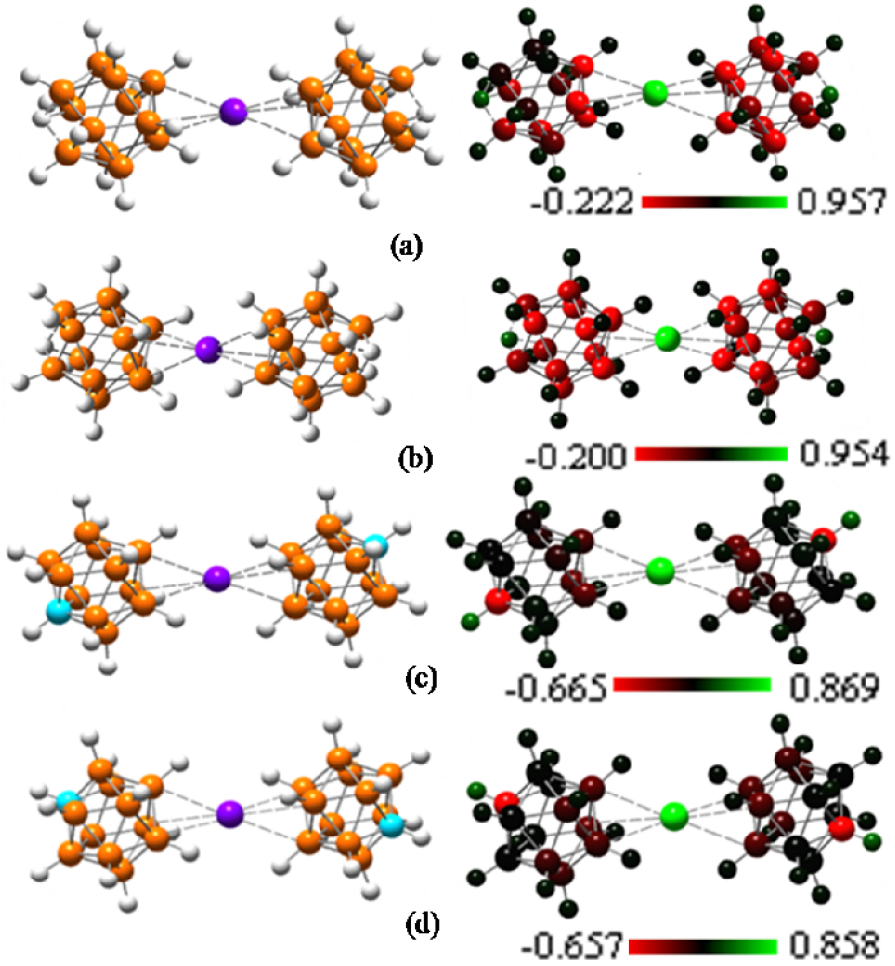

Figure 14. Geometries (left) and NBO charge distributions (right) of (a) $Na(B_{12}H_{13})_2$, (b) $Na(B_{12}H_{13})_2^-$, (c) $Na(CB_{11}H_{12})_2$ and (d) $Na(CB_{11}H_{12})_2^-$

The electron affinities and vertical detachment energies are given in Table 5. We note that these values are consistently larger than those of the corresponding superhalogen building blocks shown in Table 1. Hence, they can be classified as hyperhalogens. As in the case of superhalogens, here also the electron affinities gradually decrease from Li to Cs. The differences between the EAs and VDEs lie in the range of 0.1 to 0.3 eV suggesting that the relaxations of structures following photodetachment of the extra electron are minimal.

6.1.2.3 Weakly Coordinating Anions vis a vis Superhalogens:

Classes of bulky anions that interact weakly with cations are often referred to in the literature as weakly coordinating anions. These have attracted considerable attention due to their commercial importance in olefin polymerization, biomedicine, catalysis, and potential as components in lithium ion battery technology. Superhalogens and hyperhalogens are also of considerable importance in chemistry since they can be used in redox reactions involving compounds with high ionization potentials. Thus, a link between these two species may guide in the synthesis of new materials. In 1986, a new class anions based on stable boron cluster framework, namely $CB_{11}H_{12}^-$ was introduced as a candidate for weakly coordinating anion.[137] Since weak binding and large distance between the metal and anion complex are characteristic signatures of weakly coordinating anions, we have calculated the binding energies of MY (M= Li, Na, K, Rb, Cs, Y=$B_{12}H_{13}$ and $CB_{11}H_{12}$) against fragmentation into M^+ cation and Y^- anion. For comparison, we have also calculated the analogous fragmentation energies for MF into M^+ and F^-. The distances between alkali metal atom and F range from 1.58 Å in LiF to 2.56 Å in CsF. The distances between the metal atom and nearest B atom in M($CB_{11}H_{12}$), on the other hand, range from 2.20 Å to 3.43 Å for M= Li and Cs, respectively. Similarly, the energies to dissociate MF to M^+ and F^- range from 8.02 eV in LiF to 5.04 eV in CsF. The corresponding dissociation energies of

$M(CB_{11}H_{12})$ into M^+ and $CB_{11}H_{12}^-$ are 5.41 eV in $Li(CB_{11}H_{12})$ and 3.39 eV in $Cs(CB_{11}H_{12})$. Thus, we understand why $CB_{11}H_{12}^-$ meets the requirements of a weakly coordinating anion. We have repeated this exercise for the $M(B_{12}H_{13})$ species and confirm that $B_{12}H_{13}^-$ is also a weakly coordinating anion. Similar ideas can be extended to other superhalogens and hyperhalogens. We are currently carrying a systematic study of this topic.

6.1.2.4 Stability with respect to fragmentation

Superhalogens and hyperhalogens are of considerable importance in chemistry as they can be used in redox reactions involving compounds with high ionization potentials and, thus, can be used to synthesize novel materials. For any potential applications, it is necessary to examine their stability with respect to fragmentation. We have, therefore, calculated their binding energies (ΔE) against fragmentation into neutral and ionic species. For example, in the gas phase a neutral salt cluster (MY) would fragment into two neutral components M and Y while in a solution a MY salt would fragment into M^+ and Y^-. Here Y is a superhalogen. We have calculated the energies for different fragmentation channels using the following equations

$$\Delta E_1 = -[E(MY) - E(M) - E(Y)] \quad (1)$$

$$\Delta E_2 = -[E(MY) - E(M^+) - E(Y^-)] \quad (2)$$

$$\Delta E_3 = -[E(MY_2^-) - E(MY) - E(Y^-)] \quad (3)$$

$$\Delta E_4 = -[E(MY_2^-) - E(M^+) - 2E(Y^-)] \quad (4)$$

For comparison, we have also calculated the analogous fragmentation energies for MF and MF_2. First we discuss the stabilities of neutral closed shell clusters $M(B_{12}H_{13})$ and $M(CB_{11}H_{12})$ and

compare these against closed shell MF (M=Li-Cs). The fragmentation energies, ΔE_1 and ΔE_2 defined in Eq (1) and Eq.(2), are given in Table 6 and ΔE_3 and ΔE_4 defined in Eq (3) and Eq.(4), are given in Table 7. We note that fragmentation energies, ΔE_1 of MY and MF are very similar when they dissociate into neutral species. However, when they dissociate into ions, MY is more prone to dissociation compared to MF by about 1.6-2.6 eV. The fragmentation of negative ions of hyperhalogens, on the other hand, is somewhat different. The relevant energies ΔE_3 and ΔE_4 are given in Table 6. The fragmentation energies for MF_2^- dissociating into neutral MF and F^- are higher than those in MX_2^- by 0.6-1.5 eV. However, the fragmentation energies ΔE_4 for MF_2^- dissociating into neutral M^+ and $2F^-$ are higher than those in MY_2^- by a much larger amount, namely, 2-4 eV. This indicates that F^- is much more strongly bound to the alkali metal atoms than either $B_{12}H_{13}^-$ or $CB_{11}H_{12}^-$ in the neutral closed shell clusters as well as in the hyperhalogens. Our theoretical results corroborate the experimental finding[137] that $CB_{11}H_{12}^-$ is a weakly coordinating anion and further suggest that $B_{12}H_{13}^-$ is also one such anion.

Table 6. Fragmentation energies (eV) of neutral closed shell clusters MF, $M(B_{12}H_{13})$ and $M(CB_{11}H_{12})$ for (M=Li, Na, K, Rb, Cs)

Cluster	**ΔE_1**	**Cluster**	**ΔE_1**	**Cluster**	**ΔE_1**
LiF	5.89	$Li(B_{12}H_{13})$	5.18	$Li(CB_{11}H_{12})$	5.18
NaF	4.75	$Na(B_{12}H_{13})$	4.52	$Na(CB_{11}H_{12})$	4.53
KF	5.01	$K(B_{12}H_{13})$	4.84	$K(CB_{11}H_{12})$	4.84
RbF	4.45	$Rb(B_{12}H_{13})$	4.66	$Rb(CB_{11}H_{12})$	4.65
CsF	4.51	$Cs(B_{12}H_{13})$	4.78	$Cs(CB_{11}H_{12})$	4.77
Cluster	**ΔE_2**	**Cluster**	**ΔE_2**	**Cluster**	**ΔE_2**
LiF	8.02	$Li(B_{12}H_{13})$	5.37	$Li(CB_{11}H_{12})$	5.41
NaF	6.68	$Na(B_{12}H_{13})$	4.52	$Na(CB_{11}H_{12})$	4.56
KF	6.02	$K(B_{12}H_{13})$	3.92	$K(CB_{11}H_{12})$	3.94
RbF	5.29	$Rb(B_{12}H_{13})$	3.57	$Rb(CB_{11}H_{12})$	3.60
CsF	5.04	$Cs(B_{12}H_{13})$	3.37	$Cs(CB_{11}H_{12})$	3.39

Table 7. Fragmentation energies (eV) of anions of hyperhalogen clusters $M(B_{12}H_{13})_2^-$ and $M(CB_{11}H_{12})_2^-$ for (M=Li, Na, K, Rb,Cs). The results are compared with MF_2^-.

Cluster	ΔE_3	Cluster	ΔE_3	Cluster	ΔE_3
LiF_2^-	3.07	$Li(B_{12}H_{13})_2^-$	1.51	$Li(CB_{11}H_{12})_2^-$	1.55
NaF_2^-	2.73	$Na(B_{12}H_{13})_2^-$	1.55	$Na(CB_{11}H_{12})_2^-$	1.58
KF_2^-	2.14	$K(B_{12}H_{13})_2^-$	1.40	$K(CB_{11}H_{12})_2^-$	1.42
RbF_2^-	2.15	$Rb(B_{12}H_{13})_2^-$	1.37	$Rb(CB_{11}H_{12})_2^-$	1.39
CsF_2^-	1.97	$Cs(B_{12}H_{13})_2^-$	1.29	$Cs(CB_{11}H_{12})_2^-$	1.31
Cluster	**ΔE_4**	**Cluster**	**ΔE_4**	**Cluster**	**ΔE_4**
LiF_2^-	11.08	$Li(B_{12}H_{13})_2^-$	6.88	$Li(CB_{11}H_{12})_2^-$	6.96
NaF_2^-	9.42	$Na(B_{12}H_{13})_2^-$	6.07	$Na(CB_{11}H_{12})_2^-$	6.14
KF_2^-	8.16	$K(B_{12}H_{13})_2^-$	5.31	$K(CB_{11}H_{12})_2^-$	5.36
RbF_2^-	7.45	$Rb(B_{12}H_{13})_2^-$	4.94	$Rb(CB_{11}H_{12})_2^-$	4.98
CsF_2^-	7.01	$Cs(B_{12}H_{13})_2^-$	4.66	$Cs(CB_{11}H_{12})_2^-$	4.71

6.1.3 Conclusions

In summary, we have shown that superhalogens designed by the Wade-Mingo's rule can be utilized to build salts and hyperhalogens. The superhalogens based on borane derivatives are weakly coordinating anions with potential for applications. We hope that the present work will motivate experimentalists to search for new bulky negative ions governed by the Wade-Mingos rule.

6.2 Stabilization of Unusually High Oxidation States

6.2.1 Introduction

The oxidation state is a "measure of the degree of oxidation of an atom in a substance"[138] and it is the fundamental key to understanding redox reactions, reaction mechanisms, catalysis etc. It is the charge an atom in a compound would have, *if* the bonding were completely ionic. This description makes the determination of oxidation states in covalent systems less transparent since

charges are shared between atoms and not completely transferred. In such systems, the oxidation state is determined by assigning the bonding electron pair to the more electronegative ligand. For example, the charge on the C atom in CH_4 is -0.797, but its oxidation number is -IV. Explicit rules for assigning oxidation states are available in the IUPAC Gold Book.[138] Transition metals, owing to their incomplete *d*-shells, exhibit variable oxidation states and hence form a large domain of complexes. The possibility of transforming Group 12 elements such as Zn into transition metals has fascinated chemists for decades. Due to Zn's $3d^{10}4s^2$ ground state configuration and highly stable filled *d*-orbitals its inner *d*-electrons seldom take part in bonding and oxidation states of Zn beyond +II are difficult to achieve. Needless to say, the discovery of new oxidation states of Zn will enable us to formulate new reactions and develop new chemistry. This is particularly important as zinc has many applications in the pure metallic state (in alloys), as salts (used as white pigments), as bio-complexes (metallo-enzymes) and as organometallic reagents (used in organic synthesis).

We realize that the major challenge in achieving an oxidation state of +III and higher for Group 12 elements is to involve their inner *d*-orbitals. This is particularly difficult to accomplish for Zn since its third ionization potential is the largest amongst its congeners (39.7 eV, 37.5 eV and 34.2 eV for Zn, Cd and Hg, respectively).[139] Since this decreases as we go down the periodic table, significant effort has been made in the past to achieve higher oxidation states for the heavier element mercury. In 1976, a short-lived $[Hg^{III}(cyclam)]^{3+}$ species generated through electrochemical oxidation was reported.[140]

The +IV state of Hg is expected to be more stable than the +III state since it has the same electronic configuration ($5d^8$) as that of the very stable Au^{3+} cation.[141] Consequently, HgF_4, where Hg is in a +IV oxidation state, was theoretically predicted about twenty years ago.[141-143] However, experimental observation eluded scientists until very recently when it was prepared by matrix isolation method.[144] Also, Kaupp et al. have studied weakly coordinating anions as ligands that can stabilize +IV oxidation state of Hg.[145] Unlike HgF_4, in all cases they found that Hg^{IV} complexes have at least one exothermic fragmentation pathway. Zn has not yet been shown to exist in an oxidation state of +III or higher.

We wondered if highly oxidizing ligands may enable Zn to exhibit +III oxidation state. Armed with the knowledge superhalogens[8] can have electron affinities (EA) far exceeding the value of halogen atoms, we embarked on a systematic study of the interaction of zinc with a variety of atoms and molecules with progressively increasing electron affinities. The high EA of these ligands can be expected to compensate for the large third ionization potential of Zn. In this work we address two fundamentals questions: (1) Can superhalogens stabilize the +III oxidation state of zinc? (2) Must *d*-orbitals be involved to achieve this? We have approached the problem in two ways. First, we have performed a methodical study of the equilibrium geometries and total energies of neutral and anionic ZnX_3 clusters for X = F, BO_2 and AuF_6 using density functional theory. Note that the electron affinities of F, BO_2, and AuF_6 are, respectively, 3.4[146], 4.5[71], and 8.4[25] eV. In case of ZnX_3, for zinc to be in +III oxidation state, it is necessary that zinc is bound to three individual monovalent ligands (X) which are more electronegative than zinc. Second, we have studied a simple ZnF_4^- system and its corresponding ionic salt, $KZnF_4$. Here also, the oxidation state of Zn has to be +III to satisfy the net charge of -1 for the ZnF_4 anion.

6.2.2 Results and Discussions

6.2.2.1 ZnX_3 super and hyperhalogens

The optimized structures of neutral and anionic ZnX_3 are given in Figure 15. ZnX_3^- molecules are expected to be very stable negative ions with large vertical detachment energies (VDE).

Table 8 shows the adiabatic detachment energies (ADE) and vertical detachment energies of ZnX_3^- clusters. The ADE was determined by calculating the energy difference between the anion ground state of a cluster and its neutral. The VDE, on the other hand, was calculated by taking the energy difference between the anion and the neutral, both at the anion ground state geometry. Our calculations show that, indeed, ZnF_3 is a superhalogen, $KZnF_3$ being a well-known perovskite salt.[146] Similarly, we find $Zn(BO_2)_3$ and $Zn(AuF_6)_3$ to be hyperhalogens. The oxidation state of Zn is +II in these anions. To achieve +III oxidation state, ZnX_3 molecules must also be stable as neutrals. The structure, bonding and stability of neutral ZnX_3 are discussed below.

Table 8. Adiabatic Detachment Energies (ADE) and Vertical Detachment Energies (VDE) of ZnX_3 clusters for X=F, BO_2 and AuF_6

Cluster	ADE	VDE
ZnF_3^-	6.20	6.59
$Zn(BO_2)_3^-$	5.63	6.78
$Zn(AuF_6)_3^-$	9.38	9.82

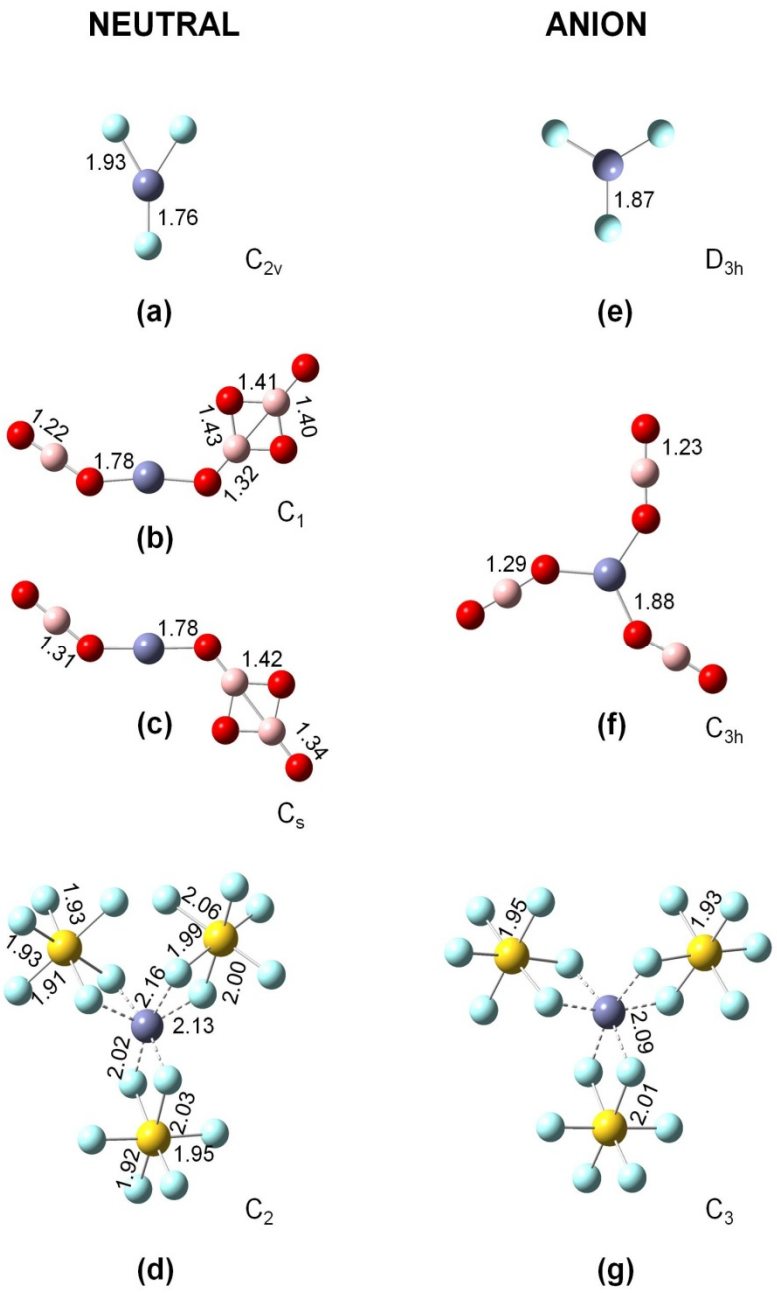

Figure 15. Optimized structures of neutral (a-d) and anionic (e-g) ZnX_3 (X=F, BO_2 and AuF_6) clusters. Bond lengths are in Å.
Purple, blue, yellow, red and pink represent Zn, F, Au, O and B respectively.

6.2.2.2 ZnF_3

ZnF_3 is planar with C_{2v} symmetry and has two Zn-F bond lengths (1.93 Å and 1.76 Å) signifying two different bond strengths. These results are in good agreement with earlier work on ZnF_3 performed at the B3LYP and CCSD(T) levels using effective core potentials, ECP of the Stuttgart group for Zn and aug-cc-pVTZ basis set for F. The F-F bond distance between the two nearest F atoms is 2.04 Å.[147] It is worthwhile to point out that this distance is only slightly longer than the F-F bond distance in F_2^- molecule (2.01 Å). This suggests that the two close F atoms in ZnF_3 are quasi-molecular. The quasi-molecular nature of two of the F atoms in ZnF_3 is further demonstrated in Figure 16 where we compare the charge density contours around the two closest F atoms in ZnF_3 with that around the F atoms in F_2^-. The presence of an F-F quasi-molecular interaction indicates that Zn should be in +II oxidation state, not +III. This can be understood by comparing the molecule with BaO_2. Conventionally, O is assigned an oxidation state of -II in most compounds. However, as there is a peroxo-linkage between the two O atoms in BaO_2, the oxidation state of O is assigned to be –I and that of Ba is not +IV, but +II. Similarly, in ZnF_3, the two quasi-molecular F atoms should each be assigned an oxidation state of -½, thereby making the formal oxidation state of zinc +II. It is important to note that the fragmentation of ZnF_3 into ZnF_2 and ½ F_2 is favorable (see Table S2 in Appendix II). The reaction is slightly exothermic (by 0.06 eV) which confirms earlier work that it is not a stable compound of Zn in +III oxidation state.[147]

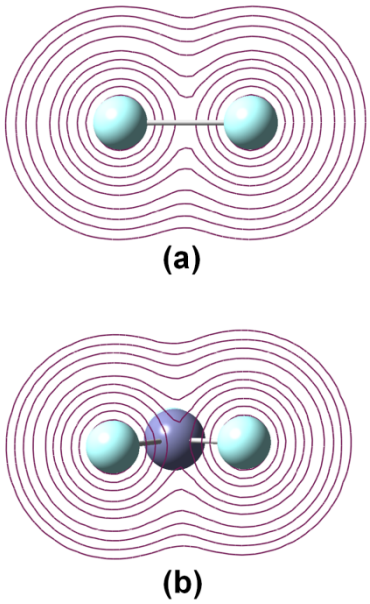

Figure 16. Contour diagrams of (a) isolated F_2^- and (b) two closest F atoms in ZnF_3. The contour diagrams were plotted using default isovalues in Gaussview 5.0. Identical isovalues were used for both molecules.

6.2.2.3 $Zn(BO_2)_3$

Unlike ZnF_3, the ground state of $Zn(BO_2)_3$ is stable with respect to fragmentation (see Table S3 in supporting information). However, here Zn is attached to one BO_2 ligand and one B_2O_4 ligand. This is because two molecules of BO_2 dimerize exothermically (-1.70 eV) to form B_2O_4. The BO_2 and B_2O_4 ligands can be both trans and cis to each other giving rise to two degenerate structures. The significance of this result is that Zn is not in +III oxidation state even though there are three BO_2 units in the molecule. We were able to determine a local minimum geometry where all the BO_2 moieties are attached individually to Zn i.e. a structure where Zn can be in +III oxidation state. However, this structure is 1.07 eV higher in energy than the ground state. Some energetically low-lying structures of neutral and anionic $Zn(BO_2)_3$ are given in Figure S4 and Figure S5.

6.2.2.4 $Zn(AuF_6)_3$

$Zn(AuF_6)_3$ has C_2 symmetry. Zn is surrounded by three AuF_6 units. The three Au atoms form the vertices of an isosceles triangle with the Au-Au distance being 5.92 Å for the equal sides of the triangle and the remaining Au-Au distance being 4.56 Å. The Zn atom is at a distance of 3.15 Å from one Au atom and 3.26 Å from the other two Au atoms. Zn is hexa-coordinated with six F atoms. We note that as in the case of ZnF_3, here also, two AuF_6 moieties are close to each other. However, in contrast to ZnF_3, $Zn(AuF_6)_3$ is stable against all the fragmentation channels studied (see Table S4). Therefore, $Zn(AuF_6)_3$ is a *stable* molecule of Zn in the +III oxidation state.

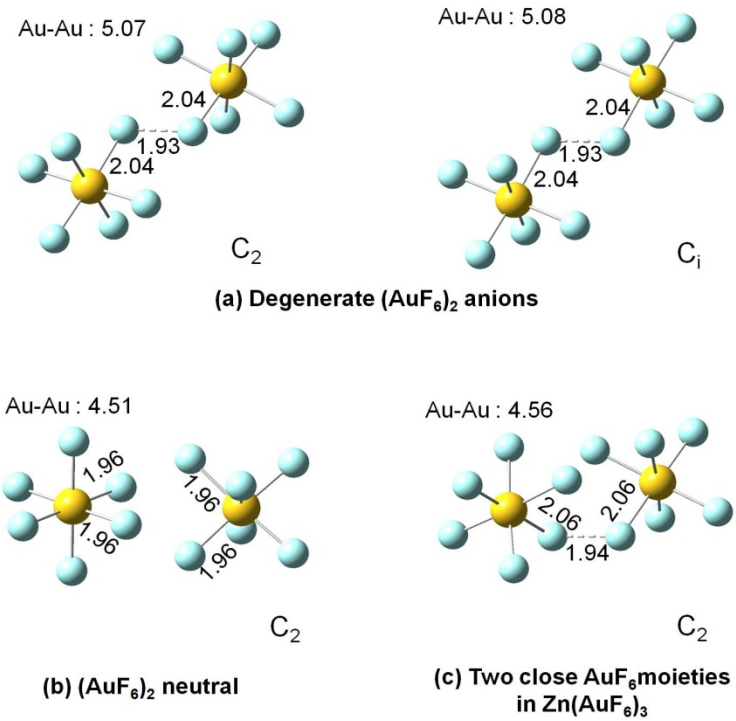

Figure 17. Optimized structures of (a) two degenerate $(AuF_6)_2^-$ anions, (b) isolated $(AuF_6)_2$ and (c) the two close AuF_6 moieties in $Zn(AuF_6)_3$.
Bond lengths are in Å.

6.2.2.5 Charge distribution and stability

Now the question arises if the inner 3*d* electrons are involved in bonding or not in the ZnX_3 clusters. To understand the nature of bonding involved, we computed the Natural Bond Orbitals (NBO) charge distributions (see Table S6 in supporting information). The natural population analysis indicates that the *d*-orbitals of Zn are completely filled in ZnF_3. The NBO charge on Zn is 1.682. The charge on one of the F atoms is -0.821 while the charge on each of the other two quasi-molecular F atoms is about -0.430. This indicates that while one 4*s* electron of Zn is "transferred" to one F atom, the other electron is shared between the remaining two F atoms. In both the cis and trans isomers of $Zn(BO_2)_3$, the charge on Zn is 1.655 while those on the BO_2 and B_2O_4 units are -0.844 and -0.811 respectively, indicating that the two *s* electrons of Zn are transferred to the two ligands. As before, the *d*-orbitals in Zn are completely occupied. In $Zn(AuF_6)_3$, one AuF_6 moiety has a charge of -0.893 whereas the two AuF_6 groups closer to each other have a charge of -0.428 indicating that one *s* electron of Zn is transferred to one AuF_6 ligand while the other *s* electron is shared by the remaining two AuF_6 groups. This is similar to the case of ZnF_3. Again, the natural population analysis suggests that the *d*-orbitals of Zn are completely occupied in $Zn(AuF_6)_3$. To understand why Zn should be in +III oxidation state in $Zn(AuF_6)_3$ while it is in +II oxidation state in ZnF_3, we point out a major difference between the bonding in ZnF_3 and $Zn(AuF_6)_3$. As stated before, the two closest F atoms in ZnF_3 appear to form a quasi-molecular F_2^- unit. Hence, even if ZnF_3 were stable with respect to fragmentation, the oxidation state of Zn would still be +II. This possibility is negated in case of $Zn(AuF_6)_3$. Though two of the AuF_6 moieties are close to each other, they do *not* form a quasi-molecular $(AuF_6)_2^-$ unit. This is because $(AuF_6)_2^-$ itself is *not* a stable molecule as F_2^- is and it fragments into $Au_2F_{11}^-$ and ½ F_2 releasing 0.42 eV of energy. Similarly, neutral $(AuF_6)_2$ is also unstable by

2.02 eV (see Table S1). Also, comparison of the optimized geometries of $(AuF_6)_2$ and $(AuF_6)_2^-$ with the geometry of the two close AuF_6 moieties in $Zn(AuF_6)_3$ show stark differences in the structures (see Figure 17) which further reduce the possibility of quasi-molecular interaction between the two close AuF_6 moieties in $Zn(AuF_6)_3$. Therefore, $Zn(AuF_6)_3$ is a genuine and stable compound of Zn in +III oxidation state. As far as the direct participation of *d*-orbitals in bonding is concerned, we note that NBO charge of +3 in Zn is only possible if bonding is purely ionic. In neutral $Zn(AuF_6)_3$ the bonding is not purely ionic, rather a combination of covalent and ionic bonding is featured. We want to emphasize that here the focus is on Zn in +III oxidation state and *not* in +3 cationic state. We show that Zn does not have to give up a *d*-electron to be in +III oxidation state, though it is a requirement for it to be in +3 cationic state. In this connection, we note that in AuF_6^-, a d^6 system, Au exists in a +V oxidation state, but the NBO charge on Au is not +5, but +2.116. Also, the natural electron configuration is [core] $6s^{0.38}\ 5d^{8.46}$ as opposed to [core] $5d^6$. Moreover, in case of $Hg^{IV}F_4$ (which has been experimentally confirmed[144]), Hg does not give up two *d*-electrons to become a "true" +4 cation according to natural population analysis. As a matter of fact, the NBO charge on Hg is +2.019 and its electronic configuration is [core] $6s^{0.56}\ 5d^{\ 9.37}$ whereas for a true Hg^{4+} cation it should be [core] $5d^8$. Therefore, the formal oxidation state and partial atomic charges are two fundamentally different concepts as had been pointed out earlier by Kaupp and Schnering.[148] Our results imply that to attain the +III oxidation state of Zn, two criteria should be simultaneously satisfied: we require ligands with higher electron affinity and ligands that do not preferentially dimerize. The success of AuF_6 as a ligand is attributed to the fulfillment of these two requirements.

An alternate approach to stabilize Zn(III) is in the form of an anionic molecule. We have studied ZnF_4^- and $KZnF_4$ as potential candidates. Optimized structures and fragmentation energies are given the in the supporting information (Figure S7 and Table S5). We note that an earlier gas phase study had shown that ZnF_4^- is stable with respect to atomic or molecular fluorine ejection.[147] It was suggested that the stability can be increased further by building salts with a counterion. Our calculations indicate that ZnF_4^- is stable in the gas phase. However, it is likely that the formation of the energetically more favorable salt K_2ZnF_4, where zinc is in +II oxidation state, will be preferred over that of $KZnF_4$, especially in the condensed phase. The energies corresponding to the lowest energy fragmentation pathway of all the clusters studied are given in Table 9. To verify the magnitude of these energies, the structures were re-optimized at the M06[134] level using SDD basis[99,100] for Au, aug-cc-pVTZ[135] basis for Zn, B, O, F and 6-311+G* for K.

Table 9. Fragmentation energies of neutral ZnX_3 clusters, ZnF_4^- and $KZnF_4$ for the lowest energy pathways. B3LYP zero-point corrected energies are given in parentheses

Cluster	**Fragmentation Pathway**	**Fragmentation Energy (eV)**	
	Method	B3LYP	M06
	Basis	Au: SDD; Zn, B, O, F, K: 6-311+G*	Au: SDD; K: 6-311+G*; Zn, B, O, F: aug-cc-pvtz
ZnF_3	$ZnF_2 + ½\ F_2$	-0.06 (-0.05)	-0.23
$Zn(BO_2)_3$	$Zn(BO_2)_2 + ½\ B_2O_4$	1.07 (1.03)	1.32
$Zn(AuF_6)_3$	$Zn(AuF_6)_2 + ½\ Au_2F_{10} + ½\ F_2$	0.26 (0.23)	0.17
ZnF_4^-	$ZnF_3^- + ½\ F_2$	0.11 (0.11)	0.01
$KZnF_4$	$½\ K_2ZnF_4 + ½\ ZnF_2 + ½\ F_2$	-0.07 (-0.06)	-0.16

It should be mentioned here that Riedel, Straka and Kaupp have tried to utilize 'weakly coordinating anions' such as AlF_4^-, $Al_2F_7^-$, AsF_6^- etc. to stabilize the +IV oxidation state of Hg.[145]

In their work they have also stated that aggregation of the ligands is a major obstacle to achieving higher oxidation states. Furthermore, it is interesting to note that the weakly coordinating ligands tested were all superhalogens, that is, they all have high electron affinities. In fact, we believe that most weakly coordinating ligands are superhalogens and hence they derive their property to stabilize high oxidation states of metals. Our results open the door for the synthesis of new compounds containing metals in unusual oxidation states with potential for applications. It has already been demonstrated that unusually high oxidations states of elements have important consequences. For example, high valent iron (Fe) such as Fe^{IV} (in oxoferryl porphyrins) and Fe^{V} (in nitridoirons) are important in biochemistry[149] whereas Fe^{VI} (in FeO_4^{2-}) has been used for waste water management.[150]

6.2.3 Conclusions

In summary, we have shown that higher and unusual oxidation states of metals can be achieved using ligands with large electron affinities such as superhalogens. We have demonstrated this with the particular case of $Zn(AuF_6)_3$ in which zinc is in a hitherto unknown +III oxidation state. In addition to bearing large electron affinities, it is also important that these ligands have no tendency to dimerize since the contrary would favor fragmentation of the metal-ligand complex. Equally important, we show that ZnF_3 is a superhalogen with a vertical detachment energy (VDE) of 6.59 eV while $Zn(AuF_6)_3$ is a hyperhalogen with a VDE of 9.82 eV. Consequently, these molecules are predicted to form very stable negative ions. However, in the neutral form, whereas ZnF_3 is *not* stable with respect to fragmentation, $Zn(AuF_6)_3$ *is* by 0.26 eV. Though the oxidation state of zinc in the latter molecule is +III, it seems from the NBO charge distribution and natural population analysis that the *d*-orbitals of zinc are not directly involved in bonding.

We note that the NBO charge alone can be used to determine the oxidation state *if* the bonding is purely ionic, i.e. there is complete charge transfer between the metal and the ligand. However, the situation is less clear when the bonding is partly ionic and partly covalent. Nonetheless, our results show that even in the absence of significant direct involvement of *d*-electrons, it is still possible to increase the degree of oxidation of a species and hence form new compounds by using specific ligands. This finding not only demonstrates a way to enhance the chemistry of zinc but also opens the door for the synthesis of unusual compounds by using the strong oxidizing property of superhalogens.

Chapter 7 Summary

In summary, traditional superhalogens are metal-halogen clusters that supersede Cl in terms of electron affinity. We have studied two types of unconventional superhalogens, namely, borane-based superhalogens and pseudohalogen-based superhalogens.

We find that the Wade-Mingo's rule can also be used as an electron counting rule to design novel superhalogens of borane-derivatives. Unlike conventional superhalogens which have a metal atom at the core surrounded by halogen atoms, the superhalogens formed using the Wade-Mingos rule do not have to have either halogen or metal atoms. We demonstrate this by using $B_{12}H_{13}$ and its isoelectronic cluster, $CB_{11}H_{12}$ as examples. We also show that while conventional superhalogens containing alkali atoms require at least two halogen atoms, only one borane-like moiety is sufficient to render $M(B_{12}H_{12})$ (M=Li, Na, K, Rb, Cs) clusters superhalogen properties. In addition, hyperhalogens can be formed by using the above superhalogens as building blocks. Examples include $M(B_{12}H_{13})_2$ and $M(CB_{11}H_{12})_2$ (M=Li - Cs). This finding opens the door to an untapped source of superhalogens and weakly coordinating anions with potential applications.

Similarly, we find that pseudohalogens can also be used in place of halogens to design new superhalogens. We have shown that when a central Au atom is surrounded by CN moieties, superhalogens can be created with electron detachment energies as high as 8.4 eV. However, there is a stark contrast between the stability of these superhalogens and that of conventional

AuF_n superhalogens. Whereas AuF_n complexes are stable upto n=5 for neutrals and n=6 for anions, $Au(CN)_n$ complexes (with CN moieties attached individually) are metastable beyond n=1 for neutrals and n=3 for anions. This is a major limitation of pseudohalogens in building superhalogens. In addition, we have elucidated important distinctions between electron affinity (EA) and adiabatic detachment energy (ADE), two terms that are often used synonymously in literature.

Furthermore, we have shown one very important application of superhalogens. Superhalogens are expected to be strong oxidizing agents due to their high electron affinities. We have shown that by choosing specific ligands it is possible to increase the oxidation state of a metal beyond what is currently known. We have demonstrated this with the example of $Zn(AuF_6)_3$ where Zn is in a hitherto unknown +III oxidation state.

Currently, we are working on studying how the superhalogen properties of borane-based clusters evolve with size and composition. We are also testing the applications of superhalogens in designing high energy density salts. Since theory based on density functional theory has predictive power, we hope that our research will motivate experimentalists to synthesize bulk materials containing superhalogens and test their applications.

References

1. Nishikawa, K.; Nojima, H. *Jpn. J. Appl. Phys. Part 2 Lett.* **2001**, *40*, L835-L837.

2. Miller, N. J. *J. Ment. Health Adm.* **1984**, *11*, 36-7.

3. Goel, N.; Etwaroo, G. R. *Psychol. Med.* **2006**, *36*, 1253-1263.

4. Marshakov, A. I.; Chebotareva, N. P.; Lukina, N. B. *Prot. Met.* **1992**, *28*, 301-307.

5. Bartlett, N. *Proc. Chem. Soc.* **1962**, 218.

6. Korobov, M. V.; Kuznetsov, S. V.; Sidorov, L. N.; Shipachev, V. A.; Mitkin, V. N. *Int. J. Mass Spectrom. Ion Processes* **1989**, *87*, 13-27.

7. Hotop, H.; Lineberger, W. C. *J. Phys. Chem. Ref. Data* **1985**, *14*, 731-750.

8. Gutsev, G. L.; Boldyrev, A. I. *Chem. Phys.* **1981**, *56*, 277-283.

9. Anusiewicz, I.; Skurski, P. *Chem. Phys. Lett.* **2002**, *358*, 426-434.

10. Anusiewicz, I.; Sobczyk, M.; Dabkowska, I.; Skurski, P. *Chem. Phys.* **2003**, *291*, 171-180.

11. Goebbert, D. J. *Comput. Theo. Chem.* **2011**, *976*, 201-208.

12. Gutsev, G. L. *J. Chem. Phys.* **1993**, *99*, 3906-3912.

13. Gutsev, G. L. *Chem. Phys.* **1992**, *163*, 59-67.

14. Gutsev, G. L. *Chem. Phys. Lett.* **1991**, *184*, 93-98.

15. Gutsev, G. L.; Bartlett, R. J.; Boldyrev, A. I.; Simons, J. *J. Chem. Phys.* **1997**, *107*, 3867-3875.

16. Gutsev, G. L.; Jena, P.; Bartlett, R. J. *Chem. Phys. Lett.* **1998**, *292*, 289-294.

17. Wang, X. B.; Ding, C. F.; Wang, L. S.; Boldyrev, A. I.; Simons, J. *J. Chem. Phys.* **1999**, *110*, 4763-4771.

18. Sikorska, C.; Smuczynska, S.; Skurski, P.; Anusiewicz, I. *Inorg. Chem.* **2008**, *47*, 7348-7354.

19. Elliott, B. M.; Koyle, E.; Boldyrev, A. I.; Wang, X. B.; Wang, L. S. *J. Phys. Chem. A* **2005**, *109*, 11560-11567.

20. Zhao, X. -.; Litherland, A. E. *Nucl. Instrum. Meth. B* **2007**, *259*, 224-229.

21. Marchaj, M.; Freza, S.; Skurski, P. *J. Phys. Chem. A* **2012**, *116*, 1966-1973.

22. Yang, X.; Wang, X. B.; Wang, L. S.; Niu, S. Q.; Ichiye, T. *J. Chem. Phys.* **2003**, *119*, 8311-8320.

23. Yang, J.; Wang, X.; Xing, X.; Wang, L. *J. Chem. Phys.* **2008**, *128*, 201102.

24. Wang, Q.; Sun, Q.; Jena, P. *J. Chem. Phys.* **2009**, *131*, 124301.

25. Koirala, P.; Willis, M.; Kiran, B.; Kandalam, A. K.; Jena, P. *J. Phys. Chem. C* **2010**, *114*, 16018-16024.

26. Pradhan, K.; Gutsev, G. L.; Jena, P. *J. Chem. Phys.* **2010**, *133*, 144301.

27. Pradhan, K.; Gutsev, G. L.; Weatherford, C. A.; Jena, P. *J. Chem. Phys.* **2011**, *134*, 234311.

28. Joseph, J.; Behera, S.; Jena, P. *Chem. Phys. Lett.* **2010**, *498*, 56-62.

29. Joseph, J.; Pradhan, K.; Jena, P.; Wang, H.; Zhang, X.; Jae Ko, Y.; Bowen, K. H. J. *J. Chem. Phys.* **2012**, *136*, 194305.

30. Wu, M. M.; Wang, H. P.; Ko, Y. J.; Wang, Q.; Sun, Q.; Kiran, B.; Kandalam, A. K.; Bowen, K. H.; Jena, P. *Angew. Chem. Int. Ed.* **2011**, *50*, 2568-2572.

31. Craciun, R.; Picone, D.; Long, R. T.; Li, S.; Dixon, D. A.; Peterson, K. A.; Christe, K. O. *Inorg. Chem.* **2010**, *49*, 1056-1070.

32. Siddiqui, S. A. *Struct. Chem.* **2012**, *23*, 267-274.

33. Siddiqui, S. A.; Pandey, A. K.; Rasheed, T.; Mishra, M. *J. Fluorine Chem.* **2012**, *135*, 285-291.

34. Siddiqui, S. A.; Rasheed, T.; Pandey, A. K. *Comput. Theo. Chem.* **2012**, *979*, 119-127.

35. Anusiewicz, I. *J. Phys. Chem. A* **2009**, *113*, 11429-11434.

36. Anusiewicz, I. *J. Phys. Chem. A* **2009**, *113*, 6511-6516.

37. Boldyrev, A. I.; Simons, J. *J. Chem. Phys.* **1993**, *99*, 4628-4637.

38. Boldyrev, A. I.; Vonniessen, W. *Chem. Phys.* **1991**, *155*, 71-78.

39. Enlow, M.; Ortiz, J. V. *J. Phys. Chem. A* **2002**, *106*, 5373-5379.

40. Gutsev, G. L.; Jena, P.; Zhai, H. J.; Wang, L. S. *J. Chem. Phys.* **2001**, *115*, 7935-7944.

41. Gutsev, G. L.; Khanna, S. N.; Rao, B. K.; Jena, P. *Phys. Rev. A* **1999**, *59*, 3681-3684.

42. Gutsev, G. L.; Rao, B. K.; Jena, P.; Wang, X. B.; Wang, L. S. *Chem. Phys. Lett.* **1999**, *312*, 598-605.

43. Gutsev, G. L.; Weatherford, C. A.; Pradhan, K.; Jena, P. *J. Comput. Chem.* **2011**, *32*, 2974-2982.

44. Pradhan, K.; Gutsev, G. L.; Weatherford, C. A.; Jena, P. *J. Chem. Phys.* **2011**, *134*, 144305.

45. Swierszcz, I.; Anusiewicz, I. *Chem. Phys.* **2011**, *383*, 93-100.

46. Swierszcz, I.; Skurski, P. *Chem. Phys. Lett* **2012**, *537*, 27-32.

47. Zhai, H. J.; Li, J.; Wang, L. S. *J. Chem. Phys.* **2004**, *121*, 8369-8374.

48. Pathak, B.; Samanta, D.; Ahuja, R.; Jena, P. *Chemphyschem* **2011**, *12*, 2422-2427.

49. Mingos, D. M. P. *Acc. Chem. Res.* **1984**, *17*, 311-319.

50. Mingos, D. M. P. *Nat. Phys. Sci.* **1972**, *236*, 99-&.

51. Wade, K. *Chem. Commun.* **1971**, 792.

52. Wade, K. *Adv. Inorg. Chem. Radiochem.* **1976**, *18*, 1.

53. Samanta, D.; Wu, M. M.; Jena, P. *Inorg. Chem.* **2011**, *50*, 8918-8925.

54. Samanta, D.; Wu, M. M.; Jena, P. *J. Phys. Chem. Lett.* **2011**, *2*, 3027-3031.

55. Samanta, D.; Jena, P. *J. Am. Chem. Soc.* **2012**, *134*, 8400-8403.

56. Miller, T. M.; Leopold, D. G.; Murray, K. K.; Lineberger, W. C. *J. Chem. Phys.* **1986**, *85*, 2368-2375.

57. Lewis, G. N. *J. Am. Chem. Soc.* **1916**, *38*, 762-785.

58. Langmuir, I. *J. Am. Chem. Soc.* **1919**, *41*, 868-934.

59. Langmuir, I. *Science* **1921**, *54*, 59-67.

60. Mitchell, P. R.; Parish, R. V. *J. Chem. Educ.* **1969**, *46*, 811-814.

61. Jensen, W. B. *J. Chem. Educ.* **2005**, *82*, 28-28.

62. Franklin, J. L.; Harland, P. W. *Ann. Rev. Phys. Chem.* **1974**, *25*, 485-526.

63. Alexandrova, A. N.; Boldyrev, A. I.; Fu, Y. J.; Yang, X.; Wang, X. B.; Wang, L. S. *J. Chem. Phys.* **2004**, *121*, 5709-5719.

64. Anusiewicz, I. *Aust. J. Chem.* **2008**, *61*, 712-717.

65. Anusiewicz, I.; Skurski, P. *Chem. Phys. Lett.* **2007**, *440*, 41-44.

66. Gutsev, G. L. *Chem. Phys.* **1991**, *158*, 33-39.

67. Sikorska, C.; Skurski, P. *Chem. Phys. Lett.* **2012**, *536*, 34-38.

68. Yin, B.; Li, J.; Bai, H.; Wen, Z.; Jiang, Z.; Huang, Y. *Phys. Chem. Chem. Phys.* **2012**, *14*, 1121-1130.

69. Freza, S.; Skurski, P. *Chem. Phys. Lett.* **2010**, *487*, 19-23.

70. Wang, X. B.; Wang, L. S. *J. Chem. Phys.* **2000**, *113*, 10928.

71. Zhai, H.; Wang, L.; Li, S.; Wang, L. *J. Phys. Chem. A* **2007**, *111*, 1030-1035.

72. Willis, M.; Gotz, M.; Kandalam, A. K.; Gantefor, G. F.; Jena, P. *Angew. Chem. Int. Ed.* **2010**, *49*, 8966-8970.

73. Sikorska, C.; Skurski, P. *Inorg. Chem.* **2011**, *50*, 6384-6391.

74. Bae, G.; Cha, J.; Lee, H.; Park, W.; Park, N. *Carbon* **2012**, *50*, 851-856.

75. Wudl, F. *Acc. Chem. Res.* **1984**, ***17,*** 227-232.

76. Yang, H.; Li, Y.; Wu, D.; Li, Z. *Int. J. Quantum Chem.* **2012**, *112*, 770-778.

77. Smuczynska, S.; Skurski, P. *Inorg. Chem.* **2009**, *48*, 10231-10238.

78. Schrodinger, E. *Phys. Rev.* **1926**, *28*, 1049-1070.

79. Born, M.; Oppenheimer, J. R. *Ann. Physik.* **1927**, *41*, 457-484.

80. Hartree, D. R. *Proc. Cambridge. Philos. Soc.* **1928**, *24*, 89-110.

81. Fock, V. *Z. Physik.* **1930**, *61*, 126-148.

82. Moller, C.; Plesset, M. S. *Phys. Rev.* **1934**, *46*, 618-622.

83. Cizek, J. *J. Chem. Phys.* **1966**, *45*, 4256-4266.

84. Thomas, L. H. *Proc. Cambridge. Philos. Soc.* **1927**, *23*, 542-548.

85. Fermi, E. *Rend. Accad. Naz. Lincei* **1927**, *6*, 602-607.

86. Dirac, P. A. M. *Proc. Cambridge. Philos. Soc.* **1930**, *26*, 376-385.

87. Hohenberg, P.; Kohn, W. *Phys. Rev.* **1964**, *136*, B864-B871.

88. Kohn, W.; Sham, L. J. *Phys. Rev.* **1965**, *140*, A1133-A1138.

89. Vosko, S. J.; Wilk, L.; Nusair, M. *Can. J. Phys.* **1980**, *58*, 1200-1211.

90. Becke, A. D. *Phys. Rev. A* **1988**, *38*, 3098-3100.

91. Perdew, J. P.; Wang, W. *Phys. Rev. B* **1992**, *45*, 13244-13249.

92. Becke, A. D. *J. Chem. Phys.* **1993**, *98*, 5648-5652.

93. Lee, C. T.; Yang, W. T.; Parr, R. G. *Phys. Rev. B* **1988**, *37*, 785-789.

94. Slater, J. C. *Phys. Rev.* **1930**, *36*, 57-64.

95. Gill, P. M. W. *Adv. Quantum Chem.* **1994**, *25*, 141-205.

96. Hehre, W. J.; Stewart, R. F.; Pople, J. A. *J. Chem. Phys.* **1969**, *51*, 2657-2664.

97. Krishnan, R.; Binkley, J. S.; Seeger, R.; Pople, J. A. *J. Chem. Phys.* **1980**, *72*, 650-654.

98. Mclean, A. D.; Chandler, G. S. *J. Chem. Phys.* **1980**, *72*, 5639-5648.

99. Schwerdtfeger, P.; Dolg, M.; Schwarz, W. H. E.; Bowmaker, G. A.; Boyd, P. D. W. *J. Chem. Phys.* **1989**, *91*, 1762-1774.

100. Dolg, M.; Wedig, U.; Stoll, H.; Preuss, H. *J. Chem. Phys.* **1987**, *86*, 866-872.

101. Frish, M. J. et al. Gaussian 03, Revision D.02, Gaussian, Inc., Wallingford CT, 2004.

102. Frish, M. J. et al. Gaussian 09, Revision B.01, Gaussian, Inc., Wallingford CT, 2010.

103. Feakes, D. A.; Waller, R. C.; Hathaway, D. K.; Morton, V. S. *Proc. Natl. Acad. Sci. U. S. A.* **1999**, *96*, 6406-6410.

104. Lesnikowski, Z. J.; Paradowska, E.; Olejniczak, A. B.; Studzinska, M.; Seekamp, P.; Schussler, U.; Gabel, D.; Schinazi, R. F.; Plesek, J. *Bioorg. Med. Chem.* **2005**, *13*, 4168-4175.

105. Locher, G. L. *Am. J. Roentgenol. Rad. Ther.* **1936**, *36*, 1-13.

106. Shelly, K.; Feakes, D. A.; Hawthorne, M. F.; Schmidt, P. G.; Krisch, T. A.; Bauer, W. F. *Proc. Natl. Acad. Sci. U. S. A.* **1992**, *89*, 9039-9043.

107. Sivaev, I. B.; Bregadze, V. V. *Eur. J. Inorg. Chem.* **2009**, *2009*, 1433-1450.

108. Lesnikowski, Z. J. *Collect. Czech. Chem. Commun.* **2007**, *72*, 1646-1658.

109. Greenwood, N. N. *Coord. Chem. Rev.* **2002**, *226*, 61-69.

110. Finze, M.; Bernhardt, E.; Willner, H. *Angew. Chem. Int. Ed.* **2007**, *46*, 9180-9196.

111. Jelinek, T.; Baldwin, P.; Scheidt, W. R.; Reed, C. A. *Inorg. Chem.* **1993**, *32*, 1982-1990.

112. Zuttel, A.; Wenger, P.; Rentsch, S.; Sudan, P.; Mauron, P.; Emmenegger, C. *J. Power Sources* **2003**, *118*, 1-7.

113. Srinivasu, K.; Ghosh, S. K. *J. Phys. Chem. C* **2011**, *115*, 1450-1456.

114. Lin, Y.; Mao, W. L.; Mao, H. K. *Proc. Natl. Acad. Sci. U. S. A.* **2009**, *106*, 8113-8116.

115. Jemmis, E. D.; Balakrishnarajan, M. M.; Pancharatna, P. D. *Chem. Rev.* **2002**, *102*, 93-144.

116. Li, X.; Grubisic, A.; Stokes, S. T.; Cordes, J.; Gantefoer, G. F.; Bowen, K. H.; Kiran, B.; Willis, M.; Jena, P.; Burgert, R.; Schnoeckel, H. *Science* **2007**, *315*, 356-358.

117. Li, S.; Willis, M.; Jena, P. *J. Phys. Chem. A* **2010**, *114*, 16849-16854.

118. Mebel, A. M.; Najafian, K.; Charkin, O. P.; Schleyer, P. V. *J. Mol. Struct. Theochem* **1999**, *461*, 187-202.

119. Kardahakis, S.; Koukounas, C.; Mavridis, A. *J. Chem. Phys.* **2005**, *122*, 054312.

120. Wu, Z. J.; Kawazoe, Y. *Chem. Phys. Lett.* **2006**, *423*, 81-86.

121. Birckenbach, L.; Kellerman, K. *Ber. Dtsch. Chem. Ges.* **1925**, *58B*, 786-794.

122. Bergendahl, T. J. *J. Chem. Educ.* **1975**, *52*, 731-732.

123. Wannenmacher, E. A. J.; Lin, H.; Jackson, W. M. *J. Phys. Chem.* **1990**, *94*, 6608-6615.

124. Rubo, A.; Kellens, R.; Reddy, J.; Steier, N.; Hasenpusch, W. *Alkali Metal Cyanides*; Wiley-VCH Verlag GmbH & Co. KGaA: Weinheim, Germany, **2006**.

125. Kjeldsen, P. *Water Air Soil Poll.* **1999**, *115*, 279-307.

126. Tsuchida, R. *Bull. Chem. Soc. Jpn.* **1938**, *13*, 388-400.

127. Wang, X. B.; Wang, Y. L.; Yang, J.; Xing, X. P.; Li, J.; Wang, L. S. *J. Am. Chem. Soc.* **2009**, *131*, 16368-16370.

128. Wu, X.; Qin, Z. B.; Xie, H.; Cong, R.; Wu, X. H.; Tang, Z. C.; Fan, H. J. *J. Phys. Chem. A* **2010**, *114*, 12839-12844.

129. Yates, R. E.; Blauer, J. A.; Greenbau, M. A; Farber, M. *J. Chem. Phys.* **1966**, *44*, 498-504.

130. Botschwina, P.; Flugge, J. *Chem. Phys. Lett.***1991**, *180*, 589-593.

131. Ding, Y. H.; Huang, X. R.; Li, Z. S.; Sun, C. C. *J. Chem. Phys.* **1998**, *108*, 2024-2027.

132. Jiang, Z. Y.; Xu, X. H.; Wu, H. S.; Jin, Z. H. *Int. J. Mass Spectrom.* **2003**, *230*, 33-39.

133. Hay, P. J.; Wadt, W. R. *J. Chem. Phys.* **1985**, *82*, 299-310.

134. Zhao, Y.; Truhlar, D. G. *Theo. Chem. Acc.* **2008**, *120*, 215-241.

135. Kendall, R. A.; Dunning, T. H.; Harrison, R. J. *J. Chem. Phys.* **1992**, *96*, 6796-6806.

136. Gutsev, G. L.; Khanna, S. N.; Jena, P. *Phys. Rev. B* **2000**, *62*, 1604-1606.

137. Shelly, K.; Reed, C. A.; Lee, Y. J.; Scheidt, W. R. *J. Am. Chem. Soc.* **1986**, *108*, 3117-3118.

138. IUPAC. *Compendium of Chemical Terminology*, 2nd ed. (the"Gold Book"); McNaught, A. D.; Wilkinson, A., compilers; Blackwell Scientific Publications: Oxford, U.K., 1997.

XML online corrected version: Nic, M.; Jirat, J.; Kosata, B., creators; Jenkins, A., update compiler; http://goldbook.iupac.org (accessed March 26, 2012).

139. Moore, C. E. *Ionization Potentials and Ionization Limits Derived from the Analysis of Optical Spectra*; National Standard Reference Data Series 34; National Bureau of Standards: Washington, DC, 1970.

140. Deming, R. L.; Allred, A. L.; Dahl, A. R.; Herlinger, A. W.; Kestner, M. O. *J. Am. Chem. Soc.* **1976**, *98*, 4132-4137.

141. Jorgensen, C. K. *Z. Anorg. Und Allg. Chem.* **1986**, *541*, 91-105.

142. Kaupp, M.; Vonschnering, H. G. *Angew. Chem. Int. Ed.* **1993**, *32*, 861-863.

143. Kaupp, M.; Dolg, M.; Stoll, H.; Vonschnering, H. G. *Inorg. Chem.* **1994**, *33*, 2122-2131.

144. Wang, X.; Andrews, L.; Riedel, S.; Kaupp, M. *Angew. Chem. Int. Ed.* **2007**, *46*, 8371-8375.

145. Riedel, S.; Straka, M.; Kaupp, M. *Chem.-Eur. J.* **2005**, *11*, 2743-2755.

146. Parhi, P.; Manivannan, V. *Mater. Lett.* **2008**, *62*, 3468-3470.

147. Riedel, S.; Kaupp, M.; Pyykkoe, P. *Inorg. Chem.* **2008**, *47*, 3379-3383.

148. Kaupp, M.; von Schnering, H. G. *Angew. Chem. Int. Ed.* **1995**, *34*, 986.

149. Nakamoto, K. *Coord. Chem. Rev.* **2002**, *226*, 153-165.

150. Ghernaout, D.; Naceur, M. W. *Desalin. Water Treat.* **2011**, *30*, 319-332.

Appendix I

Isomers of $Au(CN)_3$

To search for the ground state of the anionic and neutral geometry of the $Au(CN)_3$ cluster, we started the optimization with 22 different initial structures. In all cases, the frequencies were found to be positive after optimization indicating these structures are at least dynamically stable.

I-1 Dissociative attachment of CN to Au in $Au(CN)_3$ and $Au(CN)_3^-$

We optimized 6 different geometries for this mode of attachment and they are shown in Figure S1. Blue represents N, grey represents C and yellow represents Au.

I-2 Attachment of CN after dimerization to Au in $Au(CN)_3$ and $Au(CN)_3^-$

We optimized eight different geometries for this mode of attachment and they are shown in Figure S2.

I-3 Attachment of CN after trimerization to Au in $Au(CN)_3$ and $Au(CN)_3^-$

We optimized 8 different geometries for this mode of attachment and they are shown in Figure S3. Other configurations outside those shown below are also possible. However, note that the energies of all the isomers are about 3 eV higher than the ground state structures shown in Figure 1 (a) and therefore, are not of significant interest.

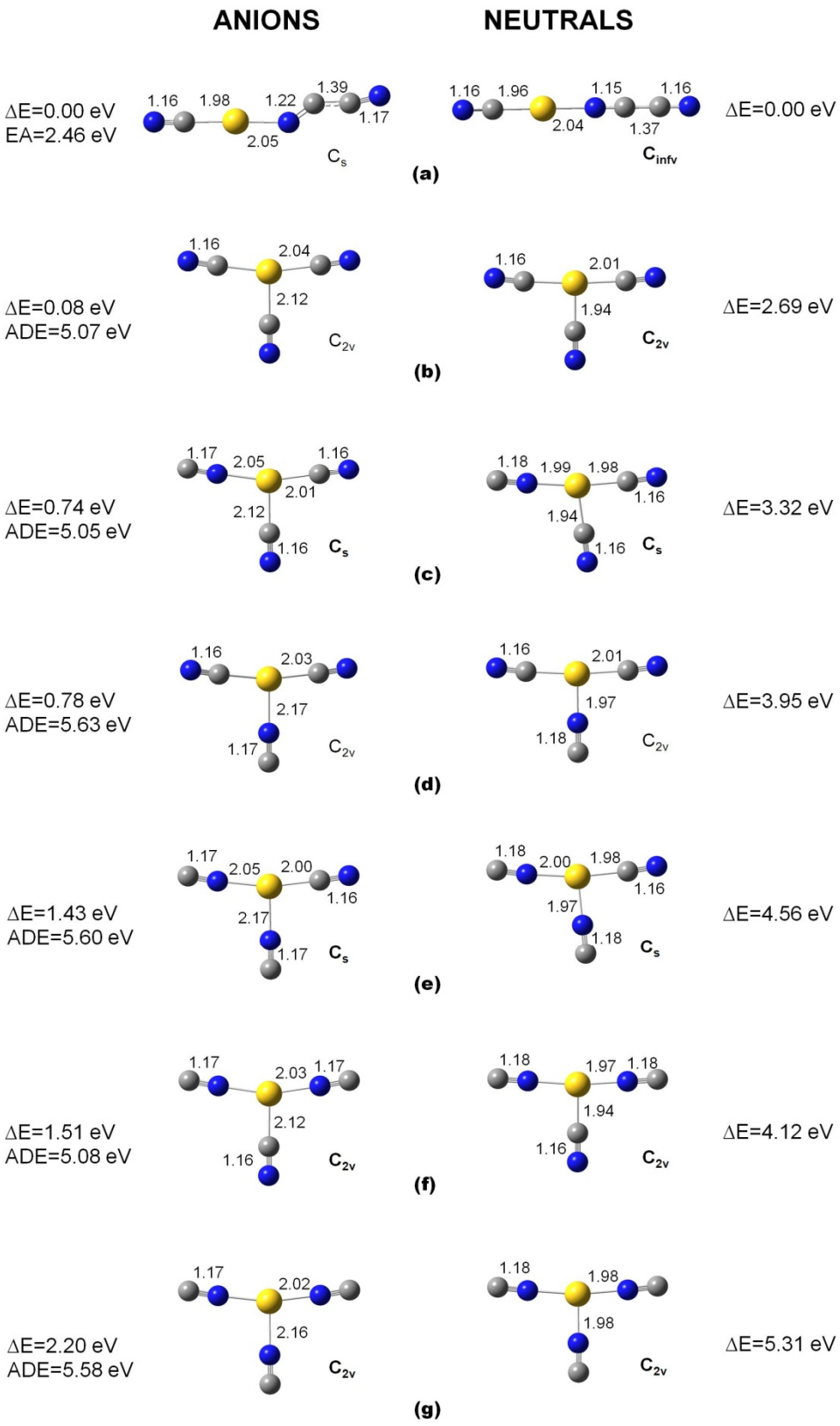

Figure S1. Isomers of $Au(CN)_3$ for dissociative attachment of CN

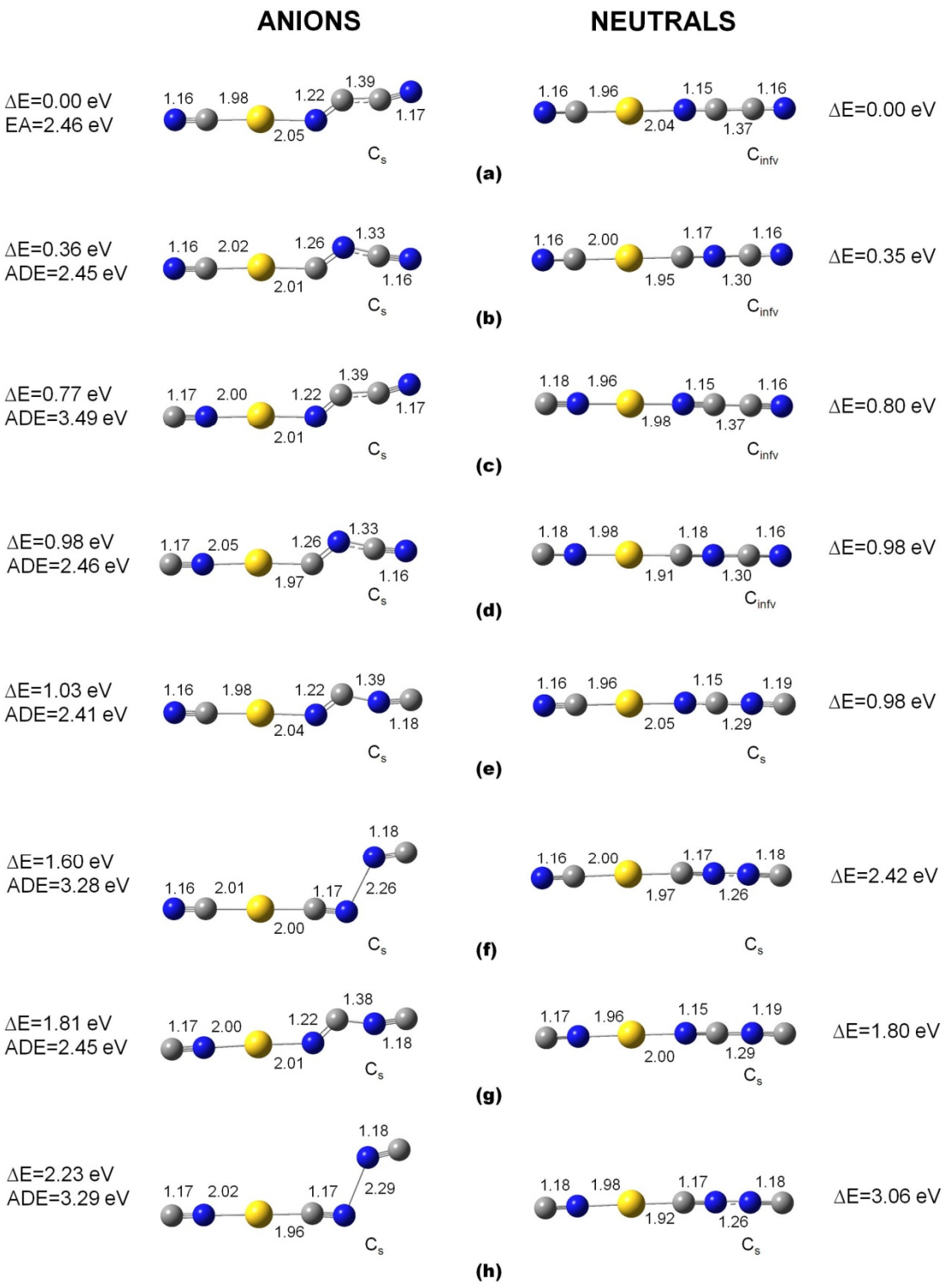

Figure S2. Isomers of $Au(CN)_3$ for attachment of CN after dimerization

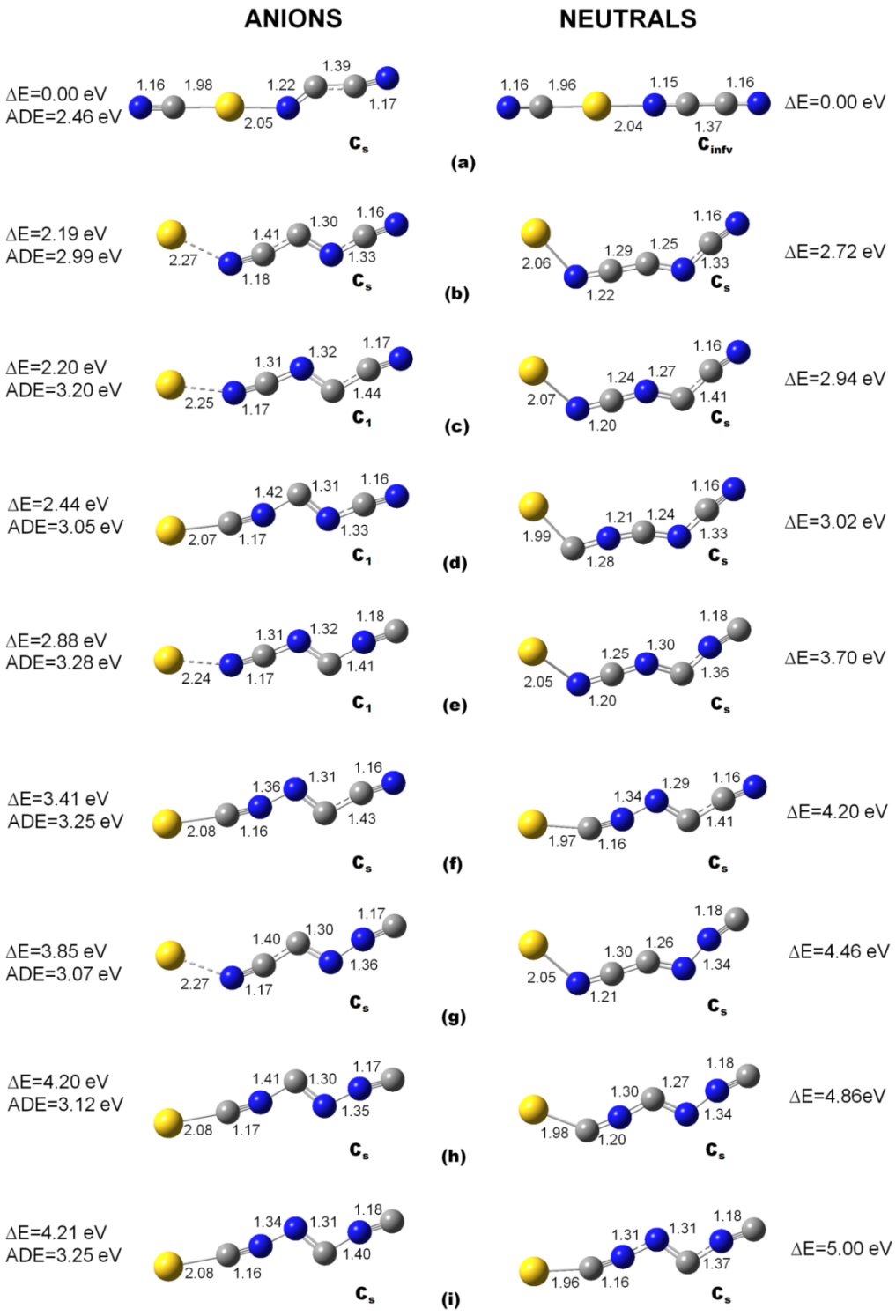

Figure S3. Isomers of $Au(CN)_3$ for attachment of CN after trimerization

Appendix II

Supporting Information for Zn in +III Oxidation State

II-1 Optimized geometries of isomers of $Zn(BO_2)_3$

To obtain the lowest energy structures, calculations were performed at the B3LYP/6-311+G* level starting with several initial geometries. Calculations revealed that indeed many isomers are possible for both neutral and anionic $Zn(BO_2)_3$ clusters. Some of the energetically low-lying isomers are shown in Figure S4 and Figure S5. Note, more isomers, especially rotamers may also exist. All the structures presented below are optimized structures and they contain no imaginary frequencies indicating their dynamic stability.

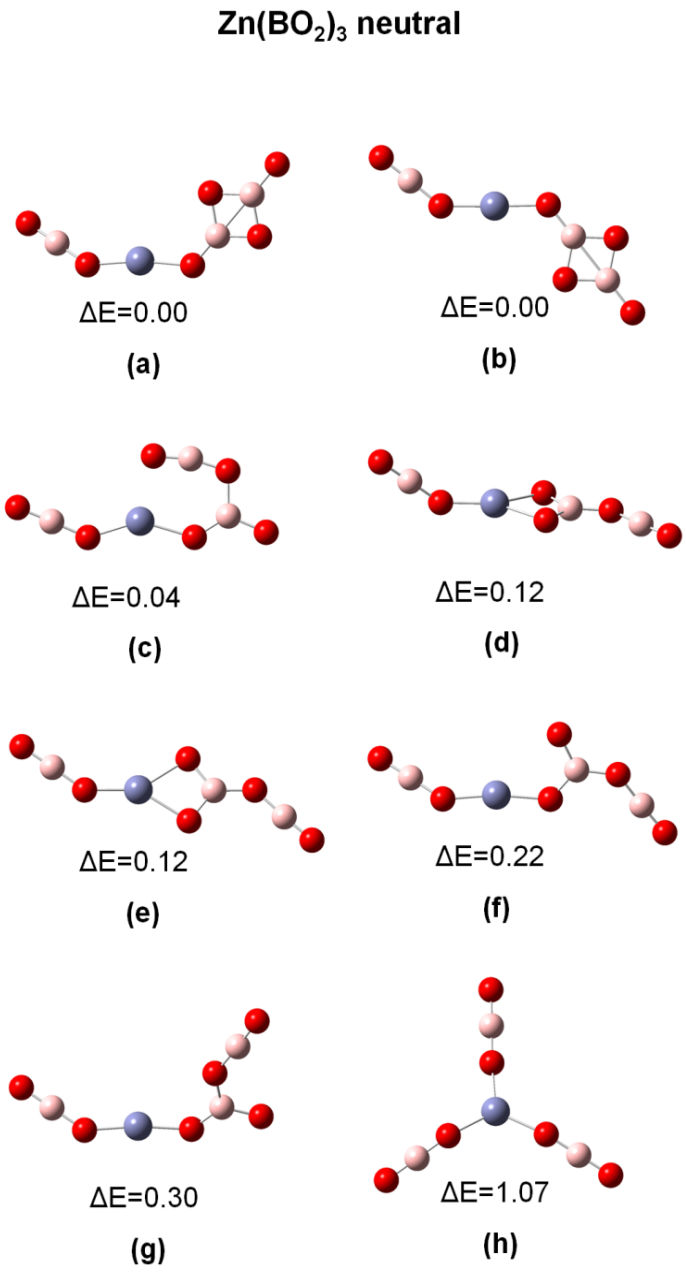

Figure S4. Some energetically low-lying isomers of neutral $Zn(BO_2)_3$

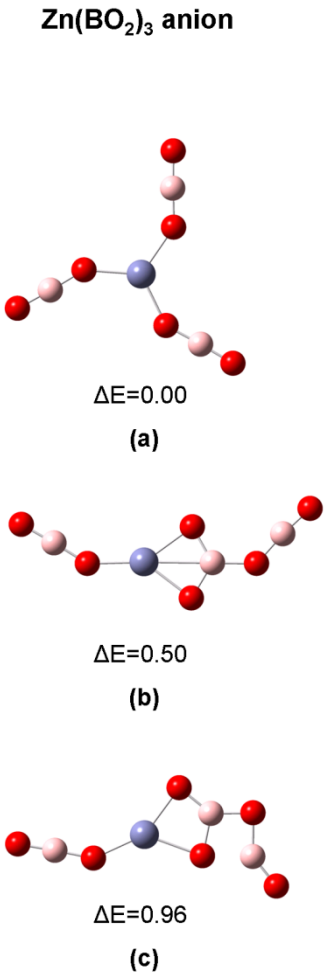

Figure S5. Some energetically low-lying isomers of $Zn(BO_2)_3$ anion

II-2 Fragmentation energies of the clusters studied

To study the thermodynamic stability of these molecules, we calculated the energies associated with different fragmentation pathways. We report all energies without zero point corrections as these do not alter thermochemistry significantly. All calculations have been done using the B3LYP hybrid functional for exchange-correlation potential. The 6-311+G* basis set for Zn, F, B and O and Stuttgart pseudopotential SDD for Au have been used.

The fragmentation energies (ΔE), i.e. the energy needed to fragment the parent cluster into the products are tabulated in Table S1-Table S5. Note that positive value of ΔE means that the parent cluster is stable against the dissociation channel indicated. During the fragmentation of a negative ion species, the negative charge will be borne by the fragment with a higher ADE value. For example, when ZnF^- fragments into Zn and F, the negative charge will be on F (electron affinity of F is 3.40 eV) and not on Zn (electron affinity of Zn is 1.03 eV). Also, species that form stable dimers will not be ejected as monomers. For example, ZnF will not dissociate preferentially into Zn and F, but to Zn and ½ F_2.

To understand ligand behavior, first we have calculated the fragmentation energies of neutral and anionic X_2 where X=F, BO_2 and AuF_6. Then we have calculated fragmentation energies of neutral and anionic ZnX_3 clusters, ZnF_4^- and $KZnF_4$. Since dispersion interactions are important for the stability of clusters such as $(AuF_6)_2$ and $(AuF_6)_2^-$, we have repeated the calculation of lowest energy fragmentation pathway of these two clusters at the M06 level using SDD basis for Au and aug-cc pVTZ for F. These energy values are given in parenthesis in Table S1.

Table S1. Fragmentation energies of neutral and anionic X_2 (X= F, BO_2 and AuF_6)

Clusters	Fragmentation Products	ΔE
F_2	2 F	1.38
F_2^-	F^- + ½ F_2	1.12
	F + F^-	1.81
$(BO_2)_2$	2 BO_2	1.70
$(BO_2)_2^-$	BO_2^- + ½ B_2O_4	1.21
	BO_2 + BO_2^-	2.06
$(AuF_6)_2$	Au_2F_{10} + F_2	-2.02 (-2.04)
	2 AuF_4 + 2 F_2	-0.80
	AuF_6 + AuF_6	-0.16
$(AuF_6)_2^-$	$Au_2F_{11}^-$ + ½ F_2	-0.42 (-0.61)
	$Au_2F_{11}^-$ + F	0.27
	$Au_2F_{10}^-$ + F_2	0.32
	AuF_4 + F_2 + AuF_6^-	1.07
	AuF_6 + AuF_6^-	1.39
	Au_2F_{10} + F_2^-	4.06

Table S2. Fragmentation energies of neutral and anionic ZnF_3 clusters

Clusters	Fragmentation Products	ΔE
ZnF_3	$ZnF_2 + ½ F_2$	-0.06[a]
	$ZnF_2 + F$	0.63[a]
	$ZnF + F_2$	4.16[a]
ZnF_3^-	$ZnF_2 + F^-$	3.35
	$ZnF_2^- + ½ F_2$	4.89
	$ZnF_2^- + F$	5.58
	$ZnF + F_2^-$	6.44
	$ZnF^- + F_2$	8.24

[a] Earlier work by Riedel et al. has found these energies to be -0.24 eV, 0.56 eV and 3.97 eV respectively, at the B3LYP level and -0.61 eV, 0.18 eV and 3.90 eV respectively at the CCSD(T) level using effective core pseudopotential for Zn and aug-cc-pVTZ for F atom.[147] Our value is different since we have used an all electron basis set 6-311+G* for Zn.

Table S3. Fragmentation energies of neutral and anionic $Zn(BO_2)_3$ clusters

Cluster	Fragmentation Products	ΔE
$Zn(BO_2)_3$	$Zn(BO_2)_2 + ½ B_2O_4$	1.07[α]
	$Zn(BO_2)_2 + BO_2$	1.92
	$ZnBO_2 + B_2O_4$	4.11
$Zn(BO_2)_3^-$	$Zn(BO_2)_2 + BO_2^-$	3.20
	$Zn(BO_2)_2^- + ½ B_2O_4$	4.07
	$Zn(BO_2)_2^- + BO_2$	4.92
	$ZnBO_2 + B_2O_4^-$	5.03
	$ZnBO_2^- + B_2O_4$	6.80

Table S4. Fragmentation energies of neutral and anionic $Zn(AuF_6)_3$ clusters

Cluster	Fragmentation products	ΔE
	$Zn(AuF_6)_2 + ½\ Au_2F_{10} + ½\ F_2$	0.26
	$Zn(AuF_6)_2 + AuF_4 + F_2$	0.87
	$Zn(AuF_6)_2 + AuF_6$	1.19
	$ZnAuF_6 + Au_2F_{10} + F_2$	2.16
$Zn(AuF_6)_3$	$ZnF_2 + {}^3/_2\ Au_2F_{10} + ½\ F_2$	2.57
	$ZnF_2 + Au_2F_{10} + AuF_4 + F_2$	3.18
	$ZnAuF_6 + 2\ AuF_4 + 2F_2$	3.38
	$ZnAuF_6 + 2\ AuF_5 + F_2$	4.50
	$ZnF_2 + 3\ AuF_3 + {}^7/_2\ F_2$	7.20
	$Zn(AuF_6)_2 + AuF_6^-$	2.13
	$Zn(AuF_6)_2^- + ½\ Au_2F_{10} + ½\ F_2$	2.84
	$Zn(AuF_6)_2^- + AuF_4 + F_2$	3.44
$Zn(AuF_6)_3^-$	$ZnAuF_6 + (AuF_6)_2^-$	3.57
	$Zn(AuF_6)_2^- + ½\ (AuF_6)_2$	3.85
	$Zn(AuF_6)_2 + ½\ Au_2F_{10}^- + ½\ F_2^-$	3.85
	$ZnAuF_6 + Au_2F_{10}^- + F_2$	3.89

[α]This energy at the M06 optimized level using aug-cc-pVTZ for Zn, B, O and F is 1.32 eV. The M06 optimized $Zn(BO_2)_3$ structure contains one imaginary frequency. If the imaginary frequency is removed, the energy of the structure will further decrease, thereby increasing ΔE. That is, the cluster will be slightly more stable than indicated by these numbers.

Table S5. Fragmentation energies of neutral and anionic ZnF_4^- and $KZnF_4$ clusters

Cluster	Fragmentation products	ΔE
ZnF_4^-	$ZnF_3^- + ½\ F_2$	0.11
	$ZnF_3^- + F$	0.80
	$ZnF_2 + F_2^-$	2.34
	$ZnF_3 + F^-$	3.52
	$ZnF_2^- + F_2$	5.00
	$ZnF^- + {}^3/_2\ F_2$	8.35
$KZnF_4$	$½\ K_2ZnF_4 + ½\ ZnF_2 + ½\ F_2$	-0.07
	$KZnF_3 + ½\ F_2$	0.41
	$KZnF_3 + F$	1.10
	$KF + ZnF_2 + ½\ F_2$	2.09

II-3 NBO charge distribution in neutral and anionic ZnX_3 clusters (X=F, BO_2, AuF_6), ZnF_4^- and $KZnF_4$

Natural Bond Orbital (NBO) charges were calculated for the lowest energy ZnX_3, ZnF_4^- and $KZnF_4$ clusters where X=F, BO_2, AuF_6. These NBO charges denote the electronic charge distribution over each atom and hence are indicative of the nature of bonding involved. The NBO charges for the lowest energy structures of different ZnX_3 clusters studied are presented below in Table S6. Figure S6 shows the numbering scheme used for the atoms.

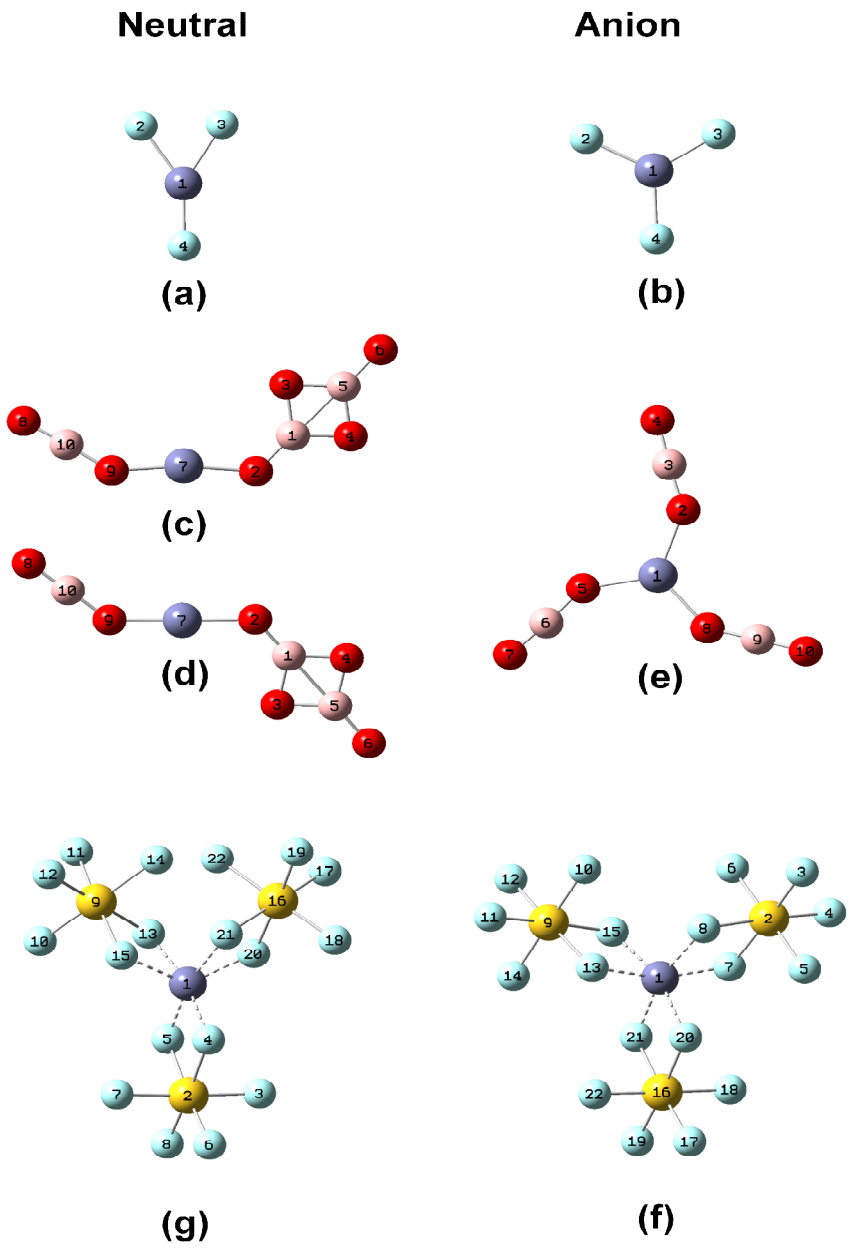

Figure S6. Numbering scheme for the atoms in ZnX_3 and ZnX_3^- clusters

Table S6. NBO charge distribution in ZnX_3 and ZnX_3^- clusters

Cluster	Neutral				Anion		
	Atom	Number	Natural Charge		Atom	Number	Natural Charge
ZnF_3	Zn	1	1.682		Zn	1	1.688
	F	2	-0.426		F	2	-0.896
	F	3	-0.434		F	3	-0.896
	F	4	-0.821		F	4	-0.896
			cis	trans			
$Zn(BO_2)_3$	B	1	1.210	1.211	Zn	1	1.751
	O	2	-1.120	-1.121	O	2	-1.181
	O	3	-0.860	-0.850	B	3	1.177
	O	4	-0.827	-0.827	O	4	-0.913
	B	5	1.107	1.106	O	5	-1.182
	O	6	-0.320	-0.321	B	6	1.177
	Zn	7	1.654	1.655	O	7	-0.913
	O	8	-0.836	-0.837	O	8	-1.181
	O	9	-1.191	-1.190	B	9	1.177
	B	10	1.184	1.183	O	10	-0.913
$Zn(AuF_6)_3$	Zn	1	1.749		Zn	1	1.753
	Au	2	2.134		Au	2	2.136
	F	3	-0.484		F	3	-0.433
	F	4	-0.631		F	4	-0.433
	F	5	-0.631		F	5	-0.493
	F	6	-0.394		F	6	-0.490
	F	7	-0.493		F	7	-0.602
	F	8	-0.394		F	8	-0.603
	Au	9	2.123		Au	9	2.136
	F	10	-0.355		F	10	-0.490
	F	11	-0.396		F	11	-0.433
	F	12	-0.399		F	12	-0.433
	F	13	-0.586		F	13	-0.603
	F	14	-0.227		F	14	-0.493
	F	15	-0.588		F	15	-0.602
	Au	16	2.123		Au	16	2.136
	F	17	-0.399		F	17	-0.433
	F	18	-0.355		F	18	-0.491
	F	19	-0.396		F	19	-0.433
	F	20	-0.589		F	20	-0.603
	F	21	-0.586		F	21	-0.603
	F	22	-0.226		F	22	-0.492

Figure S7 shows the optimized structures and numbering scheme used for ZnF_4^- and $KZnF_4$ clusters. The NBO charge distribution is shown in Table S7.

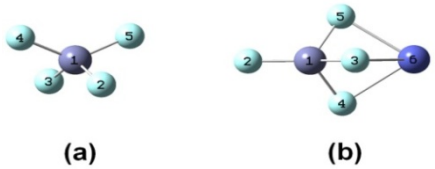

Figure S7. Optimized geometries with numbering schemes of ZnF_4^- and $KZnF_4$

Table S7. NBO charge distribution in ZnF_4^- and $KZnX_4$ clusters

Cluster	Atom	Number	Natural Charge
ZnF_4^-	Zn	1	1.855
	F	2	-0.713
	F	3	-0.714
	F	4	-0.714
	F	5	-0.714
$KZnF_4$	Zn	1	1.820
	F	2	-0.651
	F	3	-0.650
	F	4	-0.748
	F	5	-0.754
	K	6	0.983

Vita

Devleena Samanta was born on August 2, 1989 in Kolkata, India. She graduated from St. Xavier's College, Kolkata with a Bachelor of Science degree in Chemistry (honors) in 2010. She worked as a research scholar for two months at Virginia Commonwealth University (VCU) in 2008. In the summer of 2009, she interned at Central Glass and Ceramic Research Institute in Kolkata, India. Since August 2010, as a graduate student at VCU, she has been a teaching assistant for four semesters and a research assistant for two semesters. Her master's work has led to four publications, four oral and six poster presentations in national and international conferences, and one invited talk. After completing her M.S., Devleena will pursue a Ph.D in Chemistry at Stanford University starting September 2012.